Functionally segregated escape networks in zebrafish hindbrain

（ゼブラフィッシュ後脳の逃避運動回路は

感覚入力によって使い分けられる）

Tsunehiko Kohashi

Graduate School of Frontier Biosciences

Osaka University

March 2009

This thesis is based on the following articles:

1. Initiation of Mauthner- or non-Mauthner-mediated fast escape evoked by different modes of sensory input

Tsunehiko Kohashi and Yoichi Oda

The Journal of Neuroscience, 2008, 28 (42):10641-10653

2. Development of hindbrain circuits for fast escape in zebrafish

Tsunehiko Kohashi, Natsuyo Nakata and Yoichi Oda

(in preparation)

Table of contents

General introduction

A fundamental role of the nervous system is to integrate external and internal information to produce appropriate behavioral output. The idea that different brain regions are specialized for different functions, which can be traced back to Franz-Josef Gall's theory of phrenology in the eighteenth century, is today a widely-accepted view to understand functional architecture of the brain underlying behavior (Kandel, 2000).

In the brainstem, one of the main parts of the vertebrate brain, reticulospinal (RS) neurons form a phylogenetically conserved (Nieuwenhuys et al., 1998; Butler and Hodos, 2005), descending motor control system which converges sensory inputs to generate motor command for the spinal cord (Rossignol et al., 2006; Grillner et al., 2008). Subpopulations of RS neurons located in discrete brainstem regions are recruited in the control of different components of sensorimotor integration. In mammals, RS neurons in the nucleus reticularis gigantocellularis and the nucleus reticularis magnocellularis (Orlovsky et al., 1999), the caudal pontine reticular formation (Yeomans et al., 2002) and the rostral ventrolateral medulla (Dampney, 1994) are known to elicit locomotion, acoustic startle reflex and sensory-evoked regulation of blood pressure, respectively. In lampreys, RS neurons in the middle and posterior rhombencephalic reticular nuclei are thought to play pivotal roles in sensory-evoked lateral turn and roll turn (Ullen et al., 1997; Fagerstedt et al., 2001). In frogs, the visually-evoked reactions of turning toward prey and turning away from threats are separately impaired by lesions in different brainstem regions (King and Comer, 1996). In teleost fish, lesion experiments and imaging of neuronal activity suggest that subpopulations of RS neurons in the midbrain, dorsomedial and ventromedial hindbrain are important for the control of visual prey capture (Gahtan et al., 2005), fast escape (see below) and optomotor response (Orger et al., 2008), respectively. Nevertheless, it is almost completely unknown how sensory inputs are processed into a particular motor command by individual RS neurons within a brainstem region.

A fascinating concept has been raised to connect the cytoarchitecture of the RS system to its physiological function (Kimmel et al., 1982; Foreman and Eaton, 1993; Eaton et al., 2001). The concept is based on the segmental arrangement of the RS neurons along the neuraxis, particularly in the hindbrain. During development of the vertebrate embryo, the hindbrain is transiently subdivided into repeated segments, resulting in a series of 7 or 8 neuromeres called rhombomeres (Lumsden and Keynes, 1989; Keynes and Lumsden, 1990; Lumsden and Krumlauf, 1996). These hindbrain segments serve as repeated compartments of neuronal differentiation and organization (Kiecker and Lumsden, 2005). Each RS neuron belongs to a group of neurons arranged in one of the hindbrain segments (Glover, 2001). The arrangement of the RS neurons has been investigated in detail, especially in the hindbrain of larval zebrafish, where only about 100 RS neurons in total can be morphologically identified on each side (Kimmel et al., 1985; Metcalfe et al., 1986; Gahtan and O'Malley, 2001). The RS neurons, which are the first neurons to develop in the brain (Kimmel et al., 1978; Mendelson, 1986a), differentiate at the center of each rhombomere (Hanneman et al., 1988). The segmental arrangement of the RS neurons is preserved during development (Lee and Eaton, 1991). Kimmel and his colleagues first explained that the hindbrain RS neurons of larval zebrafish are arranged as if placed upon seven successive rungs of a ladder lying along the neuraxis. Most interestingly, neurons with similar morphological characteristics, including soma positions, dendritic fields and axonal pathways, are repeatedly found in adjacent segments (Kimmel et al., 1982). In addition to the RS neurons, T reticular interneurons also show a ladder-like arrangement in the caudal hindbrain (Kimmel et al., 1985). These observations inspired Kimmel et al. to propose that the neurons in the hindbrain reticular formation are segmentally organized (Kimmel et al., 1985). Further, they classified the twenty-seven types of RS neurons into seven groups based on their morphological homology, and proposed that the morphologically homologous RS neurons which repeatedly appear in adjacent segments are segmental homologs (Metcalfe et al., 1986). They then proposed the hypothesis that each segment may have evolved through successive duplication and subsequent divergence of the ancestral segment (Metcalfe et al., 1986), and that the segmental homologs are functionally and developmentally related to each other (Kimmel et al., 1982; Metcalfe et al., 1986; Lee and Eaton, 1991; Lee et al., 1993). In the embryonic

hindbrains of chicks (Clarke and Lumsden, 1993) and mice (Auclair et al., 1999) as well, RS neurons which share mediolateral position of somata and laterality of axonal trajectories (descending ipsilaterally or contralaterally) are found in adjacent rhombomeres. Thus, the concept of segmentally homologous RS neurons seems applicable to vertebrate hindbrains in general.

In terms of development, it has been demonstrated in zebrafish that dorsally located sets of segmental homologs are born and extend their axons earlier than ventrally located sets (Mendelson, 1986a, b). In addition, the homologs share antigen expression and histochemical properties at early developmental stages (Hanneman et al., 1988). Thus the segmental homologs seem to undergo similar developmental processes. The functional relationships among the homologs, however, have scarcely been elucidated, except for one set of segmentally homologous RS neurons occurring in teleost fish: three bilateral pairs of identified RS neurons repeated in the 4th through the 6th successive hindbrain segments, named the Mauthner (M-) cell, MiD2cm and MiD3cm. These are collectively known as the M-series (Lee and Eaton, 1991). The M-series neurons are located dorsally within each segment; they extend two principal dendrites dorsolaterally and ventrolaterally and send an axon descending into the contralateral spinal cord (Metcalfe et al., 1986).

The M-cell, the largest RS neuron in zebrafish and goldfish, is thought to initiate fast escape starting with a C-shaped body bending, since it has been shown in goldfish that the onset of the C-shaped bending is tightly correlated with the preceding extracellular field potential of M-cell spiking (Zottoli, 1977; Eaton et al., 1981; Eaton et al., 1988; Weiss et al., 2006) and that an action potential elicited in an M-axon excites the contralateral trunk muscle to bend the body (Fetcho, 1991)(see the introduction to Chapter 1 for more details). This Mauthner-initiated fast escape is called M-escape here. It is worth noting that a similar fast escape still occurs after M-cell ablation (Eaton et al., 1982; DiDomenico et al., 1988; Liu and Fetcho, 1999; Zottoli et al., 1999), indicating that there is another pathway for fast escape which is not initiated by M-cell firing (non-M-escape) (Eaton et al., 1984). In larval zebrafish, the lesioning of all the M-series neurons abolished fast escape with short latency (Liu and Fetcho, 1999), indicating that the M-cell homologs are involved in the non-M-escape pathway. In addition to this observation, Ca^{2+} imaging of M-series neurons in response to a head-tap stimulus (O'Malley et al., 1996), along with electrophysiological and morphological

analysis of the sensory nerve projection to the M-series (Nakayama and Oda, 2004), have led to a proposal that the M-series neurons act as a functional unit which is involved in initiation and control of fast escape elicited by sound, vibratory or head-tactile stimulus. Yet the functional relationship among the activities of the M-series neurons, as well as the means by which sensory inputs are processed into an escape command through the M-series neurons, remain to be elucidated, because RS neuron activity has not yet been observed directly during escape.

In vivo confocal Ca^{2+} imaging of the M-series neurons during escape in larval zebrafish was expected to be a particularly suitable approach by which to investigate the functional relationship among the neurons. Taking advantage of the transparency of the larvae, *in vivo* Ca^{2+} imaging enables us to monitor the activities of several neurons simultaneously during larval behavior (Fetcho et al., 1997, 1998; O'Malley et al., 2003), which was difficult with the conventional electrophysiological approaches. In addition, the non-invasive nature of *in vivo* imaging ensures that the local circuitry involving the recorded neurons is left intact (Takahashi et al., 2002). Moreover, the benefits associated with Ca^{2+} imaging as compared to imaging of the membrane potential itself, including the higher signal-to-noise ratio (Tsien, 1988) and the larger fluorescence changes (an increase per action potential of several to several dozen percent as opposed to a typical value of <0.5 % [cf. Grinvald, 1985]), allow us to obtain a significant optical signal even without signal averaging. As a result, the relationship between M-series activity and the corresponding behavior can be compared from trial to trial. Although *in vivo* Ca^{2+} imaging of RS neurons was once performed only in larva embedded in agar (O'Malley et al., 1996; Gahtan et al., 2002), recently, the activities of spinal neurons have been successfully imaged simultaneously with tail movement of partially restrained larva (Ritter et al., 2001; Bhatt et al., 2007).

Here, I have developed a novel experimental setup for *in vivo* confocal Ca^{2+} imaging of RS neurons combined with simultaneous monitoring of the freely moving tails of head-restrained larval zebrafish (Fig. 1-1). In chapter 1, I use this optical setup to show the relationship between the initiation of fast escape and spiking of the M-cell. In chapter 2, I describe the relationships among the activities of M-series neurons during fast escape, especially the relationship between the activities of the M-cell and MiD3cm. In chapter

3, I describe how the escape networks, including both M- and non-M-escape pathways, are activated by sensory systems. Finally, in chapter 4, I propose a hypothesis about the way in which fast escape in zebrafish, which occurs only in response to tactile stimulation at the time of hatching, develops to occur in response to sound/vibratory stimulation. These results will contribute to our understanding of the functional organization of the sensorimotor network in the hindbrain.

References for general introduction

Auclair F, Marchand R, Glover JC (1999) Regional patterning of reticulospinal and vestibulospinal neurons in the hindbrain of mouse and rat embryos. J Comp Neurol 411:288-300.

Bhatt DH, McLean DL, Hale ME, Fetcho JR (2007) Grading movement strength by changes in firing intensity versus recruitment of spinal interneurons. Neuron 53:91-102.

Butler AB, Hodos W (2005) Comparative Vertebrate Neuroanatomy: Evolution and Adaptation, Second Edition. Hoboken, NJ: John Wiley and Sons, Inc.

Clarke JD, Lumsden A (1993) Segmental repetition of neuronal phenotype sets in the chick embryo hindbrain. Development 118:151-162.

Dampney RA (1994) Functional organization of central pathways regulating the cardiovascular system. Physiol Rev 74:323-364.

DiDomenico R, Nissanov J, Eaton RC (1988) Lateralization and adaptation of a continuously variable behavior following lesions of a reticulospinal command neuron. Brain Res 473:15-28.

Eaton RC, Lavender WA, Wieland CM (1981) Identification of Mauthner-initiated response patterns in goldfish: Evidence from simultaneous cinematography and electrophysiology. J Comp Physiol [A] 144:521-531.

Eaton RC, Lavender WA, Wieland CM (1982) Alternative neural pathways initiate fast-start responses following lesions of the Mauthner neuron in goldfish. J Comp Physiol [A] 145:485-496.

Eaton RC, Nissanov J, Wieland CM (1984) Differential activation of Mauthner and non-Mauthner startle circuits in the zebrafish: Implications for functional substitution. J Comp Physiol [A] 155:813-820.

Eaton RC, DiDomenico R, Nissanov J (1988) Flexible body dynamics of the goldfish C-start: implications for reticulospinal command mechanisms. J Neurosci 8:2758-2768.

Eaton RC, Lee RK, Foreman MB (2001) The Mauthner cell and other identified neurons of the brainstem escape network of fish. Prog Neurobiol 63:467-485.

Fagerstedt P, Orlovsky GN, Deliagina TG, Grillner S, Ullen F (2001) Lateral turns in the Lamprey. II. Activity of reticulospinal neurons during the generation of fictive turns. J Neurophysiol 86:2257-2265.

Fetcho JR (1991) Spinal network of the Mauthner cell. Brain Behav Evol 37:298-316.

Fetcho JR, Cox KJ, O'Malley DM (1997) Imaging neural activity with single cell resolution in an intact, behaving vertebrate. Biol Bull 192:150-153.

Fetcho JR, Cox KJ, O'Malley DM (1998) Monitoring activity in neuronal populations with single-cell resolution in a behaving vertebrate. Histochem J 30:153-167.

Foreman MB, Eaton RC (1993) The direction change concept for reticulospinal control of goldfish escape. J Neurosci 13:4101-4113.

Gahtan E, O'Malley DM (2001) Rapid lesioning of large numbers of identified vertebrate neurons: applications in zebrafish. J Neurosci Methods 108:97-110.

Gahtan E, Tanger P, Baier H (2005) Visual prey capture in larval zebrafish is controlled by identified reticulospinal neurons downstream of the tectum. J Neurosci 25:9294-9303.

Gahtan E, Sankrithi N, Campos JB, O'Malley DM (2002) Evidence for a widespread brain stem escape network

in larval zebrafish. J Neurophysiol 87:608-614.

Glover JC (2001) Correlated patterns of neuron differentiation and Hox gene expression in the hindbrain: a comparative analysis. Brain Res Bull 55:683-693.

Grillner S, Wallen P, Saitoh K, Kozlov A, Robertson B (2008) Neural bases of goal-directed locomotion in vertebrates--an overview. Brain Res Rev 57:2-12.

Grinvald A (1985) Real-time optical mapping of neuronal activity: from single growth cones to the intact mammalian brain. Annu Rev Neurosci 8:263-305.

Hanneman E, Trevarrow B, Metcalfe WK, Kimmel CB, Westerfield M (1988) Segmental pattern of development of the hindbrain and spinal cord of the zebrafish embryo. Development 103:49-58.

Kandel ER (2000) The brain and behavior. In: Principles of neural science, Fourth edition Edition (Kandel ER, Schiwartz JH, Jessell TM, eds). New York: McGraw-Hill.

Keynes R, Lumsden A (1990) Segmentation and the Origin of Regional Diversity in the Vertebrate Central-Nervous-System. Neuron 4:1-9.

Kiecker C, Lumsden A (2005) Compartments and their boundaries in vertebrate brain development. Nat Rev Neurosci 6:553-564.

Kimmel CB, Sessions SK, Kimmel RJ (1978) Radiosensitivity and time of origin of Mauthner neuron in the zebra fish. Dev Biol 62:526-529.

Kimmel CB, Powell SL, Metcalfe WK (1982) Brain neurons which project to the spinal cord in young larvae of the zebrafish. J Comp Neurol 205:112-127.

Kimmel CB, Metcalfe WK, Schabtach E (1985) T reticular interneurons: a class of serially repeating cells in the zebrafish hindbrain. J Comp Neurol 233:365-376.

King JR, Comer CM (1996) Visually elicited turning behavior in Rana pipiens: Comparative organization and neural control of escape and prey capture. J Comp Physiol A 178:293-305.

Lee RK, Eaton RC (1991) Identifiable reticulospinal neurons of the adult zebrafish, Brachydanio rerio. J Comp Neurol 304:34-52.

Lee RK, Eaton RC, Zottoli SJ (1993) Segmental arrangement of reticulospinal neurons in the goldfish hindbrain. J Comp Neurol 329:539-556.

Liu KS, Fetcho JR (1999) Laser ablations reveal functional relationships of segmental hindbrain neurons in zebrafish. Neuron 23:325-335.

Lumsden A, Keynes R (1989) Segmental Patterns of Neuronal Development in the Chick Hindbrain. Nature 337:424-428.

Lumsden A, Krumlauf R (1996) Patterning the vertebrate neuraxis. Science 274:1109-1115.

Mendelson B (1986a) Development of reticulospinal neurons of the zebrafish. I. Time of origin. J Comp Neurol 251:160-171.

Mendelson B (1986b) Development of reticulospinal neurons of the zebrafish. II. Early axonal outgrowth and cell body position. J Comp Neurol 251:172-184.

Metcalfe WK, Mendelson B, Kimmel CB (1986) Segmental homologies among reticulospinal neurons in the hindbrain of the zebrafish larva. J Comp Neurol 251:147-159.

Nakayama H, Oda Y (2004) Common sensory inputs and differential excitability of segmentally homologous

reticulospinal neurons in the hindbrain. J Neurosci 24:3199-3209.

Nieuwenhuys R, ten Donkelaar HJ, Nicholson C (1998) The central nervous system of vertebrates. Berlin: Springer-Verlag.

O'Malley DM, Kao YH, Fetcho JR (1996) Imaging the functional organization of zebrafish hindbrain segments during escape behaviors. Neuron 17:1145-1155.

O'Malley DM, Zhou Q, Gahtan E (2003) Probing neural circuits in the zebrafish: a suite of optical techniques. Methods 30:49-63.

Orger MB, Kampff AR, Severi KE, Bollmann JH, Engert F (2008) Control of visually guided behavior by distinct populations of spinal projection neurons. Nat Neurosci 11:327-333.

Orlovsky GN, Deliagina TG, Grillner S (1999) Initiation of locomotion. In: Neuronal control of locomotion: from mollusc to man, pp 205-214. New York: Oxford University Press.

Ritter DA, Bhatt DH, Fetcho JR (2001) In vivo imaging of zebrafish reveals differences in the spinal networks for escape and swimming movements. J Neurosci 21:8956-8965.

Rossignol S, Dubuc R, Gossard JP (2006) Dynamic sensorimotor interactions in locomotion. Physiol Rev 86:89-154.

Takahashi M, Narushima M, Oda Y (2002) In vivo imaging of functional inhibitory networks on the Mauthner cell of larval zebrafish. J Neurosci 22:3929-3938.

Tsien RY (1988) Fluorescence measurement and photochemical manipulation of cytosolic free calcium. Trends Neurosci 11:419-424.

Ullen F, Deliagina TG, Orlovsky GN, Grillner S (1997) Visual pathways for postural control and negative phototaxis in lamprey. J Neurophysiol 78:960-976.

Weiss SA, Zottoli SJ, Do SC, Faber DS, Preuss T (2006) Correlation of C-start behaviors with neural activity recorded from the hindbrain in free-swimming goldfish (Carassius auratus). J Exp Biol 209:4788-4801.

Yeomans JS, Li L, Scott BW, Frankland PW (2002) Tactile, acoustic and vestibular systems sum to elicit the startle reflex. Neuroscience and Biobehavioral Reviews 26:1-11.

Zottoli SJ (1977) Correlation of the startle reflex and Mauthner cell auditory responses in unrestrained goldfish. J Exp Biol 66:243-254.

Zottoli SJ, Newman BC, Rieff HI, Winters DC (1999) Decrease in occurrence of fast startle responses after selective Mauthner cell ablation in goldfish (Carassius auratus). J Comp Physiol [A] 184:207-218.

Chapter 1

Mauthner and non-Mauthner-mediated fast escape in larval zebrafish characterized by *in vivo* calcium imaging of neuronal activity during behavior

Summary

I have developed a novel optical system to monitor activities of brain neurons during behavior in larval zebrafish. As the first step, I examined correlation between initiation of fast escape and accompanying activity of the M-cell. The neuronal activities were monitored with Ca^{2+} elevation in the soma of the M-cell, associated with spiking of the cell. To measure the somatic Ca^{2+} response, the Mauthner (M-) cell in larval zebrafish (5-9 days postfertilization; dpf) was retrogradely labeled with a dextran-conjugated fluorescent calcium indicator, Oregon Green BAPTA-1 dextran. For simultaneous imaging of the neuronal activity and body movement, the rostral body of the fish was fixed in agar, allowing the tail to move freely. Tail flip response elicited by water pulse applied to the otic vesicle was monitored in the semi-fixed preparation with a high-speed camera and fluorescence response of the M-cell was imaged simultaneously with confocal microscopy. The tail flip response reflects that of freely-swimming larva at the points of contralateral directionality to the stimulus, short-onset latency and fast angular velocity of initial bending. Sixty-three out of ninety-one fast tail flips were initiated with short onset latency and associated with a prominent fluorescence increase in the ipsilateral M-cell as large as that evoked by single antidromic spike of each cell, supporting the previous notion that single spiking of the M-cell initiates contralateral escape (M-escape). Interestingly, fast tail flip was also observed without M-cell firing (non-M-escape), the angular velocity of

which was similar to that of M-escape but the onset was delayed (>6 ms). Selective laser ablation of the M-cell abolished escape with onset latencies shorter than 6 ms. Thus, these results suggest that firing of an M-cell is necessary to produce fast escape with short latency.

Introduction

One goal of neuroethology is to account for an innate behavior at the level of single, identifiable cells (Bullock, 1990). Escape or startle responses, which are widely observed in animal species, have been the subject of a number of studies related to this issue (Eaton, 1984). Escapes have commonly been viewed as an abrupt and stereotyped behavior triggered by a sudden aversive stimulus. From the highly stereotyped motor output and extremely-short onset latency of the behavior, the neural circuits for the initiation of escape are generally believed to be relatively simple and identifiable from sensory organs to muscles (Korn and Faber, 1996; Yeomans and Frankland, 1996; Edwards et al., 1999).

One of the best-characterized escapes is the fast escape exhibited by fusiform-shaped teleost fishes (Domenici and Blake, 1997), which starts with a C-shaped body bending opposite to the stimulus. Most of the fast escapes are believed to be initiated by an action potential in one of the paired M-cells. It has been shown in goldfish that initiation of the fast escape is tightly correlated with the preceding extracellular field potential of the contralateral M-cell spiking (Zottoli, 1977; Eaton et al., 1981; Eaton et al., 1988; Weiss et al., 2006). It was also shown that firing of the M-cell, elicited by electrical stimulation of the axon, is sufficient to activate the contralateral trunk muscle (Hackett and Faber, 1983; Hackett and Greenfield, 1986) to produce initial phase of the C-bend toward the opposite side (Nissanov et al., 1990) by direct activation of contralateral spinal motoneurons along the body (Fetcho and Faber, 1988). These observations have strengthened the idea that the M-cell is involved in every fast escape.

Lesion studies of the M-cell, however, demonstrated that the fast escape similar to that of M-cell intact animal can be initiated even in the absence of the M-cell (Kimmel et al., 1980; Eaton et al., 1982; DiDomenico et al., 1988; Liu and Fetcho, 1999; Zottoli et al., 1999). The possibility that such fast escape occurred without M-cell firing can be initiated in intact brain was also suggested in restrained larval zebrafish preparation (Eaton et al., 1984). These led to a hypothesis that there are two types of fast escape in intact fish brain; one is initiated by firing of the M-cell, termed M-escape, and the other is not but by that of the other reticulospinal (RS) neurons, termed non-M-escape.

Activities of identified RS neurons other than the M-cell, however, have not been reported yet during escape in freely-moving preparation. This is mainly because it is very hard with extracellular field potential recordings to identify multiple neurons which are activated, although spiking of the M-cell can be exceptionally identified from very large and distinctive field potential in the vicinity of the soma (Furshpan and Furukawa, 1962). In the first place, even activities of bilateral M-cells has not been monitored simultaneously until recently (Weiss et al., 2006). Compared with extracellular recordings, *in vivo* confocal Ca^{2+} imaging of neuronal activity in transparent larval zebrafish has great advantage in recording of multiple neurons (Fetcho et al., 1997, 1998). Furthermore, since all the RS neurons are morphologically identifiable in larval zebrafish (Metcalfe et al., 1986), activities of them can be assessed at the level of single identified neurons by labeling retrogradely with dextran-conjugated fluorescent Ca^{2+} indicators injected into the spinal cord (O'Malley et al., 1996; Gahtan et al., 2002). In addition, the non-invasive nature of this recording technique allows us to monitor neuronal activity in unanesthetized behaving animal.

Thus, as the first step of my study, I tried to confirm the direct correlation between M-cell activity and initiation of fast escape by *in vivo* confocal Ca^{2+} imaging. I developed a novel upright confocal microscope equipped with an inverted optical system to monitor tail movement of partially-restrained larval zebrafish simultaneously. Here, I demonstrate that the M-cell indeed fires an action potential during fast escape (M-escape). In addition, I showed that similar fast escape occurred without firing of the M-cell (non-M-escape) but the onset was delayed from that of M-escape.

Materials and methods

Animals. Experiments were performed on 5 to 9-days-postfertilization (dpf) larval zebrafish (*Danio rerio*) at room temperature (27-29 ºC). Larvae were obtained from an adult zebrafish colony and raised at 28.5 ºC. By this stage, larvae start swimming, feeding and showing escape in response to tactile and vibratory stimulation (Budick and O'Malley, 2000; Burgess and Granato, 2007). All procedures were performed in compliance with the guidelines approved by the Animal Care and Use Committee of Nagoya University and stipulated by the Osaka University Committee on Animal Research.

Retrograde labeling of RS neurons. Hindbrain RS neurons were labeled with a fluorescent Ca^{2+} indicator Oregon-green BAPTA-1 dextran (OGB1; 10,000 molecular weight; Invitrogen, Eugene, OR) as follows. Larvae were anesthetized with 0.01% 3-aminobenzoic acid ethyl ester (MS222; Sigma, St. Louis, MO) in 10% Hank's solution (HBSS; in mM, 13.7 NaCl, 0.54 KCl, 0.025 Na_2HPO_4, 0.044 KH_2PO_4, 0.13 $CaCl_2$, 0.1 $MgSO_4$, and 0.42 $NaHCO_3$, pH 7.2) chilled on ice. To label RS neurons neurons retrogradely, a 33% solution of OGB1 in 10% HBSS was pressure-injected via a glass microcapillary (tip diameter: approximately 10 μm) into the caudal spinal cord (at approximately the level of the 22nd myotome) using a Picospritzer III (Parker Hannifin Corp., Fairfield, NJ) (Fig. 1-1A). A small injection did not disturb the movement of the body rostral to the injection site. After the injection, larvae were allowed to recover in 10% HBSS (28.5 ºC) for more than 9 hours.

Semi-fixed preparation. For simultaneous monitoring of RS neuron activity and behavioral response, the larvae were placed in an agar-coated glass recording chamber. The rostral half of the body was embedded in 3.5% agar (low-melting point agarose, gelled at 28 ºC; Invitrogen, Gaithersburg, MD) with its dorsal side up (modified from Ritter et al., 2001). The chamber was filled with 10% HBSS after the agar had congealed. For application of water pulse stimuli to the head, the agar covering the otic vesicle (OV) was cut out on one side. For monitoring tail movements, the tail caudal to the cloaca and well anterior to the OGB1-injected site was exposed (Fig. 1-1B). During all experiments, the viability of the fish was carefully monitored by observing the fast blood flow in thin vessels within the brain.

Behavioral analysis of fast escape. Escape responses were elicited by a water pulse applied every 5 min to the otic vesicle (OV) or rostral head skin through a syringe needle (26 gauge; inner diameter: 220 μm; Terumo, Tokyo, Japan). In some experiments, the water pulse was applied to one side of the tail at level of the cloaca. The water pulses were generated by a pressure pulse of 3 ms duration delivered from a Picospritzer. The pressure was normally adjusted to < 30 psi, unless otherwise noted. When the semi-fixed larva was stimulated, the needle tip was kept 0.5 mm apart from the surface of the fish with a micromanipulator (MM-200; Narishige, Tokyo, Japan). To observe escape in the unrestrained preparations, the larvae were placed in a Petri dish (3.5 cm) filled with 10% HBSS at a depth of 3 to 4 mm and the tip of the water stimulus needle was positioned 1 to 3 mm from the fish.

Sequential images of the escape response were captured with a high-speed digital camera (captured every 1 ms, Fastcam Ultima 1024 or Fastcam 1024 PCI; Photoron, Tokyo, Japan) and saved with Fastcam Viewer ver.2.4.3.2 software (Photoron). Latency was defined as the time from the arrival of the water pulse to the head of the fish to the beginning of tail movement. The water arrival time in the semi-fixed preparations, estimated as the time of delivery of the water to 0.5 mm from the syringe needle in air, was 0.41, 0.44 and 0.65 ms for stimulus pulses at a pressure of 20, 15 and 10 psi, respectively. The estimated time was confirmed by the observation of a slight depression of the otic vesicle in response to a strong water pulse (> 20 psi). In the unrestrained preparations, the water arrival time was visually determined as the time it took the ripple of water stimulus to reach the head of the fish.

Tail flexion responses with latency shorter than 15 ms were analyzed (see Results and Discussion). The tail flexion angle (θ) was measured from the three dots on the midline as shown in Fig. 1-2C1 and C2. The dots were positioned at the cloaca (dot 2), L/12 rostral (dot 1) and L/6 caudal (dot 3) to dot 2; L represents the distance from the caudal end of the swim bladder to the tip of the tail. All the dots were rostral to the OGB1 injection site. Assignment of the dots and measurement of the flexion angle were performed with motion analysis software (Dipp-Motion 2D; Ditect, Tokyo, Japan). The angular velocity was calculated from flexion angles smoothed with a three-point moving average filter.

Optics for simultaneous monitoring of RS neuron activity and behavior (Fig. 1-1C-E). Calcium im-

aging of RS neurons was performed with an upright microscope (BX51WI; Olympus, Tokyo, Japan) with a water immersion objective (LUMPlanFL 40xW/IR; 40X; NA0.8; Olympus). The inverted optics for behavioral recording was attached below a manipulation stage and consisted of a low-magnification objective (XLFluor 2x/340; 2X; NA 0.14; Olympus), a dual port (U-DP; Olympus) with an imaging lens unit (U-DP1xC; Olympus) and a high-speed digital camera (Fastcam Ultima 1024 or Fastcam 1024 PCI). The tail of the semi-fixed preparation was illuminated with orange light (wavelengths, 590-670 nm) that did not interfere with confocal imaging. The manipulation stage was completely isolated from both of the optics. The axes of the two optical systems could be moved independently to focus on neurons and the tail.

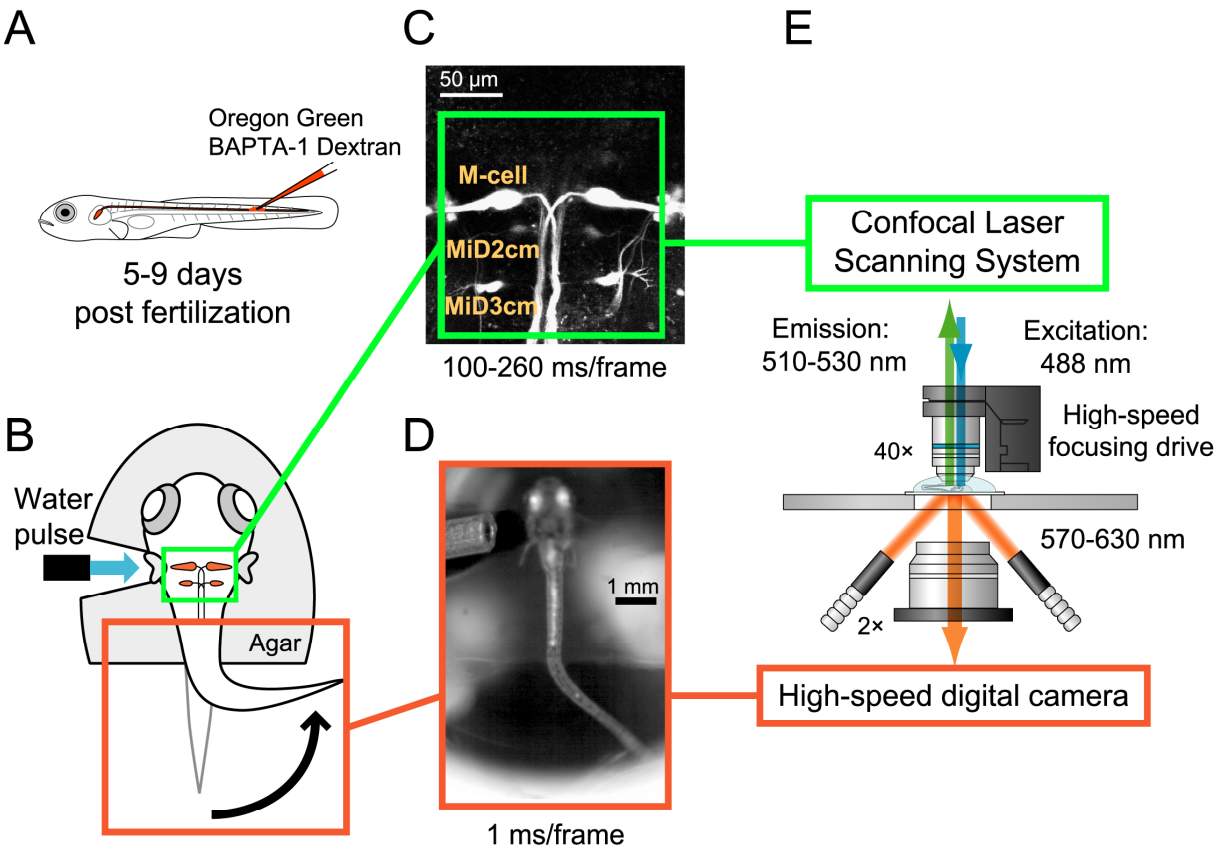

Figure. 1-1. Experimental setup for simultaneous monitoring of RS neuron activity and behavior. **A,** RS neurons were labeled retrogradely with a fluorescent Ca^{2+} indicator, Oregon Green BAPTA-1 dextran, injected into caudal spinal cord. **B-E,** The rostral body, anterior to the cloaca, of the larval zebrafish was embedded in agar (**B**). A water pulse was usually applied to the otic vesicle (OV; a premature organ of inner ear). The evoked fluorescence responses in the RS neurons (green) and tail movement (orange) were monitored simultaneously with confocal microscopy (**C and E, upright optics**) and a high-speed digital camera (**D and E, inverted optics**), respectively. The tail of the semi-fixed larva was illuminated with orange light that did not interfere with confocal imaging. The high-speed focusing drive, which enabled us to switch focal planes alternately during image acquisition, was used in Chapter 2 and 3. See Materials and Methods for detail.

Calcium imaging with confocal microscopy. RS neurons were illuminated with a 488 nm argon laser line and the fluorescence images of them were captured with a conventional confocal scanner (FV300; Olympus; emission filter, 510-530 nm). Before each trial, a series of horizontal optical sections spanning the cells was collected and the brightest plane of each cell to image was determined, which ensured that the increase in fluorescence of the cell was not a result of its movement into a brighter plane (O'Malley et al., 1996). Images (512 × 512 pixels) were collected every 260 ms. I used Fluoview ver.3.3 software (Olympus) for operation of the confocal scanner and image acquisition.

After Ca^{2+} imaging of the RS neurons during escape, fluorescence responses associated with antidromic (AD) action potentials of the same neurons were examined. The larvae were anesthetized with 0.01% MS222, re-embedded in 3.5% agar and immobilized with injection of d-tubocurarine chloride solution (3 mg/ml; Sigma) to prevent tail movement evoked by AD stimulation from injury to the spinal cord. To stimulate the axons of the RS neurons (Furshpan and Furukawa, 1962; Eaton and Farley, 1975; Takahashi et al., 2002; Nakayama and Oda, 2004), a bipolar tungsten electrode was placed on the spinal cord rostral to the OGB1-injected site through a small hole cut in the agar and bipolar pulsed currents were delivered (pulse duration: 80 μs).

Quantification of fluorescence response. Prior to the quantification of fluorescence, background correction was done on the raw fluorescence images. Fluorescence intensities of the cell bodies were measured and the relative changes in fluorescence from the resting intensity ($\Delta F/F$) were calculated. The first frame after stimulation was excluded from the analysis since it was affected by the movement of the larva. For the M-cell, the second frame after stimulation was used to measure the amplitude of the response.

Laser ablation of M-cells. To ablate M-cells, an FV300 system with a 60x water objective (LUMPLanFL60x, NA0.9; Olympus) was used and the laser beam was applied to the fluorescence-labeled M-cell of zebrafish embedded in agar, as described elsewhere (Liu and Fetcho, 1999). The argon laser at maximum strength was focused on the middle of the M-cell soma in the point-scanning mode. Exposure for 15 min was usually required to ablate the M-cell. After the exposure, the fish was gently removed from the agar and held in 10% HBSS for half to one day before a postlesion behavioral test. The success of the ablation

was verified by observing no recovery of fluorescence at the soma of the M-cell and its truncated axon with the FV300 system on the day after ablation (Fig. 1-6A).

Statistics. Results were presented as the mean ± SEM. The statistical significance was assessed using the Student's t-test after verifying the normality of the distributions by the Kolmogorov-Smirnov test ($p > 0.05$) and the equality of the variance with the F-test ($p > 0.05$), unless otherwise noted.

Results

Escape response of partially restrained larvae

A key aspect of this study was reproduction of the fast escape in the partially restrained (semi-fixed) larval zebrafish in which Ca^{2+} imaging of hindbrain RS neurons was performed. I examined the tail movements elicited by applying a water pulse stimulus to the otic vesicle (OV) on one side of the semi-fixed larva and compared them with those of the fast escape in freely moving (unrestrained) fish (Kimmel et al., 1974; Kimmel et al., 1980; Liu and Fetcho, 1999; Budick and O'Malley, 2000; Burgess and Granato, 2007) (Fig. 1-2A, B). Both unrestrained and semi-fixed preparations exhibited tail flexions contralateral to the stimuli (20 out of 22 responses and 96 out of 101 responses, respectively). The time from the water pulse arrival to the tail movement onset (latency: 3 to 12, 5.7 ± 0.6 ms and 3 to 15, 5.3 ± 0.3 ms, respectively) and angular velocity of the initial tail flexion (20 to 48, 31.5 ± 1.5 degrees and 17 to 41, 29.5 ± 0.5 degrees during 8 ms after movement onset, respectively) were not significantly different (Fig. 1-2C; $p > 0.1$, Mann-Whitney U-test) between the two preparations. Thus, the tail flips observed in the semi-fixed larva reflect the tail movements during the initial phase of fast escape.

These tail responses started within 15 ms after the stimulus arrival. In a few cases, behavioral responses with long latencies (>15 ms, 24-92 ms) also occurred in both preparations. However, I excluded them from the following analysis, because they showed significantly slower initial bending (13.9 ± 4.6 degrees, n = 4, and 10.3 ± 2.4 degrees, n = 8, during the initial 8 ms in unrestrained and semi-fixed preparations, respectively, $p < 0.001$) than during the short-latency fast responses, as reported previously (Burgess and Granato, 2007).

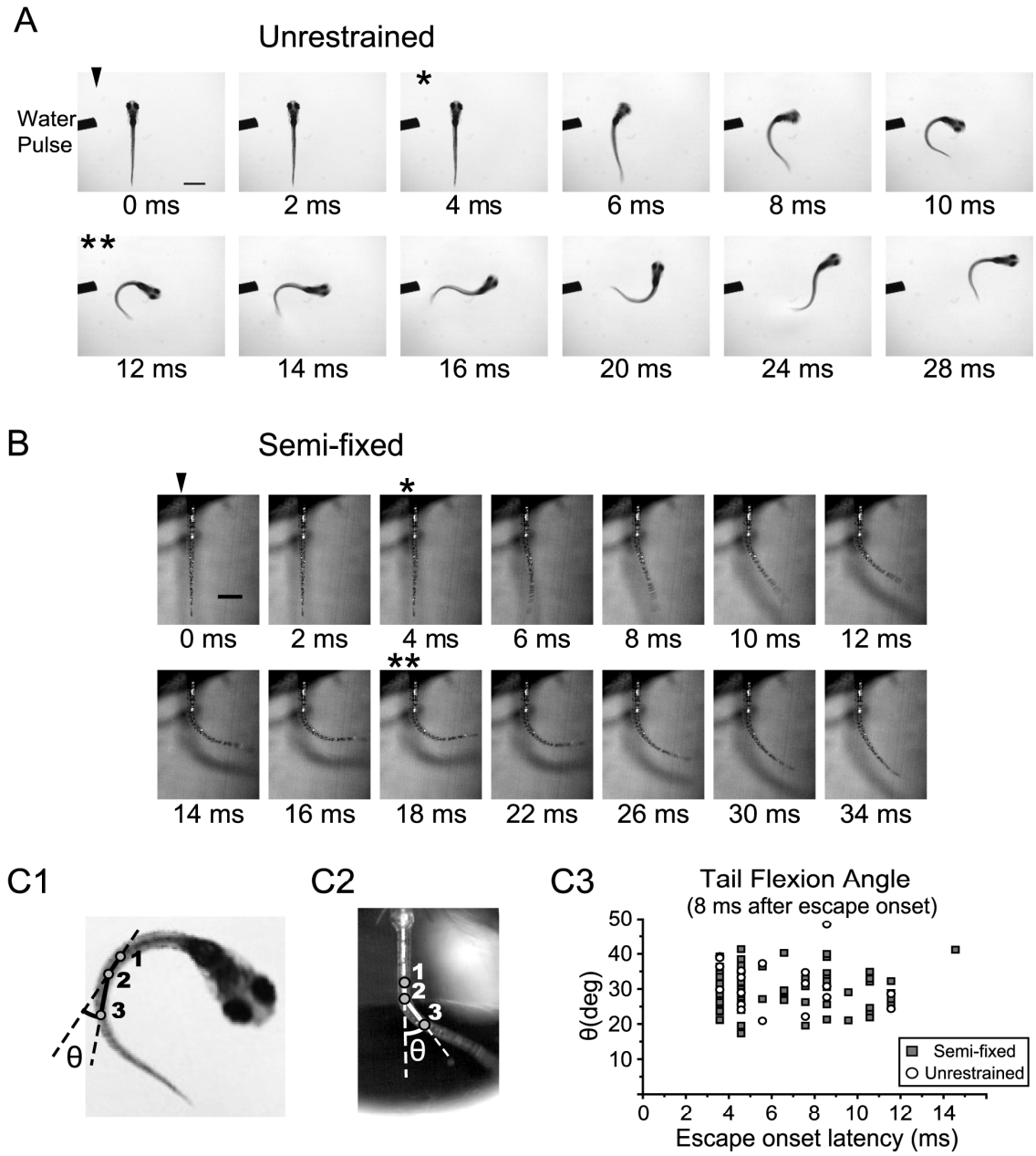

Figure 1-2. Comparison of the tail movements of unrestrained and partially-restrained zebrafish larvae. **A**, The fast escape of unrestrained fish elicited by a water pulse applied to head. The initial strong bend along the whole length of the body, away from the stimulus and the following counter bend represent the typical features of the fast escape of teleosts. The time from the water pulse arrival (arrowhead) is denoted. Single asterisk: response onset. Double asterisks: maximum bending. Scale bar: 1 mm. **B**, Tail flip response of the partially restrained (semi-fixed) larva. In response to the water pulse stimulus to the otic vesicle, a contralateral tail flip and following return movement were observed. Arrowhead, single and double asterisks are the same as in **A**. Scale bar: 0.5 mm. **C**, The tail flexion angles (θ) of unrestrained fast escape (**C1**) and semi-fixed tail flip (**C2**) were measured from the three dots on the midline of the body (1, 2 and 3, see Materials and Methods for details). **C3**, The flexion angles 8 ms after the escape onset (ordinate) are plotted against escape onset latency (abscissa). Data of the semi-fixed tail flips (squares) are in the same range as those of unrestrained fast escapes (circles).

Single spiking of the M-cell associated with initiation of fast escape with short latency

Field potential recordings of M-cell spiking in freely moving goldfish have shown that onset of fast escape is closely correlated with preceding firing of the M-cell (Zottoli, 1977; Eaton et al., 1981; Eaton et al., 1988; Weiss et al., 2006). Here, I examined the correlation by Ca^{2+} imaging of the M-cells during the tail flip of the semi-fixed larva. The M-cells were retrogradely labeled with a Ca^{2+} indicator (Oregon green BAPTA-1 dextran) and were imaged with confocal microscopy (FV300, see Materials and Methods) as exemplified in Figs. 1-3 and 4. The majority of the fast escapes elicited by a water pulse applied to an OV to activate auditory or vestibular sensory afferents were associated with an observed increase in fluorescence ($\Delta F/F$) in the ipsilateral M-cell, whereas no or much smaller fluorescence responses were obtained in the contralateral M-cell (Fig. 1-3A, B). Typically, an increase of more than 20% from the resting fluorescence intensity was observed in the ipsilateral M-cell soma associated with the fast escape (n = 60 out of 91, 17 fish).

To assess whether the fluorescence response of the M-cell during the fast escape reflects spiking of the cell, I compared it with the fluorescence response of an antidromic (AD) action potential in the same cell. Application of electrical pulses with different intensities to the spinal cord induced fluorescence transients in the M-cell in an all-or-nothing manner with a steady amplitude (Fig. 1-3C; peak $\Delta F/F = 30.9 \pm 1.6$ %, 17 cells), which was mediated by Ca^{2+} influx through voltage-gated calcium channels opened during an AD action potential (Takahashi et al., 2002). Thus, I defined the fluorescence response with an amplitude greater than 0.7 times that of an AD spike (xAD) as a sign of orthodromic spiking of the M-cell (see the summarized Fig. 1-5B2). In the M-cell, repetitive firing is suppressed by its powerful recurrent inhibitory circuit (see Discussion). Previously it was shown that double AD stimulation elicits a Ca^{2+} signal in the M-cell nearly twice as large as that resulting from single AD stimulation when the recurrent inhibition was blocked pharmacologically (see Fig. 7 in Takahashi et al., 2002). The fact that the sensory-evoked responses never reached twice that of an AD response (< 1.5 xAD) suggests that the M-cell fired once during the fast escape as observed electrophysiologically in goldfish (Zottoli, 1977; Eaton et al., 1981; Eaton et al., 1988; Weiss et al., 2006).

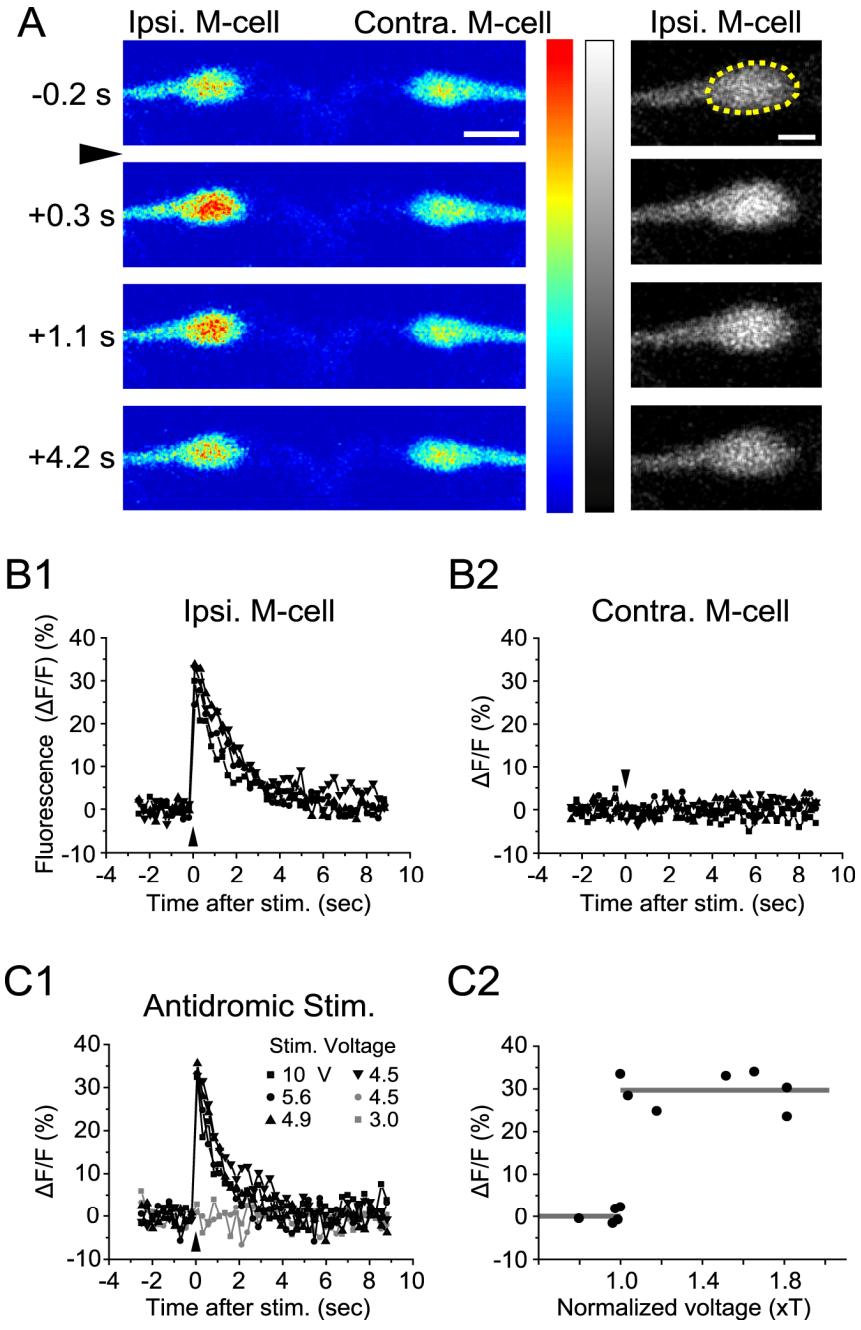

Figure 1-3. Fluorescence response of the paired M-cells associated with fast escape. **A**, Typical fluorescence responses of the paired M-cells, obtained simultaneously with the tail response of Fig. 1-1B2. Left: Pseudocolored images of the fluorescence responses before (-0.2 s) and after (+0.3, 1.1 and 4.2 s) the water pulse arrival (arrowhead). The M-cell ipsilateral to the stimulus (Ipsi. M-cell; gray scale images are shown on right) showed an apparent increase in fluorescence whereas the contralateral M-cell (Contra. M-cell) did not. Scale bars: 20 μm (left) and 10 μm (right). The color and gray scales represent fluorescence intensity (blue or black, lowest; red or white, highest). **B**, Fractional changes in fluorescence (ΔF/F; ordinate) in the somata of the M-cells (the area in the dashed yellow line in **A**) accompanied with fast escape (escape onset latencies: 3-5 ms) were plotted against the time after stimulus arrival (abscissa). Responses of 4 trials obtained from the pair shown in A are superimposed (data exemplified in **A** are shown as triangles). The ipsilateral M-cell exhibited large transient increases in fluorescence (**B1**; peak ΔF/F = 25-35%) whereas the contralateral M-cell did not show any apparent fluorescence response (**B2**). **C1**, Fluorescence responses associated with an antidromic spike of the same ipsilateral M-cell in response to electrical stimulation applied to the spinal cord, which appeared in an all-or-nothing manner with different stimulus intensity (volts) as denoted. The amplitude of suprathreshold fluorescence responses is comparable to that of the large sensory-evoked responses in **B1**. **C2**, The amplitude of the fluorescence response (ordinate) associated with the AD spike of another M-cell is plotted against the intensities of spinal cord stimulation (abscissa; normalized by the threshold voltage, T). The constant increase in fluorescence at the suprathreshold stimulus (average amplitude: 29.6%, right gray line) is consistent with the generation of a single antidromic spike (Takahashi et al., 2002). The left gray line indicates 0%.

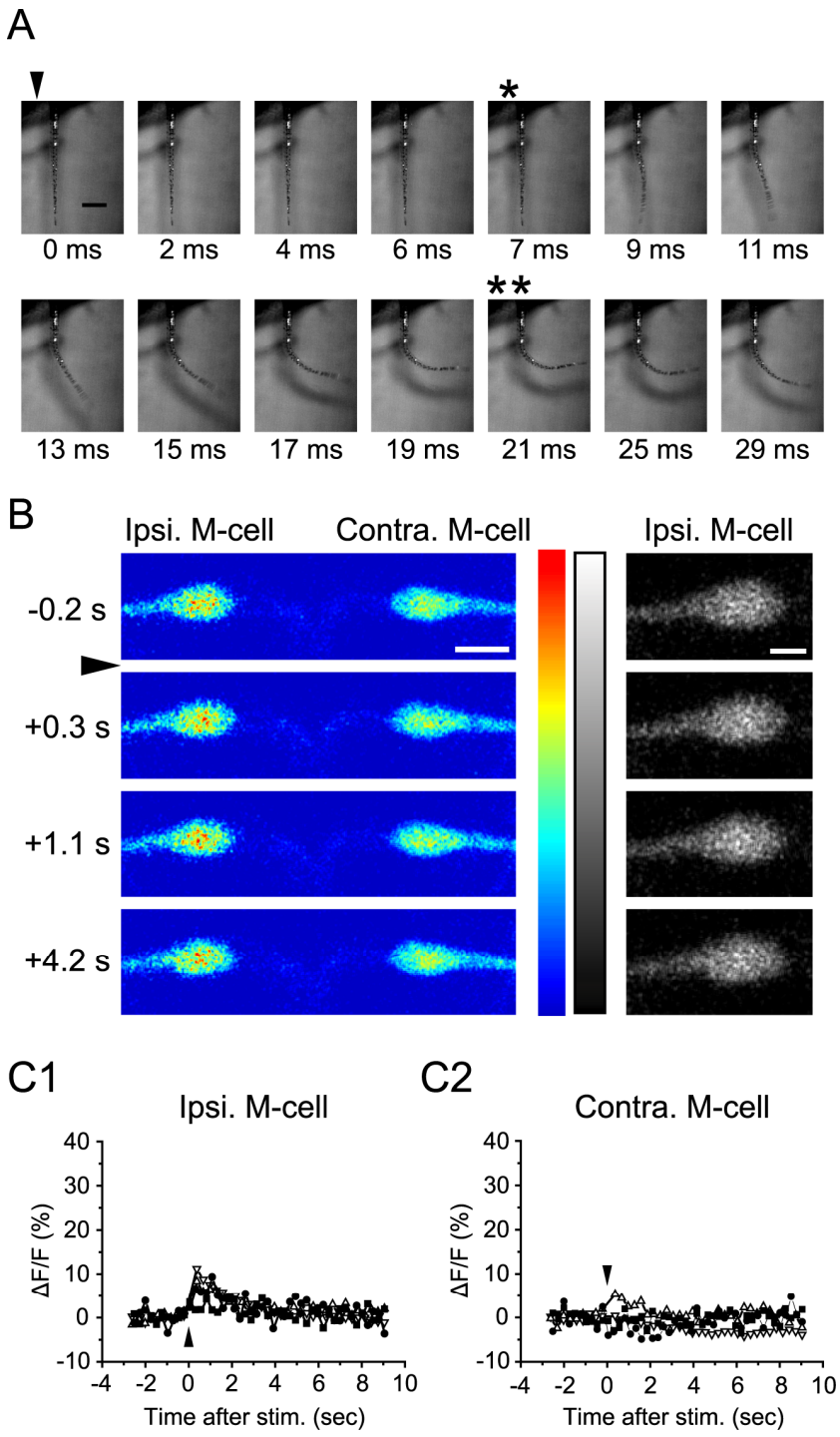

Figure 1-4. Small fluorescence response of the M-cell associated with the delayed fast escape. **A**, In some cases, onset of the tail flip was delayed in the same animal as shown in Fig. 1-1B2. Note that the time course of the delayed tail flexion after onset is similar to that with short latency. Arrowhead, single and double asterisks are the same as in Fig. 1-1. Scale bar: 0.5 mm. **B**, Fluorescence images of the paired M-cells taken simultaneously with A. Neither of the M-cells shows apparent change in fluorescence (left). Gray scale images of the ipsilateral M-cell are shown on the right. Scale bars: 20 μm (left) and 10 μm (right). **C**, Quantification of changes in fluorescence in two pairs of ipsilateral (**C1**) and contralateral (**C2**) M-cells (filled and open symbols for each pair) associated with fast escapes with an onset latency of 7-9 ms. The responses indicated by filled squares are obtained from **B**. In these trials, the M-cells exhibit only a small or no apparent increase in fluorescence.

Of 91 fast escapes obtained from 17 fish, 63 escapes were associated with a suprathreshold increase in fluorescence (> 0.7 xAD) in the ipsilateral M-cell (peak $\Delta F/F$ = 18 to 51%, 32.5 ± 0.9%, 0.74 to 1.50 xAD, 1.04 ± 0.02 xAD, Fig. 1-5A red, B). They were denoted as M-escapes. M-cell firing was never observed when an escape failed to occur at threshold (peak $\Delta F/F$ < 6.5 %, 2.2 ± 0.6 %, < 0.24 xAD, 0.09 ± 0.02 xAD, n = 17, Failure in Fig. 1-5B) or subthreshold intensity (peak $\Delta F/F$ < 5.6 %, 2.4 ± 0.6 %, < 0.14 xAD, 0.07 ± 0.02 xAD, n = 9) of the water stimulus for the tail response. These findings support the previous notion that the M-cell triggers a fast escape toward the contralateral side (Yasargil and Diamond, 1968; Zottoli, 1977; Eaton et al., 1981; Hackett and Faber, 1983; Hackett and Greenfield, 1986; Eaton et al., 1988; Weiss et al., 2006). In some fast escape responses (28 out of 91) of the same fish, however, the ipsilateral M-cell showed only subthreshold (< 0.7 xAD) fluorescence responses (Figs. 1-4, 5A blue, B; peak $\Delta F/F$ < 16%, 7.5 ± 0.9%, < 0.55 xAD, 0.26 ± 0.03 xAD), indicating that the M-cell did not fire. The subthreshold increase in fluorescence may represent the Ca^{2+} influx associated with a postsynaptic response without spiking. These fast escapes were denoted as non-M-escapes. There was a close correlation between firing of the ipsilateral M-cell and the onset latency of the fast escape (Fig.1-5B). It is clearly seen that M-escapes displayed shorter latencies than non-M-escapes (average onset latency: 3.7 ± 0.1 and 8.4 ± 0.3 ms, respectively, $p < 10^{-4}$, Mann-Whitney U-test, see also Fig. 1-5C1). In particular, escapes with latencies shorter than 6 ms were always accompanied with M-cell firing.

Once the fast escape started, however, the trajectories of the initial tail flexion during M- and non-M-escapes were indistinguishable from each other (Fig. 1-5A). The tail flexion angles (28.5 ± 1.4 and 29.2 ± 1.6 degrees, during the initial 8 ms, data from 12 fish which exhibited both M- and non-M-escapes, respectively) and maximum angular velocities (4.2 ± 0.2 and 4.3 ± 0.3 deg/ms, respectively) of the initial bending were the same as shown in Fig. 1-5C (p > 0.1, paired t-test). No significant correlations were observed between the onset latency and these kinematic parameters (R=0.08 and 0.02, respectively, p > 0.7, see also Fig. 1-2C3) although the later phase of tail movement could not be measured because the tail movement was restricted by the head-embedding agar. Nor were any significant correlations observed between latency and kinematic parameters of tail movement in the unrestrained larvae (flexion angle during

the initial 8 ms, maximum angular velocity, maximal angle and duration of the initial bending, R= -0.10, -0.05, -0.10 and 0.04, respectively, $p > 0.6$). Thus, non-M-escapes showed fast escape movement similar to that of M-escapes, but with a delay in the onset.

To assess whether M-cell firing is required for the initiation of escape with short latency (3 to 6 ms), I examined the effects of M-cell ablation. After selective photoablation of retrogradely labeled M-cells (Fig. 1-6A, see also Liu and Fetcho, 1999), fast escapes never started within 6 ms (Fig. 1-6B and C2, onset latency: 8.7 ± 0.3 ms, n = 39, 5 fish). By contrast, there were no apparent differences in the trajectories or velocities of tail movement between intact and ablated animals (tail flexion angle during the initial 8 ms: 26.8 ± 3.1 degrees, maximum angular velocity: 4.0 ± 0.4 deg/ms, $p > 0.4$). Hence, the M-cell is indispensable for initiation of the fast escape with a short delay.

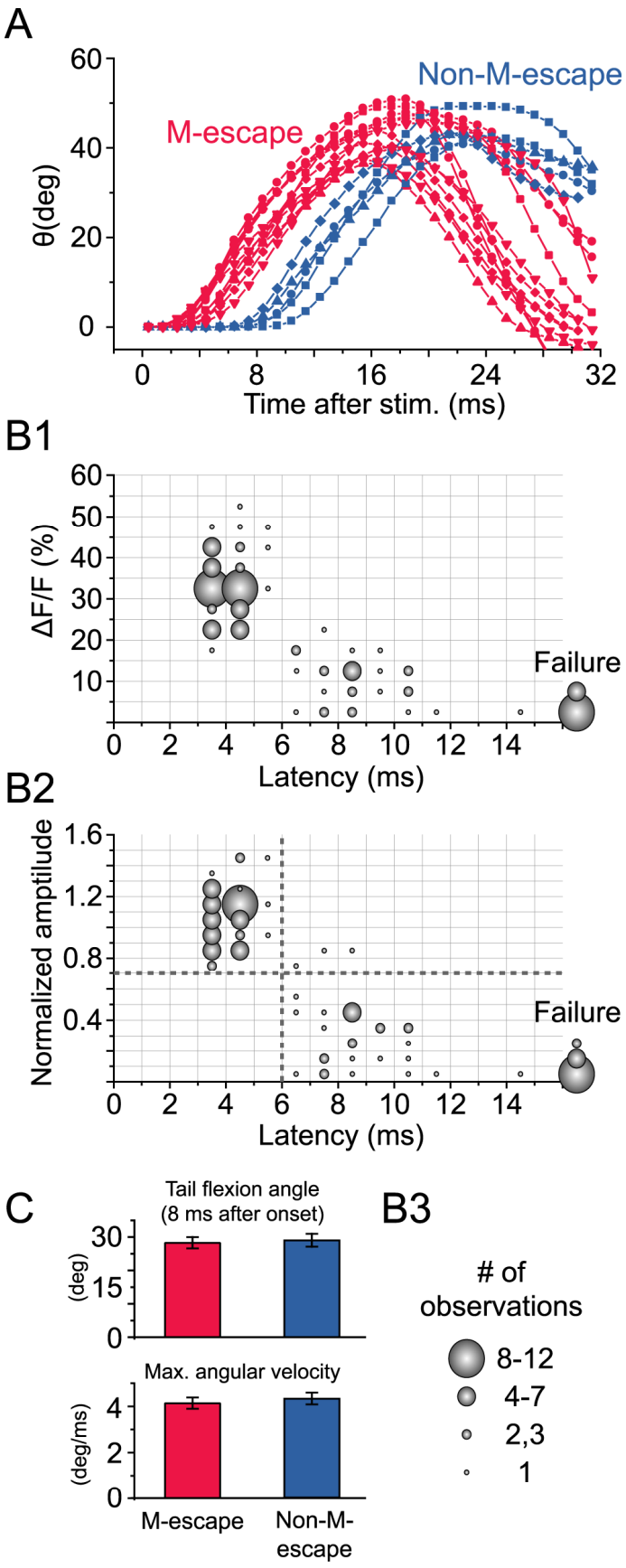

Figure 1-5. Single spiking of the M-cell tightly correlated with fast escape with short latency. **A**, Representative trajectories of tail flexion elicited by a water pulse applied to the OV. The tail flexion angle (ordinate; measured as in Fig. 1-1C2) is plotted against the time after water pulse arrival (abscissa). Exemplified tail flips (n = 19) obtained from 5 fish (denoted by different symbols for each fish) are superimposed. Red and blue represent tail flips associated with (M-escapes) and without M-cell firing (non-M-escapes), respectively (see below). **B**, The relationship between escape onset latency (abscissa) in response to the OV stimulation and accompanying fluorescence response amplitude of the ipsilateral M-cell (ordinate) is illustrated in bubble charts (n = 91, 17 fish), with the size of the bubbles representing the number of observations in each bin (**B3**). The fractional increase in fluorescence intensity (ΔF/F; **B1**, bin size: 5% and 1 ms) and the value normalized by the AD spike amplitude (xAD; **B2**, bin size: 0.1 xAD and 1 ms) are displayed. The majority of fast escapes started with short latency (3-5 ms) and were accompanied with a large apparent increase in fluorescence in the M-cell, which was comparable to that of an AD action potential, indicating that a single spiking of the M-cell was associated with the initiation of fast escape with short latency (> 0.7 xAD; denoted M-escapes, see Results). In particular, fast escapes starting within 6 ms after stimulus onset were always associated with an M-cell spike. In contrast, fast escapes without an M-cell spike, indicated by fluorescence responses smaller than the AD action potential (< 0.7 xAD; denoted non-M-escapes), started with latency longer than 6 ms. In addition,when escape failed to occur (failure), the M-cell never fired. The vertical and horizontal gray dotted lines in **B2** indicate 6 ms and 0.7 xAD, respectively. **C**, There was no significant difference in initial angle (during the initial 8 ms; top) and maximal angular velocity (bottom) of the tail flexion between the M-escapes and the non-M-escapes.

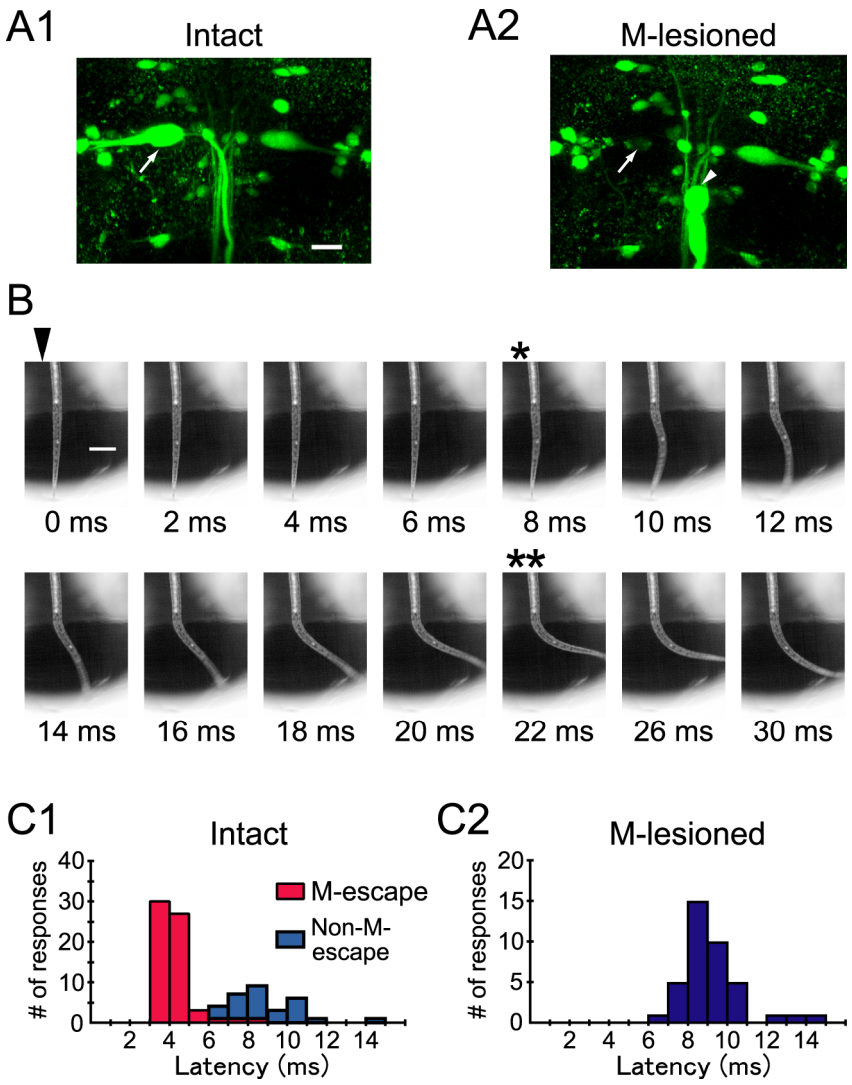

Figure 1-6. M-cells are necessary for initiating fast escape with short latency. **A**, Fluorescence images of reticulospinal neurons before (**A1**) and a day after (**A2**; M-lesioned) laser irradiation aimed at the left M-cell soma (arrows). The loss of fluorescence from soma and the stumped axon of the irradiated M-cell (arrowhead) without effect on nearby neurons show that the M-cell was successfully and selectively killed. Scale bar: 20 μm. **B**, A water pulse applied to the OV on the M-lesioned side still elicited a tail flip response to the contralateral side but the onset was delayed (8 ms, asterisk). Scale bar: 0.5 mm. **C**, Frequency distribution of onset latencies of fast escapes elicited by the OV stimulation in intact (**C1**) or M-lesioned (**C2**) fish. **C1**, Fast escapes of intact fish replotted from the data shown in Fig. 1-4B are classified into M-escapes (red) and non-M-escapes (blue) by M-cell activity simultaneously monitored. **C2**, After ablation of the M-cell, fast escape showed only delayed onset longer than 6 ms.

Discussion

In this chapter, I examined the correlation between the M-cell firing and escape behavior by *in vivo* Ca^{2+} imaging of the M-cell directly during fast escape in partially restrained larval zebrafish. The results showed that single spiking of one of the paired M-cells initiates a fast escape (M-escape) to the contralateral side with short latency, as demonstrated by field potential recordings of M-cell spike during escape in goldfish (Zottoli, 1977; Eaton et al., 1981; Eaton et al., 1988; Weiss et al., 2006). Surprisingly, similar fast escape movement also occurred without M-cell firing (non-M-escape), but the onset was delayed. Thus, at least two types of fast escape pathways exist in intact fish and the M-cell initiates fast escape with short latency.

Single spiking of the M-cell during escape

The suprathreshold fluorescence response of the M-cell (> 0.7 xAD) elicited by the water pulse stimulus represents generation of an orthodromic action potential, because its amplitude was similar to that associated with a single AD spike and was distinguishable from the subthreshold Ca^{2+} response (Figs. 1-3, 4 and 5). Simultaneous Ca^{2+} imaging and whole-cell recording in rodent cortical pyramidal neurons (Smetters et al., 1999; Berger et al., 2007) or lamprey spinal neurons (Viana di Prisco and Alford, 2004) have demonstrated that the somatic Ca^{2+} increase associated with an action potential is much larger than that with subthreshold synaptic or non-synaptic depolarization, which is thought to come through NMDA receptors or voltage-gated Ca^{2+} channels.

The M-cell shows a typical single spiking at the onset of depolarization (Nakayama and Oda, 2004). The mechanisms underlying the single-spiking property of the M-cell were suggested previously: 1) the M-cell is prevented from firing repetitively by a powerful recurrent feedback inhibitory circuit (Furukawa and Furshpan, 1963; Faber and Korn, 1978), and expression of low-threshold potassium channels as shown in goldfish (Nakayama and Oda, 2004), 2) repetitive firing was observed in goldfish only when the recurrent inhibitory circuit or the low-threshold potassium channel was blocked pharmacologically (Furukawa et al., 1964; Nakayama and Oda, 2004), and 3) the recurrent inhibitory circuit was also demonstrated in larval

zebrafish (Takahashi et al., 2002).

The M-cell initiates fast escape with short latency

From the tight correlation between M-cell firing and initiation of the fast escape (Fig. 1-5) together with the effect of M-cell lesioning on the escape onset latency (Fig. 1-6), I conclude that M-cell firing is necessary to initiate fast escape with short latency (< 6 ms) as shown in goldfish (Eaton et al., 1982; DiDomenico et al., 1988; Zottoli et al., 1999). A previous study using unrestrained larval zebrafish showed delay in the onset of escape elicited by a head-directed water pulse after lesioning of the M-cell (2.7 or 3.9 ms in prelesion and 4.6 ms in postlesion experiments), although it was not statistically significant unlike in the present study (Liu and Fetcho, 1999). The lack of significance is probably because whether the water stimulus hit the otic vesicle or head skin is critical for initiation of M- or non-M-escape, as shown in Chapter 3, or because the distance between the stimulus apparatus and the fish varied among trials and the water pulse often pushed the freely swimming larva, making it difficult to determine the escape onset latency.

Here, fast tail flexion without M-cell firing (Figs. 1-4, 5) has provided the first direct evidence for non-M-escape in intact fish, which was originally indicated by the body twitch response in fully-restrained larval zebrafish observed with extracellular recording of M-cell activity (Eaton et al., 1977; Eaton et al., 1984). The shorter latency of the M-escape is explained by output properties of the M-cell (see summarized figure 1-7). First, conduction velocity of the thick M-axon is the highest in hindbrain descending neurons (Furshpan and Furukawa, 1962; Eaton and Farley, 1975; Hatta and Korn, 1998). I calculated the spike conduction times from somata to the end of the spinal cord as 1.1 ms and 2.2 ms for the M-cell and non-M-cells, respectively, with reference to the conduction velocities [3.0 m/s and 1.5 m/s, respectively, from Eaton and Farley (1975)] and the total length (3.3 mm) of their axons. Second and probably more importantly, single spiking of the M-cell is sufficient to evoke a trunk muscle twitch (Nissanov et al., 1990), whereas bursting of non-M-cells may be necessary to evoke the muscle twitch (see Chapter 2). The different efficacy of the two systems may result from connectivity of the RS neurons onto the spinal motoneurons, especially primary motoneurons. The single action potential of M-axon activates primary motoneu-

rons monosynaptically and polysynaptically via spinal descending interneurons (Fetcho and Faber, 1988; Fetcho, 1992). In zebrafish, the descending interneurons are named as circumferential descending interneurons (CiDs) (Bernhardt et al., 1990; Hale et al., 2001). The M-axon has short unbranched axon collaterals to make effective direct contacts with primary motoneurons and with the descending interneurons at their initial segment of axons (Fetcho, 1991). The direct connection onto the primary motoneuron has not been found in other descending neurons. Rather, descending axons of the non-M-RS neurons such as morphological homologs of the M-cell exhibit rich terminal branching in the spinal cord (Gahtan and O'Malley, 2003)(see also Chapter 2), suggesting that they connect to the dendrites of motoneurons or only to interneurons. Such inefficient synaptic connections may require multiple action potentials of non-M-cells to fire the motoneurons and thus may cause the delay in the escape onset. The third possible reason for the shorter onset latency of M-escape is that shorter latency from the sensory inputs to the spiking of the M-cell and other RS neurons. This issue remains to be examined.

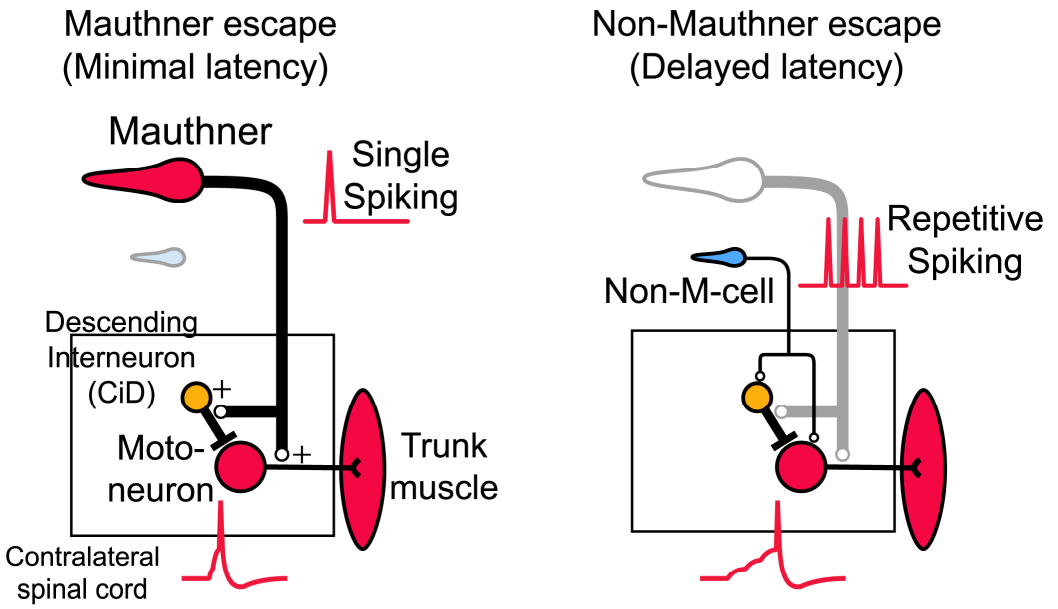

Figure. 1-7. Spinal circuit models for M- and non-M-escapes. **Left,** When the M-cell fired, an M-cell action potential travels faster than any other descending fibers. In the spinal cord, the M-axon excites motoneurons monosynaptically and polysynaptically via descending interneurons named CiD. The M-axon makes effective synaptic contact onto the initial segment of its postsynaptic neurons. Hence, the single spiking of the M-cell is enough to fire the motoneurons and initiates fast escape with minimal latency. **Right,** non-M-cell is suggested to excite motoneurons and CiDs, too. However, the non-M-axon is implied to make ineffective synapses onto soma-dendritic region of its postsynaptic neurons. Thus, non-M-cell probably need to fire repetitively to accumulate excitatory postsynaptic potential in the motoneurons to the firing threshold. Red lines indicate membrane potential change (up, positive, time flows left to right) in hindbrain neurons (upper lines) and motoneurons (bottom lines). Sharp spikes indicate action potentials. See discussion for detail.

References for chapter 1

Berger T, Borgdorff A, Crochet S, Neubauer FB, Lefort S, Fauvet B, Ferezou I, Carleton A, Luscher HR, Petersen CC (2007) Combined voltage and calcium epifluorescence imaging in vitro and in vivo reveals subthreshold and suprathreshold dynamics of mouse barrel cortex. J Neurophysiol 97:3751-3762.

Bernhardt RR, Chitnis AB, Lindamer L, Kuwada JY (1990) Identification of spinal neurons in the embryonic and larval zebrafish. J Comp Neurol 302:603-616.

Budick SA, O'Malley DM (2000) Locomotor repertoire of the larval zebrafish: swimming, turning and prey capture. J Exp Biol 203:2565-2579.

Bullock TH (1990) Goals of neuroethology. Bioscience 40:244-249.

Burgess HA, Granato M (2007) Sensorimotor gating in larval zebrafish. J Neurosci 27:4984-4994.

DiDomenico R, Nissanov J, Eaton RC (1988) Lateralization and adaptation of a continuously variable behavior following lesions of a reticulospinal command neuron. Brain Res 473:15-28.

Domenici P, Blake R (1997) The kinematics and performance of fish fast-start swimming. J Exp Biol 200:1165-1178.

Eaton RC (1984) Neural Mechanisms of Startle Behavior. New York: Plenum Press.

Eaton RC, Farley RD (1975) Mauthner neuron field potential in newly hatched larvae of the zebra fish. J Neurophysiol 38:502-512.

Eaton RC, Lavender WA, Wieland CM (1981) Identification of Mauthner-initiated response patterns in goldfish: Evidence from simultaneous cinematography and electrophysiology. J Comp Physiol [A] 144:521-531.

Eaton RC, Lavender WA, Wieland CM (1982) Alternative neural pathways initiate fast-start responses following lesions of the Mauthner neuron in goldfish. J Comp Physiol [A] 145:485-496.

Eaton RC, Nissanov J, Wieland CM (1984) Differential activation of Mauthner and non-Mauthner startle circuits in the zebrafish: Implications for functional substitution. J Comp Physiol [A] 155:813-820.

Eaton RC, DiDomenico R, Nissanov J (1988) Flexible body dynamics of the goldfish C-start: implications for reticulospinal command mechanisms. J Neurosci 8:2758-2768.

Eaton RC, Farley RD, Kimmel CB, Schabtach E (1977) Functional development in the Mauthner cell system of embryos and larvae of the zebra fish. J Neurobiol 8:151-172.

Edwards DH, Heitler WJ, Krasne FB (1999) Fifty years of a command neuron: the neurobiology of escape behavior in the crayfish. Trends Neurosci 22:153-161.

Faber DS, Korn H (1978) Neurobiology of the Mauthner Cell. New York: Raven Press.

Fetcho JR (1991) Spinal network of the Mauthner cell. Brain Behav Evol 37:298-316.

Fetcho JR (1992) Excitation of motoneurons by the Mauthner axon in goldfish: complexities in a "simple" reticulospinal pathway. J Neurophysiol 67:1574-1586.

Fetcho JR, Faber DS (1988) Identification of motoneurons and interneurons in the spinal network for escapes initiated by the Mauthner cell in goldfish. J Neurosci 8:4192-4213.

Fetcho JR, Cox KJ, O'Malley DM (1997) Imaging neural activity with single cell resolution in an intact, behaving vertebrate. Biol Bull 192:150-153.

Fetcho JR, Cox KJ, O'Malley DM (1998) Monitoring activity in neuronal populations with single-cell resolution

in a behaving vertebrate. Histochem J 30:153-167.

Furshpan EJ, Furukawa T (1962) Intracellular and extracellular responses of the several regions of the Mauthner cell of the goldfish. J Neurophysiol 25:732-771.

Furukawa T, Furshpan EJ (1963) Two inhibitory mechanisms in the Mauthner neurons of goldfish. J Neurophysiol 26:140-176.

Furukawa T, Fukami Y, Asada Y (1964) Effects of strychnine and procaine on collateral inhibition of the Mauthner cell of goldfish. Jap J Physiol 14:386-399.

Gahtan E, O'Malley DM (2003) Visually guided injection of identified reticulospinal neurons in zebrafish: a survey of spinal arborization patterns. J Comp Neurol 459:186-200.

Gahtan E, Sankrithi N, Campos JB, O'Malley DM (2002) Evidence for a widespread brain stem escape network in larval zebrafish. J Neurophysiol 87:608-614.

Hackett JT, Faber DS (1983) Mauthner axon networks mediating supraspinal components of the startle response in the goldfish. Neuroscience 8:317-331.

Hackett JT, Greenfield LJ (1986) The behavioral role of the Mauthner neuron impulse. Behav Brain Sci 9:729-730.

Hale ME, Ritter DA, Fetcho JR (2001) A confocal study of spinal interneurons in living larval zebrafish. J Comp Neurol 437:1-16.

Hatta K, Korn H (1998) Physiological properties of the Mauthner system in the adult zebrafish. J Comp Neurol 395:493-509.

Kimmel CB, Patterson J, Kimmel RO (1974) The development and behavioral characteristics of the startle response in the zebra fish. Dev Psychobiol 7:47-60.

Kimmel CB, Eaton RC, Powell SL (1980) Decreased fast-start performance of zebrafish larvae lacking Mauthner neurons. J Comp Physiol [A] 140:343-350.

Korn H, Faber DS (1996) Escape behavior - brainstem and spinal cord circuitry and function. Curr Opin Neurobiol 6:826-832.

Liu KS, Fetcho JR (1999) Laser ablations reveal functional relationships of segmental hindbrain neurons in zebrafish. Neuron 23:325-335.

Metcalfe WK, Mendelson B, Kimmel CB (1986) Segmental homologies among reticulospinal neurons in the hindbrain of the zebrafish larva. J Comp Neurol 251:147-159.

Nakayama H, Oda Y (2004) Common sensory inputs and differential excitability of segmentally homologous reticulospinal neurons in the hindbrain. J Neurosci 24:3199-3209.

Nissanov J, Eaton RC, DiDomenico R (1990) The motor output of the Mauthner cell, a reticulospinal command neuron. Brain Res 517:88-98.

O'Malley DM, Kao YH, Fetcho JR (1996) Imaging the functional organization of zebrafish hindbrain segments during escape behaviors. Neuron 17:1145-1155.

Ritter DA, Bhatt DH, Fetcho JR (2001) In vivo imaging of zebrafish reveals differences in the spinal networks for escape and swimming movements. J Neurosci 21:8956-8965.

Smetters D, Majewska A, Yuste R (1999) Detecting action potentials in neuronal populations with calcium imaging. Methods 18:215-221.

Takahashi M, Narushima M, Oda Y (2002) In vivo imaging of functional inhibitory networks on the Mauthner cell of larval zebrafish. J Neurosci 22:3929-3938.

Viana di Prisco G, Alford S (2004) Quantitative investigation of calcium signals for locomotor pattern generation in the lamprey spinal cord. J Neurophysiol 92:1796-1806.

Weiss SA, Zottoli SJ, Do SC, Faber DS, Preuss T (2006) Correlation of C-start behaviors with neural activity recorded from the hindbrain in free-swimming goldfish (Carassius auratus). J Exp Biol 209:4788-4801.

Yasargil GM, Diamond J (1968) Startle-response in teleost fish: an elementary circuit for neural discrimination. Nature 220:241-243.

Yeomans JS, Frankland PW (1996) The acoustic startle reflex: neurons and connections. Brain Res Rev 21:301-314.

Zottoli SJ (1977) Correlation of the startle reflex and Mauthner cell auditory responses in unrestrained goldfish. J Exp Biol 66:243-254.

Zottoli SJ, Newman BC, Rieff HI, Winters DC (1999) Decrease in occurrence of fast startle responses after selective Mauthner cell ablation in goldfish (Carassius auratus). J Comp Physiol [A] 184:207-218.

Chapter 2

Complementary activation of segmentally homologous hindbrain neurons during escape behavior of larval zebrafish

Summary

In vivo Ca^{2+} imaging of morphologically homologous reticulospinal (RS) neurons of the Mauthner (M-) cell was performed during fast escape to examine cellular basis of functional relationship between M- and non-M-escapes. One of the M-cell homologs, MiD3cm, showed significant Ca^{2+} increase during fast escape elicited by water pulse stimulation applied to the ipsilateral otic vesicle (OV) of larval zebrafish rostrally embedded in agar. Opposite to the case of the M-cell (Chapter 1), interestingly, the amplitude of the Ca^{2+} response was smaller during short-latency escape (< 6 ms) than during longer-latency (> 6 ms) escape. Antidromic stimulation of each MiD3cm suggested that the former reflected one or two action potentials whereas the latter repetitive firing. The inverse relationship between activities of the M-cell and MiD3cm was directly confirmed by simultaneous high-speed confocal imaging of the two cells: MiD3cm activity was low during M-escape but high during non-M-escape. Larger Ca^{2+} response in MiD3cm was correlated with larger initial bending especially during M-escape, suggesting that more action potentials in MiD3cm is associated with large bending of the tail during initial phase of fast escape. Thus, the M-cell and MiD3cm are suggested to act cooperatively to control escape trajectory, but to behave complementary as far as in the initiation of fast escape.

Introduction

The segmental arrangement of hindbrain reticulospinal (RS) neurons along neuraxis was first described in larval zebrafish (Kimmel et al., 1982)(see General introduction). The observation that the RS neurons with similar morphological features are appeared repeatedly in the successive hindbrain segments raised the concept of segmental homologs (Metcalfe et al., 1986). This concept also yielded a hypothesis that the segmental homologs have similar behavioral functions (Kimmel et al., 1982; Lee and Eaton, 1991; Foreman and Eaton, 1993; Lee et al., 1993).

Because the Mauthner (M-) cell plays a distinctive role in the initiation of fast escape (see Chapter 1), the relationship between the activities of the two segmental homologs of the M-cell (MiD2cm and MiD3cm in the hindbrain segment 5 and 6, respectively)(Metcalfe et al., 1986) and fast escape is thought to provide an unique opportunity to evaluate this hypothesis. Ca^{2+} imaging of the M-cell and its homologs, which are collectively called M-series (Lee and Eaton, 1991), suggested that they are involved in the control of fast escape, especially when the ipsilateral head was tapped, whereas only the M-cell in the M-series was activated by tail stimulus (O'Malley et al., 1996). Furthermore, it is reported that ablation of the series of homologs abolished fast escape (Liu and Fetcho, 1999). However, activities of the M-cell homologs have not been observed directly during escape yet.

Here, I performed *in vivo* confocal Ca^{2+} imaging of activities of MiD2cm or MiD3cm during fast escape in larval zebrafish. In addition, to assess their direct correlation with M-cell activity, I designed a novel high-speed confocal scanning microscope equipped with a high-speed focusing device which enabled us to monitor multiple neurons in different optical planes within the same trial. The results suggest that the M-cell's homologs, especially MiD3cm, act in a complementary manner to the M-cell in initiation of the fast escape.

Materials and methods

Calcium imaging of activities of M-cell homologs during escape. All procedures except for the quantification of Ca^{2+} response of M-cell homologs and high-speed Ca^{2+} imaging of multiple neurons were carried out as described in Chapter 1. For quantification of fluorescence responses of MiD2cm or MiD3cm, the fluorescence intensities obtained from the second to fifth frame after stimulation were averaged to improve the signal-to-noise ratio, because the responses of the two cells were smaller than that of the M-cell.

High-speed three-dimensional calcium imaging of multiple neurons. To monitor activities of the M-cell and its homologs in different confocal planes simultaneously, I developed a novel upright optics equipped with a high-speed, Nipkow disk confocal scanner (CSU-10; Yokogawa, Tokyo, Japan; emission filter, 510-550 nm) and a high-sensitivity digital camera (EM-CCD Camera C9100-12; Hamamatsu Photonics, Hamamatsu City, Japan). A piezoelectric high-speed focusing device (PIFOC P-721LLQ, operated with an E-662 amplifier and servo-controller; Physik Instrumente, Karlsruhe, Germany) was mounted on the objective lens to switch the focal plane in synchronization with the collection of fluorescence images. Typically, I imaged (512 × 512 pixels) two focal planes alternately at 130 ms intervals (Fig. 2-3A). I used MetaMorph 6.1 software (Molecular Devises Corporation, Downingtown, PA) to synchronize the CSU-10 shutter, camera shutter and focus switching.

Results

Ca^{2+} response of MiD3cm associated with an AD action potential

As in the case of the M-cell, a single electrical shock of the spinal cord evoked a transient fluorescent response, associated with an AD action potential, in MiD3cm in an all-or-nothing manner but with a much smaller amplitude than the M-cell (Fig. 2-1A, B; $\Delta F/F = 2.2 \pm 0.2\%$, 8 cells, see Materials and Methods for details). When pulse trains were applied, a stepwise increase in the amplitude of the fluorescence response was observed against the number of stimulus pulses (Fig. 2-1C; delivered at the suprathreshold strength at 50 ms intervals, 4 cells), suggesting summation of Ca^{2+} responses evoked by each stimulus pulse.

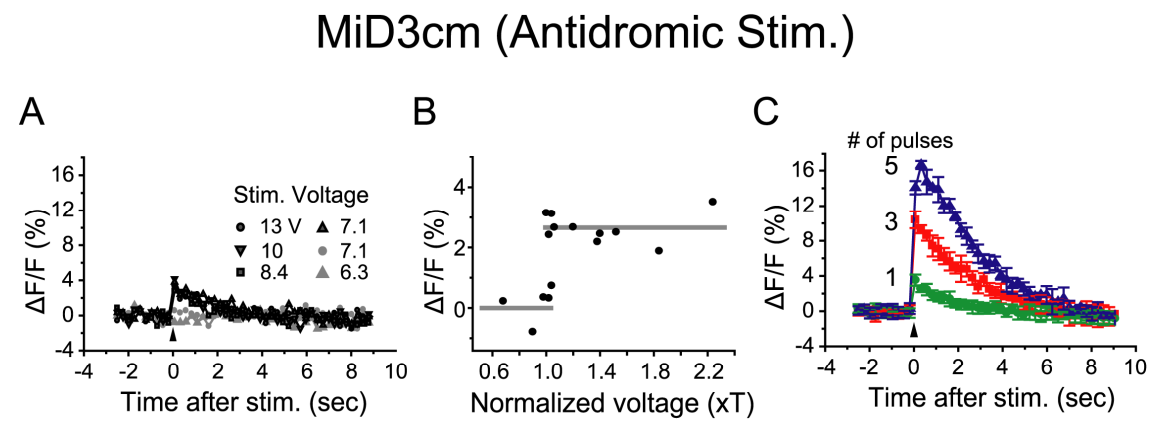

Figure 2-1. Fluorescence responses of a MiD3cm associated with antidromic action potential. **A**, Electrical stimulation of the spinal cord induced fluorescence response in the MiD3cm in an all-or-nothing manner with changes in stimulus voltage, indicating that single antidromic action potential was elicited as in the M-cell (Takahashi et al., 2002). Note that the amplitude of the MiD3cm response was apparently smaller than that of the M-cell (Fig. 1-2C). **B**, Amplitudes of fluorescence responses are plotted against stimulus voltage (normalized to the threshold voltage, T) as in Fig. 1-2C2. The left and right gray lines indicate 0% and 2.6%, respectively. **C**, As the number of stimulus pulses was increased at an intensity of 1.1 T with an interstimulus interval of 50 ms, the response amplitude increased stepwise, indicating multiple firing of the MiD3cm. Average amplitudes (mean ± SD, n = 4-7 for each trace) of the fluorescence transients elicited by 1, 3 and 5 pulses are plotted respectively.

Complementary activation of the M-cell and MiD3cm during fast escape

Significant fluorescence responses in the ipsilateral MiD3cm were elicited by either OV on one side (11 fish). Interestingly, the amplitude was significantly smaller when the tail flip started within 6 ms than when it started with a longer delay (Fig. 2-2A; $\Delta F/F = 2.7 \pm 0.4\%$ and $8.2 \pm 0.5\%$, n = 45 and 17, respectively, $p < 10^{-8}$). As shown in Fig. 2-2B, the latter response was a few times larger than that evoked by a single AD stimulus (3.6 ± 0.4 xAD, n = 9, respectively), suggesting that multiple firing of MiD3cm occurred during the delayed fast escape. In contrast, the former responses were as small as an AD spike on average (1.3 ± 0.2 xAD, n = 20). Thus, the relationship between MiD3cm activity and the behavioral onset latency seems inverse to that of the M-cell (see Chapter 1).

This relationship was directly examined by simultaneous Ca^{2+} imaging of the M-cell and MiD3cm during fast escape using a high-speed confocal microscope equipped with a high-speed focus control on the objective lens to alternately monitor the two cells located at different depths (Fig. 2-3A, see Materials and

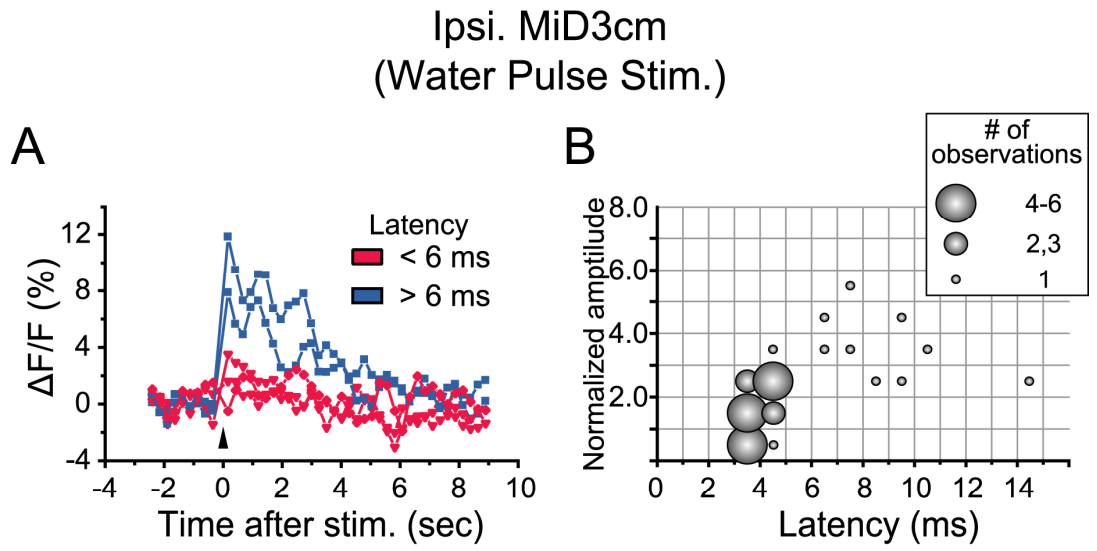

Figure 2-2. Fluorescence responses of MiD3cm associated with fast escape. **A,** Fluorescence responses in a MiD3cm, the same cell shown in Fig. 2-1, elicited by the water pulse applied to the ipsilateral OV. Five responses associated with fast escape are superimposed, demonstrating that the response amplitudes were smaller when the escapes started with shorter (< 6 ms, red) latencies than when the escape started with longer (> 6 ms, blue) latencies. **B**, Normalized amplitude of fluorescence response in MiD3cm during fast escape. Data are represented in a bubble chart as shown in Fig. 1-4. In contrast to the M-cell (see Chapter 1), the responses in MiD3cm evoked by OV were several times larger than those evoked by single AD stimulation, especially when the escape started more than 6 ms after stimulus arrival.

Methods for detail). Fig. 2-3B and C show the complementary pattern of activation in the M-cell and MiD3cm during the fast escape (4 pairs) when a water pulse was applied to the ipsilateral OV. MiD3cm exhibited only a small response when the M-cell fired (M-escape) but a large response when the M-cell did not fire (non-M-escape). Fig. 2-3D summarizes the relationships between escape onset latency and the amplitude of the fluorescence response of the M-cell and MiD3cm, demonstrating that the suprathreshold fluorescence response in the M-cell (33.1 ± 0.9%, n = 60) and the small response in MiD3cm (see above) were observed with short-latency (< 6 ms) escape, whereas the subthreshold response in the M-cell (8.9 ± 1.1%, n = 31) and the large response in MiD3cm (see above) were observed with the delayed fast escape (> 6 ms). These results above strongly suggest that greater activation of MiD3cm is involved in the non-M-escape evoked by tactile stimulus. Furthermore, MiD3cm did not show apparent fluorescence changes ($\Delta F/F$ < 1.3%, 0.6 ± 0.4%, n = 5) and none appeared to fire (< 0.4 xAD, 0.28 ± 0.11 xAD, n = 3) in response to a water pulse with subthreshold intensity for tail response.

MiD2cm shows similar tendency with MiD3cm during fast escape

The ipsilateral MiD2cm of intact fish (8 fish) showed a tendency similar to MiD3cm: smaller Ca^{2+} response during M-escape ($\Delta F/F$ = 1.1 ± 0.3%, n = 24) and larger response during non-M-escape ($\Delta F/F$ = 2.0 ± 1.2%, n = 8). Despite the fact that the amplitude of a single AD response was very small ($\Delta F/F$ = 1.4 ± 0.3%, 5 cells), MiD2cm apparently fired fewer action potentials in M-escape (0.8 ± 1.3 xAD, n = 3) than in non-M-escape (1.8 ± 0.7 xAD, n = 4). However, both the raw and normalized amplitudes of fluorescence response were too small to compare statistically ($p > 0.2$, Welch's t-test). Overall, the M-cell and its homologs are suggested to act cooperatively as a functional group, as reported previously (O'Malley et al., 1996); however, the homologs appeared to behave in a manner complementary to M-cell firing during fast escape.

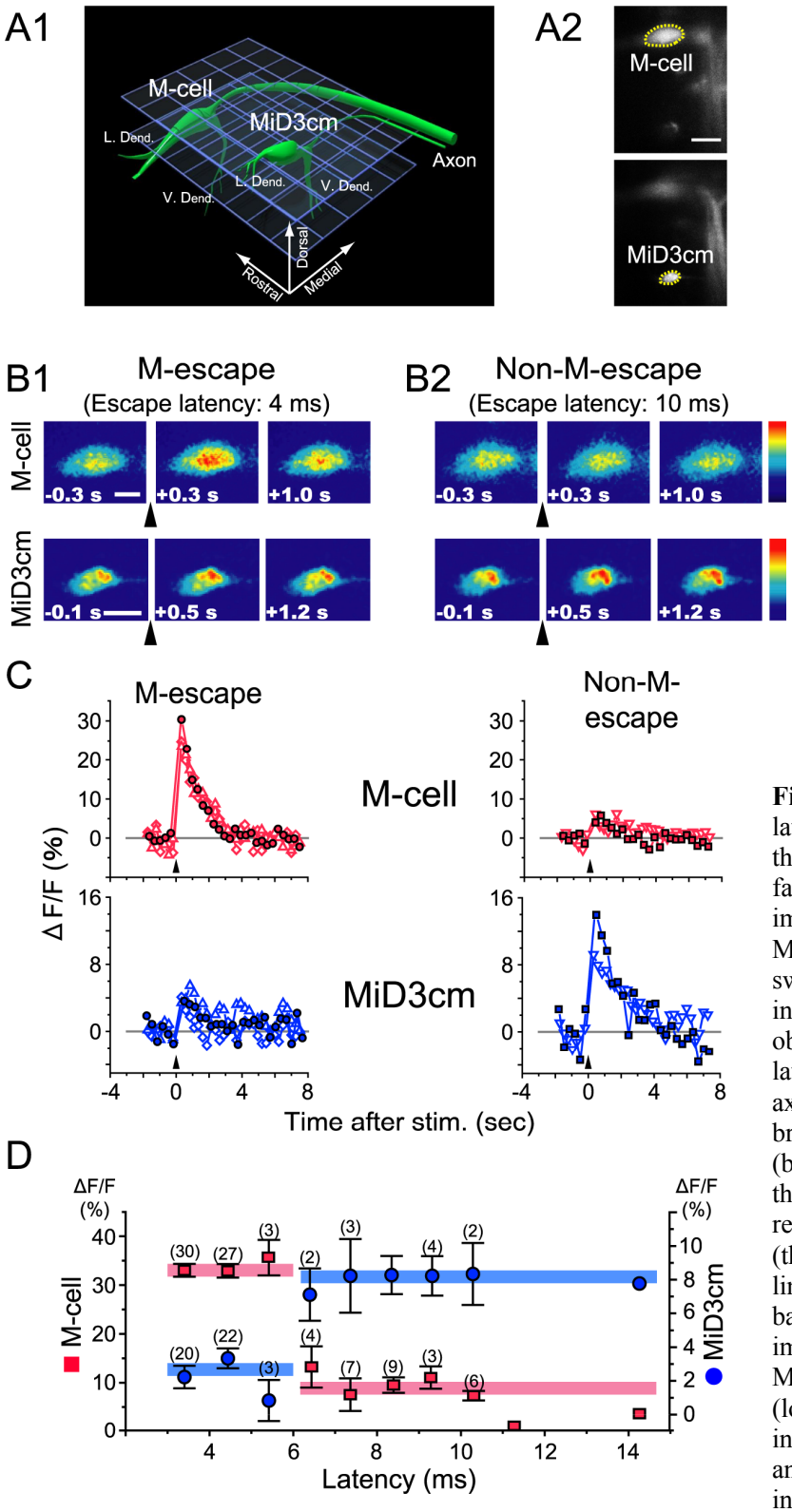

Figure 2-3. Complementary relationship between activities of the M-cell and MiD3cm during fast escape. **A1**, Alternative Ca^{2+} imaging of the M-cell and MID3cm was performed by switching two focal planes (gratings) at 7 Hz with a piezo-driven objective lens. Ventral (V.) and lateral (L.) dendrites (Dend.) and axons are indicated. **A2**, The brightest plane of MiD3cm soma (bottom) was 16 μm dorsal to that of M-cell soma (top). Fluorescence intensities of the somata (the area in the yellow dashed lines) are quantified in **C**. Scale bar: 20 μm. **B**, Pseudocolored images of the somata of the M-cell (upper) and MiD3cm (lower), the same pair as shown in **A2**, before (-0.3 and -0.1 s) and after (+0.3 to +1.2 s) applying the water pulse stimulus to the OV (arrowheads).

B1, When escape occurred with short (4 ms) latency, the M-cell showed a large fluorescence increase (M-escape), whereas MiD3cm showed only a small response. **B2**, In contrast, when escape started with longer (10 ms) latency, the M-cell did not show apparent response (non- M-escape), while the MiD3cm showed a significantly larger increase in fluorescence than in **B1**. Color scales and scale bars (10 μm) apply to both **B1** and **B2**. →

←

C, Quantification of the change in fluorescence intensity of two pairs (filled and open symbols for each pair) of M-cell (upper traces) and MiD3cm (lower traces) during three M-escapes (left column) and two non-M-escapes (right column). Responses obtained in the same trial are shown by the same symbol. The trials shown in **B1** and **B2** are indicated by circles and squares, respectively. The response amplitude of MiD3cm was complementary to that of the M-cell. The gray lines indicate 0%.**D**, Relationships between onset latency of escape and amplitude of fluorescence response elicited in the M-cell (red squares) and MiD3cm (blue circles). Escapes with short latency (< 6 ms) were accompanied with M-cell firing (see Results) and a small response in MiD3cm, whereas in the case of escape with delayed (> 6 ms) latency, the M-cell did not fire and MiD3cm showed a larger response. The number of trials is denoted above the error bar. Left and right calibrations apply to the M-cell and MiD3cm, respectively. Red and blue horizontal bars represent average response amplitudes of the M-cell and MiD3cm, respectively, for fast escape with short (< 6 ms, left bars) or delayed (> 6 ms, right bars) latency.

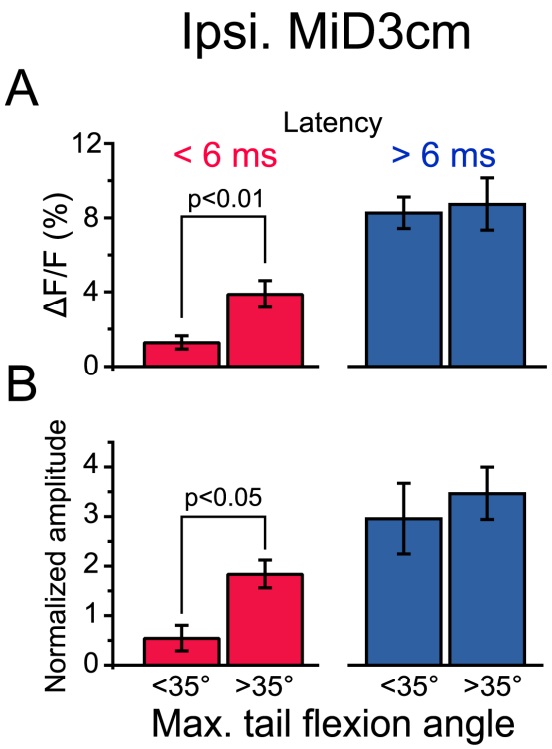

Figure 2-4. Larger activation of MiD3cm correlates with larger initial tail flexion angle during M-escape. Comparison of fluorescence response of the MiD3cm and amplitude of flexion angle of the tail flip during fast escape elicited by water pulse applied to the OV. The fractional increase in fluorescence intensity (**A**) and that normalized by the AD spike (**B**). In the tail flips with shorter onset latencies (< 6 ms) as in M-escapes, larger fluorescence responses were associated with larger tail flexions (Maximum angle: > 35 degrees). In the delayed tail flips with longer (> 6 ms) latencies as in non-M-escapes, however, there was no significant correlation between the two.

Activity of MiD3cm correlates with initial flexion angle during M-escape

Finally, I examined the possibility that MiD3cm is involved in directional control of escape, as hypothesized by Foreman and Eaton (1993). The escape trajectory was previously described with kinematic parameters on body bending during the initial turn and timing of the counter turn (Foreman and Eaton, 1993). In the present study, although the head of zebrafish was restrained in agar, the tail showed various flexion angles to some extent, which probably represent variety in activity of the trunk muscle. I compared tail flexion angle and fluorescence response of the MiD3cm (Fig. 2-4). In the M-escapes, larger fluorescence responses of the MiD3cm ($\Delta F/F = 3.9 \pm 0.7\%$, $n = 18$) were observed in association with large tail flexions (maximum flexion angle: >35 degrees) than in the case of small tail flexions (<35 degrees; $\Delta F/F = 1.3 \pm 0.4\%$, $n = 25$, $p<10^{-3}$, Welch's t-test). The difference was also significant when they were normalized by the amplitude of AD response (1.9 ± 0.3 xAD and 0.6 ± 0.3 xAD, $n = 17$ and 5, respectively, $p < 0.05$). These results indicate that more spikes in MiD3cm are associated with larger initial bending of the tail during M-escape. In fast escapes with delayed onset (>6 ms), which were virtually identical to the non-M-escapes, however, there was no significant difference between the responses of the MiD3cm associated with large (>35 degrees; $\Delta F/F = 8.3 \pm 0.8\%$ and 3.0 ± 0.7 xAD, $n = 9$ and 6, respectively) and small tail flexions (<35 degrees; $\Delta F/F = 8.8 \pm 1.4\%$ and 3.5 ± 0.5 xAD, $n = 8$ and 3, respectively; $p > 0.5$), probably because bursting of the MiD3cm at the initiation of non-M-escape masked the difference in fluorescence response associated with that in amplitude of the following tail flexion.

Discussion

In vivo Ca^{2+} imaging of the segmental homologs of the M-cell, especially MiD3cm, indicates that the homologs burst during non-M-escape. In addition, during M-escape, MiD3cm delivers more spikes in association with larger amplitude of the tail flexion than the smaller one, suggesting that the cell controls flexion amplitude of the initial bending.

MiD3cm shows different output property from the M-cell

Ca^{2+} response of MiD3cm evoked by the water pulse larger than that evoked by single AD stimulation (Fig. 2-2) suggests that the cell fires multiple action potentials during escape, in contrast to single spiking of the M-cell. This is consistent with the previous findings that the M-cell's homologs in goldfish burst at a frequency dependent on the depolarization amplitude, while the M-cell that the cell fires action potential only once at the beginning of large depolarization (Nakayama and Oda, 2004). In addition to the difference in firing property, the morphology of axonal terminals of the M-series are different from each other. The axon of MiD3cm exhibits extensive terminal arbors dorsally within the sagittal plane in the spinal cord, in contrast to the short protrusions of the M-axon (Gahtan and O'Malley, 2003). The different patterns of axonal arborization indicate that the axons of the M-cell and the homologs connect to the different population and/or regions of spinal neurons.

Firing of MiD3cm, as well as MiD2cm, during M- and non-M-escapes supports the notion that the homologs of the M-cell are involved in controlling fast escape (O'Malley et al., 1996; Liu and Fetcho, 1999), especially non-M-escape (Fig. 2-5, right). Thus, the M-cell and its homologs are suggested to be functionally related but to contribute to motor control with different output properties. Spinal neurons which are innervated by the MiD3cm are of particular interest but still remain unknown. As discussed in Chapter 1, the primary motoneurons and the CiD interneurons are the candidates.

Functional relationships between M- and non-M-escape

It appears that fluorescence response of MiD3cm, and probably MiD2cm, was suppressed during M-escape (Fig. 2-2 and 3), which may be explained by di- or polysynaptic inhibitory connection from the M-cell to the ipsilateral MiD3cm as observed in goldfish (Oda and Nakayama, 2003; Neki et al., 2007) (Fig. 2-5, left). Thus, the present results may demonstrate Mauthner-derived inhibition of non-M-escape as proposed previously (Eaton et al., 1984). Such hierarchical organization of the hindbrain RS neurons should prevent the fish from initiating non-M-escape soon after the onset of M-escape, which may result in over bending of the body to delay the forward propulsive movement of the body away from the threat.

In goldfish, spiking activity of MiD3cm is completely shut for about 10 ms after the onset of the synaptic inhibition from the M-cell (Oda and Nakayama, 2003; Neki et al., 2007), indicating that MiD3cm can fire action potentials only before or after the inhibition during M-escape. Thus, firing of MiD3cm after the inhibition (Fig. 2-5, left, pink line), which results in the additional Ca^{2+} increase, may contribute to producing the large initial tail flexion during M-escape (Fig. 2-4).

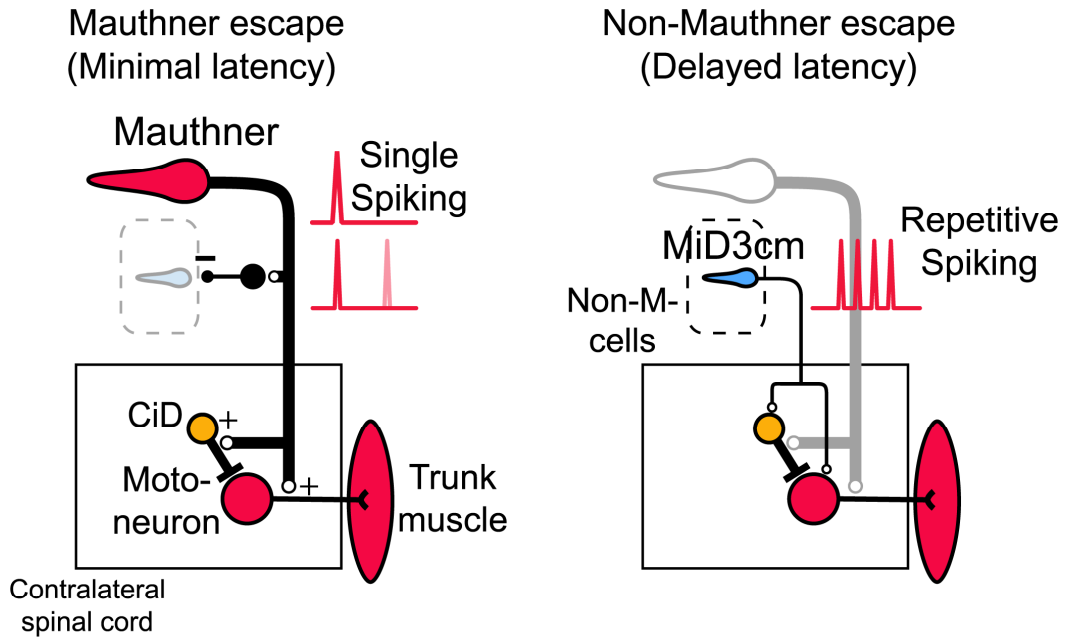

Figure 2-5. Functional relationship between the M-cell and MiD3cm. **Left**, Firing of the M-cell suppresses firing of MiD3cm via inhibitory interneuron (Oda and Nakayama, 2003; Neki et al., 2007) and may also other RS neurons that are involved in control of non-M-escape (non-M-cells, dotted lines). Firing of the MiD3cm after the suppression (pink line) may contribute to controling later phase of escape trajectory. **Right**, MiD3cm shows repetitive spiking during non-M-escape. The axon of the MiD3cm shows different spinal arborization pattern from the M-cell (Gahtan and O'Malley, 2003). It possibly connects to the primary motoneurons or CiDs via less effective synapses than the M-cell. Open and filled circles indicate excitatory and inhibitory synapses, respectively. See also Fig. 1-7.

References for chapter 2

Eaton RC, Nissanov J, Wieland CM (1984) Differential activation of Mauthner and non-Mauthner startle circuits in the zebrafish: Implications for functional substitution. J Comp Physiol [A] 155:813-820.

Foreman MB, Eaton RC (1993) The direction change concept for reticulospinal control of goldfish escape. J Neurosci 13:4101-4113.

Gahtan E, O'Malley DM (2003) Visually guided injection of identified reticulospinal neurons in zebrafish: a survey of spinal arborization patterns. J Comp Neurol 459:186-200.

Kimmel CB, Powell SL, Metcalfe WK (1982) Brain neurons which project to the spinal cord in young larvae of the zebrafish. J Comp Neurol 205:112-127.

Lee RK, Eaton RC (1991) Identifiable reticulospinal neurons of the adult zebrafish, Brachydanio rerio. J Comp Neurol 304:34-52.

Lee RK, Eaton RC, Zottoli SJ (1993) Segmental arrangement of reticulospinal neurons in the goldfish hindbrain. J Comp Neurol 329:539-556.

Liu KS, Fetcho JR (1999) Laser ablations reveal functional relationships of segmental hindbrain neurons in zebrafish. Neuron 23:325-335.

Metcalfe WK, Mendelson B, Kimmel CB (1986) Segmental homologies among reticulospinal neurons in the hindbrain of the zebrafish larva. J Comp Neurol 251:147-159.

Nakayama H, Oda Y (2004) Common sensory inputs and differential excitability of segmentally homologous reticulospinal neurons in the hindbrain. J Neurosci 24:3199-3209.

Neki D, Nakayama H, Fujii T, Oda Y (2007) Functional connection from Mauthner cell to homologous reticulospinal neurons in the goldfish hindbrain. Neurocsci Res 58:S92.

Oda Y, Nakayama H (2003) Common synaptic drive from Mauthner cell to segmentally homologous reticulospinal neurons in teleost hindbrain. In: 2003 Abstract Viewer/Itinerary Planner, p Program No. 78.79. Washington, DC: Society for Neuroscience Online.

O'Malley DM, Kao YH, Fetcho JR (1996) Imaging the functional organization of zebrafish hindbrain segments during escape behaviors. Neuron 17:1145-1155.

Chapter 3

Different modes of sensory input segregate onto different escape pathways in larval zebrafish hindbrain

Summary

Role of sensory inputs in initiation of M- and non-M-escape was examined to investigate how each of the two escape is elicited in larval zebrafish. The effects of sensory input deprivation were assessed by Ca^{2+} imaging of the M-cell during fast escape and by motion measurement of the tail movement. After elimination or lesion of the otic vesicle (OV), water pulse stimulation applied to the head still elicited fast escape. The tail movement, however, was delayed in the onset (latency > 6 ms) and never associated with M-cell firing. Thus it is suggested that auditory and/or vestibular (acousticovestibular) input from the OV is necessary to induce M-escape. The non-M-escapes were accompanied with large Ca^{2+} increase in the ipsilateral MiD3cm, indicating bursting with multiple action potentials. Stimulation of head skin exclusively elicited non-M-escape in intact fish. Thus, head-cutaneous input preferentially elicits non-M-escape via activation of the M-cell's homolog. Lateral line input unlikely contributes much to escape initiation because pharmacological blocking of lateral-line hair cells affected onset of neither M- or non-M-escapes. Laser ablation of trigeminal ganglion reduced occurrence of non-M-escape elicited by head tactile stimulus, suggesting that head-cutaneous stimulation elicits non-M-escape mainly via activation of trigeminal nerve. Thus, the present study demonstrates that hindbrain escape networks are separately activated by different mode of sensory stimulus in zebrafish.

Introduction

Fast escape in intact fish is elicited by various types of natural stimuli involving sound (Zottoli, 1977; Weiss et al., 2006), vibration or displacement (Kimmel et al., 1980; DiDomenico et al., 1988; Zottoli et al., 1999; Burgess and Granato, 2007), dropping object near the fish (Eaton et al., 1982), touch (Kimmel et al., 1974), water pulse stimulus applied to head or tail (Liu and Fetcho, 1999) or visual stimuli (Preuss et al., 2006; Weiss et al., 2006). These stimuli may activate auditory, vestibular, lateral line, cutaneous or visual inputs, either of which excites the M-cell (Kimmel et al., 1981; Kimmel et al., 1990; Faber et al., 1991; Zottoli et al., 1995) and probably other RS neurons including M-cell homologs (O'Malley et al., 1996; Gahtan et al., 2002). However, it remains to be examined whether or not the same sensory modality can activate M- and non-M-escape pathways similarly.

In this chapter, I focused on the sensory inputs evoked by the water pulse applied to the OV or the head skin. Stimulation of the OV, a premature organ of the inner ear, may activate inner ear hair cells and then statoacoustic nerve afferents to evoke acousticovestibular input. Meanwhile, stimulating the head skin may arouse tactile input via activation of the trigeminal sensory nerve which senses the deflection of the head skin. Head skin stimulation may also activate lateral line (LL) nerve which senses water flow at the skin surface via hair cells in lateral line neuromasts. To investigate the contributions of sensory inputs onto escape initiation, effects of selective deprivation of each sensory input on the M- or non-M-escape was assessed here by Ca^{2+} imaging of the M-cell and MiD3cm during escape and kinetic measurements of tail movement. The results suggest that acousticovestibular and tactile inputs effectively activate different escape pathways: the former preferentially activates the M-cell pathway, whereas the latter does the non-M-pathway involving MiD3cm.

Materials and methods

Monitoring escape behavior and calcium imaging of the M-cell and MiD3cm are performed as described in the chapters.

Ablation of otic vesicle. To eliminate sensory inputs from the OV, the otoliths on one side were ablated by intense laser pulses (Fig. 3-1B) or surgically eliminated with a fine tungsten needle. Larvae were anesthetized in 0.01% MS222, and then embedded on their side in 3.5% agar. Laser ablation was performed using a MicroPoint (Photonic Instruments, St. Charles, IL) laser system mounted on a Zeiss Axoplan 2 upright microscope with a 40x water immersion objective (Achroplan x40, NA 0.75; Zeiss). Otoliths were irradiated with a 440 nm coumarin laser pumped by a UV laser (NL100 nitrogen laser; pulse energy, 175 μJ; Stanford Research Systems, Sunnyvale, CA). Only a few laser pulses were applied to crack and split an otolith into pieces without any sign of bleeding after ablation. Soon after the fish had recovered from anesthesia, they started swimming but lost balance to keep their dorsal side up and they showed abnormal rotation. The behavioral deficits did not recover on the following days. These observations suggested successful deprivation of inner ear function. The postlesion testing was performed at 1 to 12 hours after the ablation of otoliths.

Pharmacological blockade of lateral line input. The lateral line system was blocked by degenerating neuromast hair cells pharmacologically (Fig. 3-3). Larvae were immersed in 10% HBSS containing 300-500 μM neomycin sulfate (Wako, Osaka, Japan) and incubated (at 28.5 ºC) for one hour as reported previously (Harris et al., 2003). The fish were then rinsed three times quickly in normal 10% HBSS and returned to an incubator at 28.5 ºC. The imaging tests were performed during the next 3-9 hours before the hair cells started regenerating (Harris et al., 2003). Successful elimination of the lateral line hair cells was verified by staining them through incubation in 10% HBSS containing DASPEI (0.05%, 2-[4-(dimethylamino)styryl]-N-ethylpyridinium iodide; Molecular Probes) for 20 min.

Ablation of trigeminal ganglion. Deprivation of head-tactile input was performed by laser-ablation of trigeminal ganglion neurons with the MicroPoint laser system. Trigeminal ganglion neurons were identified

by DIC optics and GFP expression in a *zCREST2/isl1-GFP* transgenic line (Uemura et al., 2005) whose M-cell was retrogradely labeled with Oregon Green BAPTA-1. Laser power was attenuated to the minimum level to kill a ganglion neuron with one or two pulses. Behavioral testing was done two to three hour after the ablation. To evaluate the ablation, the larva was fixed soon after the behavioral testing and stained with the anti-HuC/D primary antibodies (Invitrogen, 1:500 dilution). An Alexa564-conjugated secondary antibody (Invitrogen, 1:2000 dilution) was used for visualization.

Results

Acousticovestibular input is necessary for M-escape

In the previous chapters, I applied water pulse stimulus to the OV, a premature organ of the inner ear. This stimulus may activate inner ear hair cells and then statoacoustic nerve afferents. In addition, it may also activate other sensory nerves including the trigeminal sensory or lateral line (LL) nerve innervating the head skin surrounding the OV. To assess the contributions of these inputs to initiation of the fast escape, I examined the effects of lesioning the OV on the tail flip and M-cell firing (Fig. 3-1A). After the inner ear otoliths were laser-ablated (Fig. 3-1B) or the OV was surgically eliminated with a fine tungsten needle, the larvae exhibited abnormal swimming on their sides or back. However, a fast escape was still elicited in the semi-fixed preparation by a water pulse applied to the lesioned OV (OV-lesioned; Fig. 3-1C1), indicating that tactile stimulation still elicited the escape. But the onset latency was longer than that of intact fish (Fig. 3-1D1: 9.7 ± 0.3 ms, n = 47, 10 fish, $p < 10^{-4}$, Mann-Whitney U-test). In contrast, the tail flexion angle (during the initial 8 ms, 33.7 ± 1.5 degrees) and maximum angular velocity (4.9 ± 0.4 deg/ms) observed in the OV-lesioned animal was similar to that in intact fish ($p > 0.1$).

After the OV lesions, the M-cells exhibited only subthreshold fluorescence responses (Fig. 3-2A, C, $\Delta F/F$ = 5.7 ± 1.1%, 0.25 ± 0.05 xAD, n = 16, 5 fish), whereas AD stimulation still elicited robust responses as in intact fish (Fig. 3-2A1 inset, peak $\Delta F/F$ = 24.8 ± 3.4%). A suprathreshold fluorescence response was never observed, even when the maximal pressure of the stimulus apparatus was applied (50-60 psi, about 2- to 3-fold higher than behavioral threshold, n = 5, 3 fish). Similar to non-M-escape in OV-intact animal (see Chapter 2), the ipsilateral MiD3cm in OV-lesioned animal exhibited Ca^{2+} responses (Fig. 3-2B1,C 8.5 ± 0.8%, n = 7, 4 fish) with many-fold larger amplitudes than those of an AD spike (Fig. 3-2B2, 6.2 ± 0.5 xAD, n =6, 3 fish), suggesting multiple spiking. These data strongly suggest that activation of auditory or vestibular input is necessary to induce the M-cell firing which elicits a fast escape with short latency (M-escape). In addition, sensory input from the head skin may preferentially elicit a non-M-escape thorough strong activation of MiD3cm.

Tactile-evoked non-M-escape was further confirmed in OV-intact fish: suprathreshold responses was not observed in the ipsilateral M-cell when I was applied water pulse to the head skin between an eye and OV (Figs. 3-1A, 3-2A3, $\Delta F/F = 7.0 \pm 1.7\%$, 0.27 ± 0.05 xAD, n = 15, 4 fish). As shown in Figure 3-1C2 and D2, only delayed escape was elicited by the head-skin stimulation (latency: > 6 ms, 9.0 ± 0.3 ms, n = 26, 6 fish, $p < 10^{-4}$, Mann-Whitney U-test), the trajectory of which was similar to that evoked by OV stimulation (tail flexion angle during the initial 8 ms: 27.9 ± 1.1 degrees, maximum angular velocity: 4.1 ± 0.1 deg/ms, $p > 0.4$).

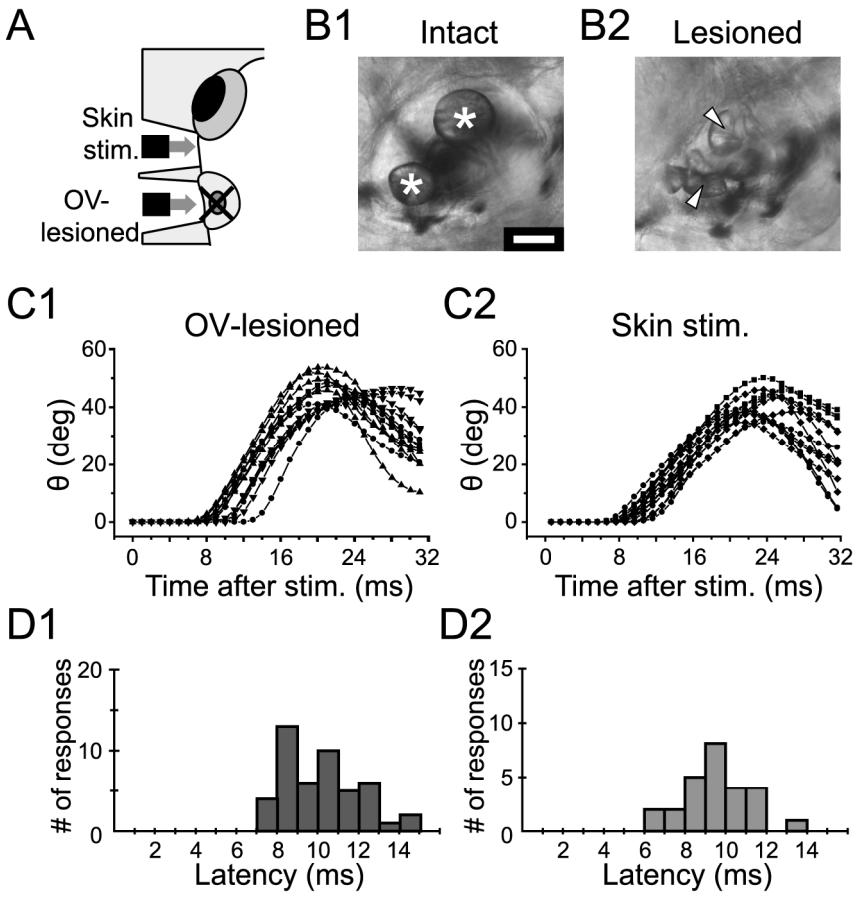

Figure 3-1. Escape response elicited by head-tactile stimulation. **A**, Tactile stimuli applied to head skin. (1) A water pulse was delivered to the OV, but the otoliths were broken by laser pulses or the OV was eliminated (OV-lesioned). (2) A water pulse was applied to the head skin between an intact OV and eye (Skin stim.). **B**, Lateral view of an OV before (**B1**) and after (**B2**) crushing two otoliths (asterisks) by laser pulse application in a 6 dpf larva. Cracked pieces of two otoliths are indicated by arrowheads in **B2**. *Left* is rostral and *up* is dorsal. Scale bar: 50 μm. **C**, Angle trajectories of the tail flexion in response to a water pulse stimulus applied to the lesioned OV (**C1**; 13 traces obtained from 4 fish) or the head skin of intact fish(**C2**; 13 traces obtained from 4 fish). The onset was always delayed. **D**, Frequency distribution of the onset latency (**D1**: OV-lesioned, **D2**: Skin stim.). The response showed latencies longer than 6 ms.

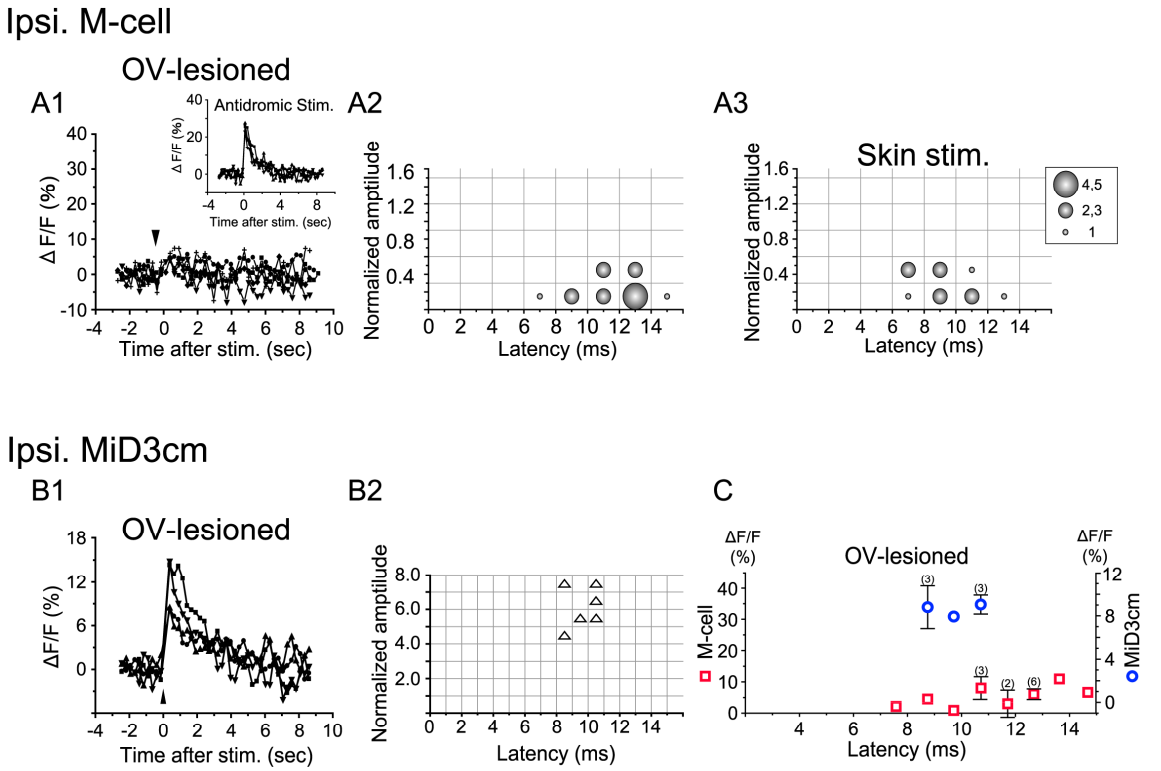

Figure 3-2. Sensory input from head skin preferentially initiates non-M-escape. **A1**, Water pulse stimulus applied to the lesioned OV produced only subthreshold fluorescence responses in the ipsilateral M-cell during fast escape (7 traces), whereas the M-cell exhibited robust fluorescence responses to the AD stimulation applied to the spinal cord (inset). **A2 and 3,** Bubble chart representation of the relationship between the amplitude of the fluorescence response of the M-cell and the onset latency of the fast escape elicited by a water pulse applied to the lesioned OV (**A2**) or the head skin (**A3**). In either case, fast escape was not elicited within 6 ms and only a small increase in fluorescence (< 0.6 xAD) was observed in the ipsilateral M-cell. Bin size: 0.3 xAD and 2 ms. The inset in **A3**, showing the number of observations, also applies to **A2**. **B**, A significant increase in fluorescence in MiD3cm was also elicited in the OV-lesioned fish. Four traces obtained from two fish are superimposed in **B1**. Such responses associated with delayed onset (> 6 ms) are several times larger in amplitude than that of single AD spike (**B2**). Bin size in **B2**: 1.0 xAD and 1 ms. Each triangle in **B2** represents a single trial. **C**. Relationships between the amplitude of the fluorescence response of the M-cell and MiD3cm and onset latency of the fast escape elicited by a water pulse applied to the lesioned OV, plotted as shown in Fig. 2-3.

Deprivation of lateral line input did not affect escape onset latency

Next, to examine whether the LL system was involved in initiating the fast escapes, I tested tail response and M-cell firing after pharmacological poisoning of the LL system with an aminoglycoside antibiotic, neomycin (300-500 μM, Harris et al., 2003). Since LL neuromasts are located only on the skin surface before 9 dpf (Webb and Shirey, 2003), a styryl pyridium dye, DASPEI, was used to label the functional hair cells in the superficial neuromasts by direct permeation through their mechanotransduction channels (Balak et al., 1990; Nishikawa and Sasaki, 1996; Gale et al., 2001; Meyers et al., 2003). The complete loss of DASPEI-labeled neuromasts after neomycin treatment (Fig. 3-3A) indicates dysfunction or degeneration of LL hair cells (Harris et al., 2003; Murakami et al., 2003; Owens et al., 2007). However, both M- (onset latency: 3.8 ± 0.2, n = 13) and non-M-escapes (7.3 ± 0.5 ms, n = 8) were still elicited by the OV stimulation as in the control (Fig. 3-3B; latency: $p > 0.05$, proportion of the two types of escape: $p > 0.4$, comparison of two proportions, 3 fish). Thus, it is unlikely that LL input makes a considerable contribution to the initiation of the fast escape.

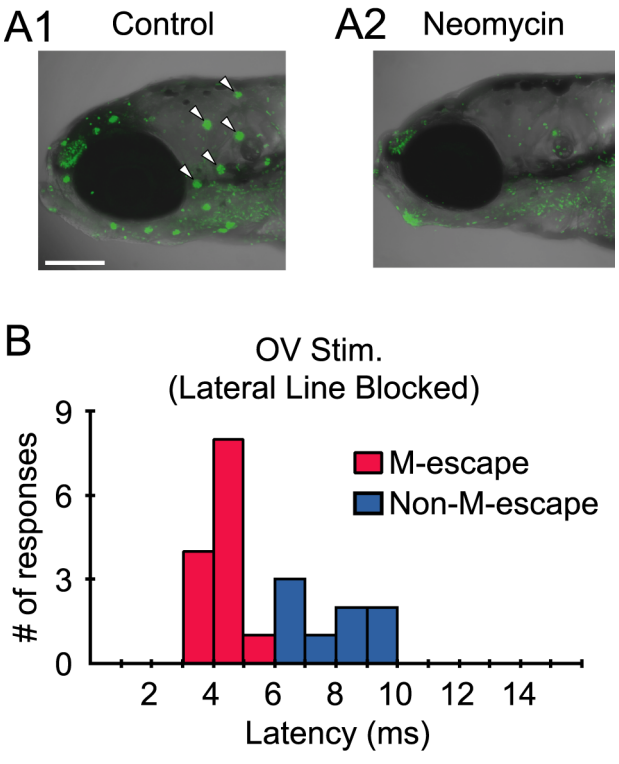

Figure 3-3. Blockade of lateral line hair cells did not affect the escape onset. **A**, Hair cells in lateral line neuromasts (those near the OV are indicated by arrowheads) were stained with DASPEI (**A1**, control). Neomycin treatment abolished the DASPEI-labeled neuromasts (**A2**). Scale bar: 200 μm. **B**, Onset latency of tail flip responses elicited by the water pulse stimulation in neomycin-treated larvae (3 fish). Simultaneous monitoring of M-cell activity revealed that neither M- (red) nor non-M-escape (blue) latency was affected after lateral line blockade.

Deprivation of trigeminal input did not affect M-escape but reduced non-M-escape

The effects of deprivation of OV or LL input on the initiation of the tail flexion suggest that activation of the remaining sensory input, the trigeminal sensory nerve innervating head skin, triggers non-M-escape. To confirm this notion, I examined the effect of selective laser ablation of the trigeminal sensory ganglion (gV)(Fig. 3-4A). Since the gV is located separately along the rostro-caudal axis from the anterior lateral ganglion (aLLg), I could ablate gV neurons with aLLg left intact (Fig. 3-4A2). I used a Tg(zCREST-2/isl1-GFP) transgenic line (Uemura et al., 2005) which express GFP in gV to enhance the identification of the neurons and efficiency of the lesion. This allowed me to kill almost all the gV neurons, evaluated by immunostaining with anti-HuC antibody (e.g. Sagasti et al., 2005) after the behavioral testing.

Water pulse applied to the OV on the gV-lesioned side (4 fish) still induced M-escape with latencies as short as that in intact fish (onset latency, 3.8 ± 0.2 ms, n = 33, $p > 0.6$, Mann-Whitney U test). This result suggests that trigeminal input does not take a decisive role in determining the timing of M-cell firing and that acousticovestibular input can solely activate the M-cell in minimum delay from sensory stimulus. Non-M-escape was also elicited with similar latency to that of intact fish (9.5 ± 0.9 ms, $p > 0.2$, Mann-Whitney U-test, n = 4), however, the proportion of non-M-escapes out of total fast escapes (11%) was significantly reduced from that of 31 % in intact fish (see Fig. 1-5, $p < 0.01$, comparison of two proportions), suggesting that trigeminal input is indeed a major input source for initiating non-M-escape. Non-M-escape after the gV lesion implies that statoasouctic input and/or lateral line inputs can also initiate non-M-escape. However, since one or two gV neurons were still detected by immunolabeling in each lesioned animal, I could not exclude the possibility that the remaining gV neurons activated the non-M-escape.

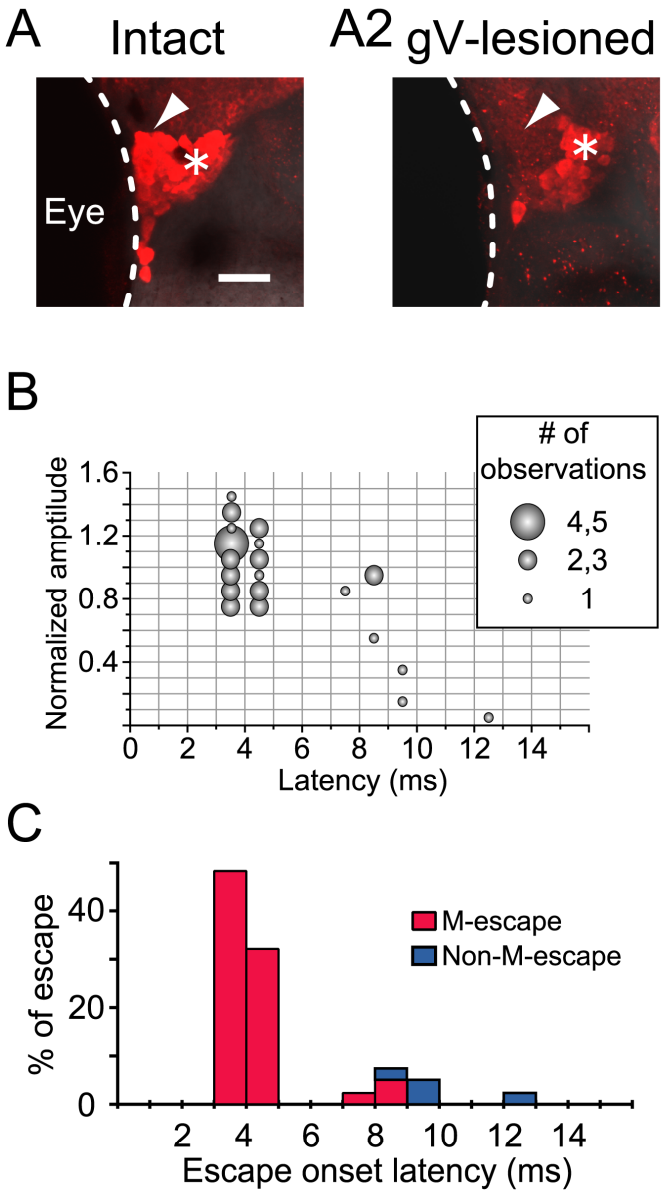

Figure 3-4. Selective ablation of trigeminal ganglion did not affect M-escape but reduced non-M-escape. **A,** Trigeminal sensory ganglion (arrow head; gV) was stained with anti-Hu C antibody (**A1**, intact). Laser ablation of gV was performed with the anterior lateral line ganglion (asterisks) left intact (**A2**). Dotted lines indicate the edge of eye ball. Scale bar: 30 μm. **B,** Bubble chart representation of the relationship between the amplitude of the fluorescence response of the M-cell and the onset latency of the fast escape elicited by a water pulse applied to the OV of the gV-lesioned larvae. Bin size: 0.1 xAD and 1 ms. **C,** Frequency distribution of the onset latency. Note that non-M-escape appeared less frequently than in intact fish (Fig. 1-5C1).

Discussion

Effects of deprivation of sensory inputs on fast escape and on activities of the M-cell and MiD3cm reveal that M- and non-M-escape circuits are activated by different sensory modalities. Acousticovestibular input activates the M-cell to initiate fast escape with minimum latency whereas head-tactile stimulation preferentially elicits the non-M-escape circuit involving MiD3cm via activation of trigeminal nerve (see summarized figure 3-5).

M-escape elicited by acousticovestibular input

In the present study, an M-escape occurred only when the water pulse was applied to an OV, suggesting that acousticovestibular input induces M-cell firing in larval zebrafish, as in adult goldfish (Faber and Korn, 1978; Oda et al., 1998; Nakayama and Oda, 2004) and zebrafish (Hatta and Korn, 1998). Acousticovestibular input may also elicit non-M-escape in intact fish. It was shown previously, however, that vibratory stimulus was virtually unable to induce fast escape in M-cell-ablated zebrafish larva, but elicited only slow escape with long latency (> 15 ms) (Burgess and Granato, 2007; see also Kimmel et al., 1980). In the present study, slow tail movement with long latency (> 15 ms) was observed in intact semi-fixed larva, but was never associated with M-cell firing (data not shown). Thus, acousticovestibular input can elicit either fast escape via M-cell firing or slow escape without M-cell firing in larval zebrafish.

Head-tactile input initiates non-M-escape via activation of MiD3cm

The effects of head-skin stimulation and lesioning OV or gV suggest that head-tactile input via the trigeminal nerve preferentially evokes non-M-escape (Figs. 3-1, 2 and 4). However, the M-cell receives direct synaptic input from the trigeminal and LL sensory nerves, as well as the statoacoustic nerve (Kimmel et al., 1990), either of which was activated by the water pulse applied to the head. The lack of M-escape upon head-skin stimulation indicates that head-tactile input is insufficient to induce M-cell firing. This may at least partly result from the low input resistance of the large-sized M-cell. The trigeminal nerve runs cau-

dally through the hindbrain and synapses onto the M-cell lateral dendrite with a small contact region (Kimmel et al., 1981), but in contrast, the statoacoustic nerve terminates over a large portion of the lateral dendrite of the M-cell which give a large depolarization to the M-cell as shown in goldfish (Faber and Korn, 1978; Szabo et al., 2007). Instead, the trigeminal nerve possibly synapses onto the dendrites of smaller RS neurons (see Kimmel et al., 1985) involving the M-cell's homologs and give efficient input to them, because of their high input resistance coming from the small size, and produce non-M-escape. Large Ca^{2+} response of MiD3cm during non-M-escape after OV lesioning (Fig. 3-2B) supports this notion.

As discussed in Chapter 2, non-M-escape pathway may be suppressed by the M-cell. Such hierarchical organization of the hindbrain RS neurons should prioritize acousticovestibular input over head-tactile input for initiating fast escape with minimum latency.

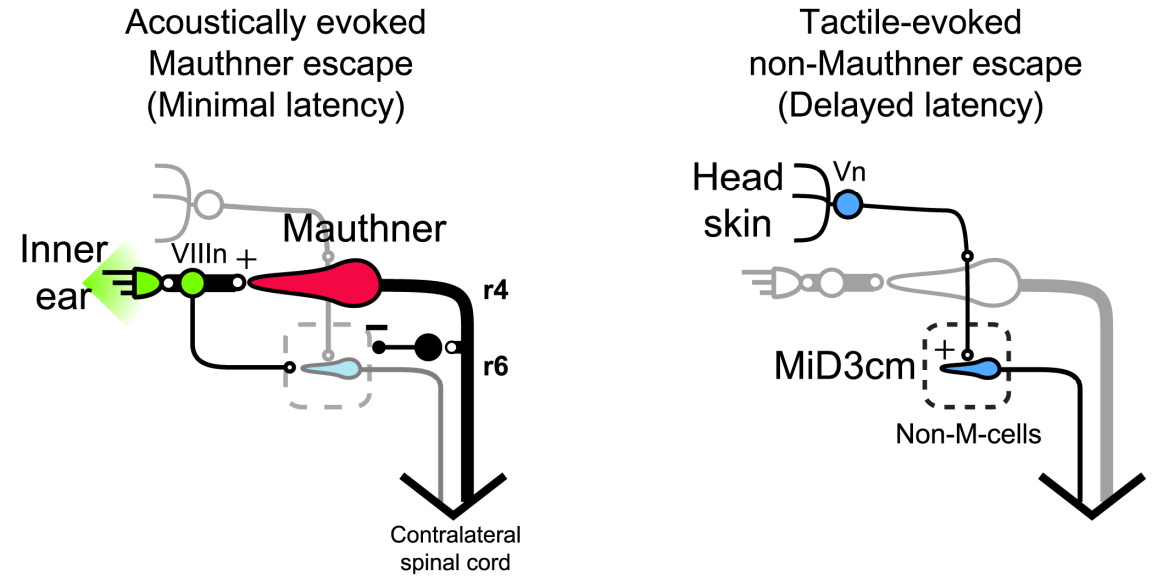

Figure 3-5. Different sensory inputs segregate on different escape networks. **Left,** Acousticovestibular input activates statoacoustic nerve (VIIIn) and the M-cell to initiate fast escape with minimal latency (M-escape), but is not so effective to elicit non-M-escape. Firing of the M-cell may suppress tactile-evoked non-M-pathway via inhibitory interneuron (right, see also Fig. 2-5). **Right,** Head-tactile stimulation activates trigeminal nerve (Vn) and MiD3cm to initiate non-M-escape, whereas it is ineffective for M-cell firing. Open and filled circles indicate excitatory and inhibitory synapses, respectively. Dotted line represents non-M-cells including MiD3cm.

References for chapter 3

Balak KJ, Corwin JT, Jones JE (1990) Regenerated hair cells can originate from supporting cell progeny: evidence from phototoxicity and laser ablation experiments in the lateral line system. J Neurosci 10:2502-2512.

Burgess HA, Granato M (2007) Sensorimotor gating in larval zebrafish. J Neurosci 27:4984-4994.

DiDomenico R, Nissanov J, Eaton RC (1988) Lateralization and adaptation of a continuously variable behavior following lesions of a reticulospinal command neuron. Brain Res 473:15-28.

Eaton RC, Lavender WA, Wieland CM (1982) Alternative neural pathways initiate fast-start responses following lesions of the Mauthner neuron in goldfish. J Comp Physiol [A] 145:485-496.

Faber DS, Korn H (1978) Neurobiology of the Mauthner Cell. New York: Raven Press.

Faber DS, Korn H, Lin JW (1991) Role of medullary networks and postsynaptic membrane properties in regulating Mauthner cell responsiveness to sensory excitation. Brain Behav Evol 37:286-297.

Gahtan E, Sankrithi N, Campos JB, O'Malley DM (2002) Evidence for a widespread brain stem escape network in larval zebrafish. J Neurophysiol 87:608-614.

Gale JE, Marcotti W, Kennedy HJ, Kros CJ, Richardson GP (2001) FM1-43 dye behaves as a permeant blocker of the hair-cell mechanotransducer channel. J Neurosci 21:7013-7025.

Harris JA, Cheng AG, Cunningham LL, MacDonald G, Raible DW, Rubel EW (2003) Neomycin-induced hair cell death and rapid regeneration in the lateral line of zebrafish (Danio rerio). J Assoc Res Otolaryngol 4:219-234.

Hatta K, Korn H (1998) Physiological properties of the Mauthner system in the adult zebrafish. J Comp Neurol 395:493-509.

Kimmel CB, Patterson J, Kimmel RO (1974) The development and behavioral characteristics of the startle response in the zebra fish. Dev Psychobiol 7:47-60.

Kimmel CB, Eaton RC, Powell SL (1980) Decreased fast-start performance of zebrafish larvae lacking Mauthner neurons. J Comp Physiol [A] 140:343-350.

Kimmel CB, Sessions SK, Kimmel RJ (1981) Morphogenesis and synaptogenesis of the zebrafish Mauthner neuron. J Comp Neurol 198:101-120.

Kimmel CB, Metcalfe WK, Schabtach E (1985) T reticular interneurons: a class of serially repeating cells in the zebrafish hindbrain. J Comp Neurol 233:365-376.

Kimmel CB, Hatta K, Metcalfe WK (1990) Early axonal contacts during development of an identified dendrite in the brain of the zebrafish. Neuron 4:535-545.

Liu KS, Fetcho JR (1999) Laser ablations reveal functional relationships of segmental hindbrain neurons in zebrafish. Neuron 23:325-335.

Meyers JR, MacDonald RB, Duggan A, Lenzi D, Standaert DG, Corwin JT, Corey DP (2003) Lighting up the senses: FM1-43 loading of sensory cells through nonselective ion channels. J Neurosci 23:4054-4065.

Murakami SL, Cunningham LL, Werner LA, Bauer E, Pujol R, Raible DW, Rubel EW (2003) Developmental differences in susceptibility to neomycin-induced hair cell death in the lateral line neuromasts of zebrafish (Danio rerio). Hear Res 186:47-56.

Nakayama H, Oda Y (2004) Common sensory inputs and differential excitability of segmentally homologous reticulospinal neurons in the hindbrain. J Neurosci 24:3199-3209.

Nishikawa S, Sasaki F (1996) Internalization of styryl dye FM1-43 in the hair cells of lateral line organs in Xenopus larvae. J Histochem Cytochem 44:733-741.

Oda Y, Kawasaki K, Morita M, Korn H, Matsui H (1998) Inhibitory long-term potentiation underlies auditory conditioning of goldfish escape behaviour. Nature 394:182-185.

O'Malley DM, Kao YH, Fetcho JR (1996) Imaging the functional organization of zebrafish hindbrain segments during escape behaviors. Neuron 17:1145-1155.

Owens KN, Cunningham DE, MacDonald G, Rubel EW, Raible DW, Pujol R (2007) Ultrastructural analysis of aminoglycoside-induced hair cell death in the zebrafish lateral line reveals an early mitochondrial response. J Comp Neurol 502:522-543.

Preuss T, Osei-Bonsu PE, Weiss SA, Wang C, Faber DS (2006) Neural representation of object approach in a decision-making motor circuit. J Neurosci 26:3454-3464.

Sagasti A, Guido MR, Raible DW, Schier AF (2005) Repulsive interactions shape the morphologies and functional arrangement of zebrafish peripheral sensory arbors. Curr Biol 15:804-814.

Szabo TM, McCormick CA, Faber DS (2007) Otolith endorgan input to the Mauthner neuron in the goldfish. J Comp Neurol 505:511-525.

Uemura O, Okada Y, Ando H, Guedj M, Higashijima S, Shimazaki T, Chino N, Okano H, Okamoto H (2005) Comparative functional genomics revealed conservation and diversification of three enhancers of the isl1 gene for motor and sensory neuron-specific expression. Dev Biol 278:587-606.

Webb JF, Shirey JE (2003) Postembryonic development of the cranial lateral line canals and neuromasts in zebrafish. Dev Dyn 228:370-385.

Weiss SA, Zottoli SJ, Do SC, Faber DS, Preuss T (2006) Correlation of C-start behaviors with neural activity recorded from the hindbrain in free-swimming goldfish (Carassius auratus). J Exp Biol 209:4788-4801.

Zottoli SJ (1977) Correlation of the startle reflex and Mauthner cell auditory responses in unrestrained goldfish. J Exp Biol 66:243-254.

Zottoli SJ, Bentley AP, Prendergast BJ, Rieff HI (1995) Comparative studies on the Mauthner cell of teleost fish in relation to sensory input. Brain Behav Evol 46:151-164.

Zottoli SJ, Newman BC, Rieff HI, Winters DC (1999) Decrease in occurrence of fast startle responses after selective Mauthner cell ablation in goldfish (Carassius auratus). J Comp Physiol [A] 184:207-218.

Chapter 4

Functional development of escape network in larval zebrafish

Summary

During development, zebrafish show fast escape first in response to touch, as known as touch response, and become to respond to sound or vibratory stimulation later. In this chapter, I compared the contributions of sensory inputs and Mauthner (M-) cell activity to initiation of fast escape in embryonic or newly-hatched larvae (40-70 hours postfertilization; hpf) to those of developed larvae (> 120 hpf) which were described in the previous chapters. I assessed the effects of deprivation of sensory inputs or of ablation of the M-cell on tail flip response in the semi-restrained preparation. Unlike the developed fish, the escape could not be elicited after ablation of the trigeminal ganglion (gV) in embryos or newly-hatched larvae before 65 hpf, indicating that tactile input is indispensable to evoke fast escape. Furthermore, ablation of the M-cell did not affect the escape onset significantly in this developmental stage, suggesting that the M-cell does not play a primary role in initiation of the escape yet. Lesion of the otic vesicle (OV) abolished short- latency escape after 80 hpf. Thus, sound-induced M-escape pathway may take over touch-induced escape pathway after 80 hpf to escape quickly from a hostile sound source before it reaches the fish.

Introduction

Attempts have been made to relate the progressive acquisition of animal behaviors to the development of underlying neuronal circuits (Bate, 1999). Zebrafish offer several advantages to assess this issue, from the levels of gene to behavior (Lewis and Eisen, 2003). During the first week of development, embryonic or larval zebrafish start to show a number of behaviors, such as coiling (large body flexion during which the tip of the tail is curled over the head), swimming or escape, in a stereotyped order (Kimmel et al., 1974; Saint-Amant and Drapeau, 1998; Drapeau et al., 2002). Development of neuronal mechanisms underlying these behaviors, involving sensory inputs (Moorman, 2001; Whitfield et al., 2002; Ghysen and Dambly-Chaudiere, 2004), central nervous system (Mendelson, 1986a, b; Lewis and Eisen, 2003), muscles (Stickney et al., 2000) and connections between them (Kimmel et al., 1990; Jontes et al., 2000) have been investigated anatomically and genetically. However, physiological basis for development of behavior remained largely to be uncovered. But over the last decade, *in vivo* Ca^{2+} imaging, whole-cell recordings and selective ablation of specific neurons have become to be employed to investigate neuronal activity during behavior, physiological characteristics of neuron or mutual connection between neurons involved in the circuit underlying behavior (Fetcho, 2006; Fetcho et al., 2008). Thus, the simplicity of fast escape network in zebrafish should provide a great opportunity to investigate functional development of neuronal circuit underlying behavioral development.

The fast escape of adult teleost fish, including zebrafish, consists of the initial C-shaped bending (C-bend), a second flexion opposite to the C-bend (counter turn), and subsequent variable and diminishing bouts of swimming (Domenici and Blake, 1997). After the onset of the fast escape, adult zebrafish travels more than one-body length during 100 ms (Kimmel et al., 1974). These features above are qualitatively accomplished in fast escape of larvae over 100 hpf (Figs 1-2A and 4-1B)(Kimmel et al., 1974). However, sensory-evoked response which appears first in developing zebrafish, named touch response, is quite distinct from the developed fast escape. At 21 hpf, decapsulated embrys start to show coiling response of up to three upon touch stimulus applied to head or tail (Kimmel et al., 1974; Saint-Amant and Drapeau, 1998).

The number of the touch-evoked tail flexion is suddenly increased and the embryo become to move its body from the initial location after 26 hpf, defined as the onset of swimming (Saint-Amant and Drapeau, 1998). The angular velocity of the initial tail flexion during the touch response enhances after its appearance, reaches to the plateau by 40 hpf (Saint-Amant and Drapeau, 1998). At the time of hatching, the angular velocity is already similar to that during fast escape of the developed larva over 100 hpf (around 50 hpf) (Fig. 4-2). Thus, the motor performance during initiation of fast escape seems well developed by the time of hatching, although the net overview of the touch response before around 70 hpf is still different from that of the developed fast escape in terms of the prolonged side-to-side body flexions which last for seconds (Kimmel et al., 1974). Nevertheless, newly-hatched larvae do not show fast escape in response to sound or vibration by 80 hpf (Fig. 4-1, see also Kimmel et al., 1974).

In the developed larvae (>120 hpf), the M-cell is required for auditory or vestibular input to initiate fast escape (Burgess and Granato, 2007) especially with short latency, whereas head-tactile input preferentially activate non-M-cells to induce fast escape (Chapter 3). Therefore, escape behaviors seems different between the newly-hatched and the developed larvae, at the point of sensory inputs to induce escape and central neurons to integrate the sensory inputs to produce motor output. To investigated the contributions of the sensory inputs and the M-cell onto fast escape in the newly-hatched larvae, effects of deprivation of sensory inputs or ablation of the M-cell onto tail flip response in larvae at 50-65 hpf was examined here. The results suggest that zebrafish acquire the sound/vibration-induced fast escape by developing acousticovestibular input to effectively activate the developing M-cell.

Materials and methods

Experiments were performed on larval zebrafish at 40-170 hpf raised at 28.5 ºC. Preparation of semi-fixed zebrafish, water pulse stimulation and ablation of the OV and the gV was done as described in the previous chapters.

Stimulation of unrestrained larva. To monitor the escape in freely-moving larva, larvae were tested in a Petri dish (3.5 cm) filled with 10% HBSS at a depth of 3 to 4 mm. Touch-induced escapes were elicitted by touching the head or the OV with a human hair or by applying water pulse to the head or the OV as described in Chapter 1. When the hair touched the larva was determined by eye. Vibratiory stimulation was applied from a loud speaker attached to the plastic plate glued to the petri dish. The stimulus wave form consisted of five cycles of sine wave at a frequency of 500 Hz, generated by a function generator (Wavefactory 1941; NF, Yokohama, Japan). The onset of the first sine wave was referred to as that of vibratory stimulation. The stimulus intensity was measured with a shock sensor (PKS1-4A1, Murata Manufacturing, Kyoto, Japan) attached on the plastic plate. The peak amplitude of the stimulus was adjusted to about 10 m/s^2, well above the behavioral threshold for fast escape in > 100 hpf larvae (Burgess and Granato, 2007).

Ablation of the M-cell in young larva. Since the M-cell can not be labeled retrogradely with dextran-conjugated fluorescence (10,000 MW; Invitrogen) before 70 hpf (Kohashi, unpublished observations), I identified the M-cell with the guide of GFP fluorescence in the Tol026 transgenic zebrafish (Tanimoto et al., 2009), which was generated by K. Horikawa, Y. Sato and H. Takeda using the Tol2 transposon-mediated enhancer trap technique (Nagayoshi et al., 2008). This transgenic line expresss green fluorescence protein (GFP) in the M-cells from approximately 35 hpf. Laser ablation of the M-cell was performed with the Micropoint system. Laser intensity was attenuated to avoid undesirable bleedings and other tissue damages in the hindbrain. Typically, the intensity was adjusted to the level at which approximately 100 laser pulses were required for successful ablation of the M-cell. Immediately after the behavioral testing, the fish was fixed, processed with the monoclonal 3A10 primary antibody (Hatta, 1992) and an Alexa 564-conjugated secondary antibody (1:2000 dilution) to confirm the loss of M-cell soma.

Statistics. Results were presented as the mean ± SD. The statistical significance was assessed using the Student's t-test after verifying the normality of the distributions by the Kolmogorov-Smirnov test ($p > 0.05$) and the equality of the variance with the F-test ($p > 0.05$), unless otherwise noted.

Results

Appearance of vibration-induced fast escape during development

Escape in newly-hatched larval zebrafish (approximately 50 hpf) is elicited by touch stimulus. Vibratory stimulus does not elicit escape at this stage, but effectively induces latter in development. Since the time course of this developmental process is determined only in zebrafish raised at lower temperature (at 25 ° C, Kimmel et al., 1974), I first confirmed the time course in zebrafish raised at 28.5 ºC. Newly-hatched larvae (approximately 50 hpf) frequently list to one side or lie upside down when at rest and rarely swim spontaneously. When the head of the larva was touched with hair, it showed abrupt and rapid whole-body bending away from the stimulus (Fig. 4-1A, top). Such touch-induced escape is followed by a series of side-to-side flexions prolonged typically for a couple of seconds, as described previously for 3-day larvae raised at 25 ºC (Kimmel et al., 1974). Vibratory stimulation does not evoke any behavioral response at this stage (Fig. 4-1A, bottom and C). By 100 hpf, larvae start floating in water appear upright at rest and show spontaneous swimming frequently. Now, virtually all larvae show fast escape (latency: < 15 ms, see Chapter 1) to the vibratory stimulus, as well as touch stimulus of the head (Fig. 4-1B and C). As described for 7-day larvae raised at 25 ºC, the movements after the escape onset are very distinct from those of 50 hpf but have all aspects of those of adult (Kimmel et al., 1974): there are the second, third and typically forth strong flexion of the body after the initial flexion and following diminishing flexions of the tail which stop typically within 200 ms after initiation of the escape. As shown in Fig. 4-1C, larvae showed fast escape in response to the vibration first at 77 hpf. The proportion of such larvae dramatically increased from 10 % at 80 hpf to 80 % at 90 hpf (50 % at 86 hpf, estimated by the Boltzmann equation). This period is corresponding to 5-to-6-day larvae at 25 ºC (Kimmel et al., 1974). Thus, these results demonstrated that vibratory stimulation become effective to elicit fast escape by 80 hpf in zebrafish.

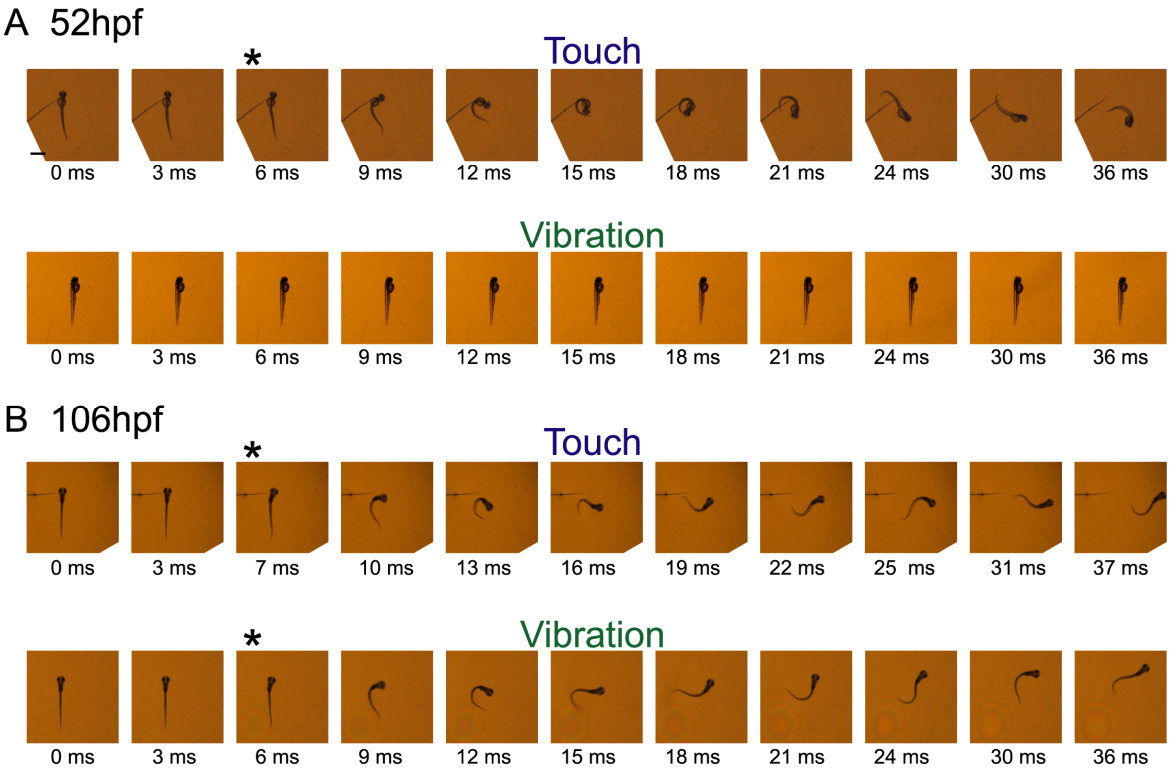

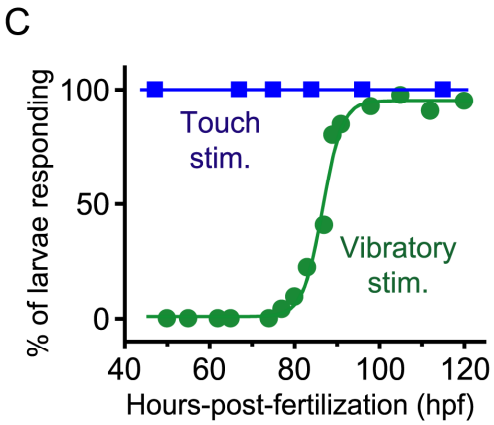

Figure 4-1. Development of fast escape evoked by head-touch or vibratory stimulation. **A, B,** Fast escape of zebrafish larvae at 52 (**A**) and 106 (**B**) hours-postfertilization (hpf) in response to head touch (top pannels) or vibration (top panels). Time after stimulus arrival is denoted. Behavioral onset is indicated by asterisk. Scale bar: 1 mm. **C,** Proportion of larvae responding (ordinate) to touch (squares) or vibratory (circles) stimulation is plotted against hpf (abscissa). Response is first observed at 77 hpf in response to the vibration and almost all the larva responded after the next 20 hours. Each larva was tested only once for vibratory stimulation and over 20 larvae were tested to generate each data point. Data points were fitted by a Boltzmann equation.

Development of escape movement during acquisition of vibration-induced response

The developmental acquisition of vibration-induced fast escape probably reflects functional development of escape network activated by acousticovestibular input, because the vibratory stimulation is expected to activate acousticovestibular input more effectively than tactile input. To test this notion, I adopted the semi-fixed preparations and elicited fast escape by applying water pulse to the OV of larvae at 40-170 hpf, as in the previous chapters. This preparation provides us fine control of the stimulus location and detailed observations on the initial tail movement during fast escape, either of which is essential in evaluating the developmental changes in escape-initiating network from sensory inputs to motor outputs.

First, I compared the fast escape of newly-hatched larvae (40-60 hpf)(Fig. 4-2A) with that of the developed larvae (120-170 hpf)(Fig. 4-2B). As I described in Chapter 1, the developed fish show two kinetically distinct types of escape: short-latency (< 15 ms) escape with faster tail flexion and long-latency (> 15 ms) escape with slow tail flexion. The former was defined as fast escape in Chapter 1. The newly hatched larvae (n = 80, 6 fish) also showed fast tail flexions with latency shorter than 15 ms (Fig. 4-3A), however, never showed tail response with longer latency than 15 ms, indicating that head-tactile stimulus elicits only fast escape in newly hatched larva. Although the overall movement during the unrestrained escape in the newly-hatched larva is quite different from that in the developed larva, the initial tail flexion angle (8 ms after initiation) of the former (26 to 50, 38.6 $\pm$ 6.8 degrees, n = 26, 6 fish) was within the similar range of that of the latter (20 to 42, 29.5 $\pm$ 5.9 degrees, n = 65, 8 fish, see also Chapter 1)(Fig. 4-2C). Thus, it is suggested that recruitment and contraction profile of the trunk muscle during fast escape is well developed by the time of hatching. Statistically, however, the tail flexion angle of the newly-hatched larva was significantly larger than that of the developed larva ($p < 0.01$), probably due to the higher viscosity resistance of water for longer tail of the developed larva.

Obvious change during development was found in the onset latency. Particularly, the minimal latency, which was 5 ms at 40 hpf, gradually decreased and reached to the minimum of 3 ms after 80 hpf. From the lack of developmental enhancement in the initial tail flexion angle which reflects angular velocity, the reduction of the latency is indicated to reflect developmental reduction in the conduction time of neuronal

pathway from sensory systems to trunk muscle. Besides the minimal value, the onset latency showed a dramatic developmental change in the distribution profile from unimodal to bimodal after 100 hpf, as if short-latency escape is added to the delayed-latency escape during development.

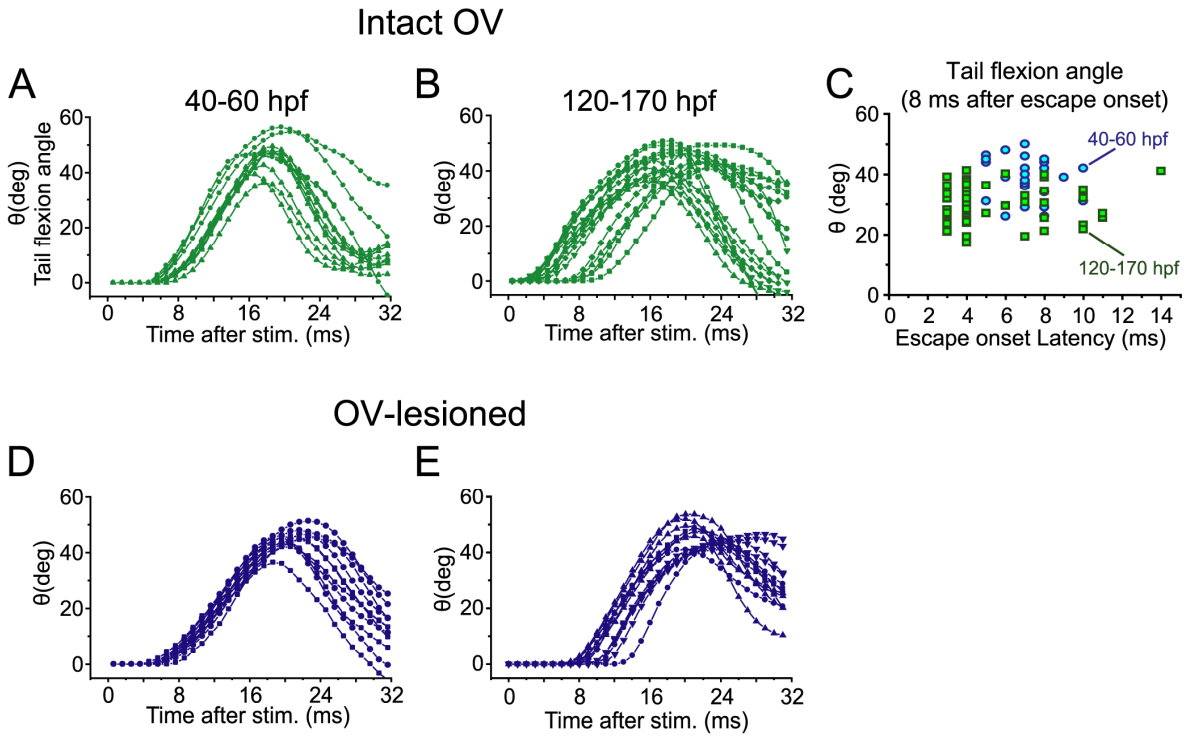

Figure 4-2. Effects of lesioning OV at different developmental stages. **A, B,** Representative angle trajectories of tail flips elicited by water pulse applied to the OV in intact fish. The tail movements of larvae at 40-60 hpf (**A**) showed similar angular velocities to those at 120-170 hpf (**B**) but the onset latencies of the former were not as short as those of the latter. Note that majority of the latter responses started before 6 ms, whereas some started later. **C,** The tail flexion angles (θ) 8 ms after the escape onset in 40-60 hpf (blue circles) and 120-170 hpf (green squares) larvae are plotted against escape onset latency. **D, E,** After the otoliths in OV were ablated by laser pulse or surgically eliminated, the onset of tail flip was delayed in larvae at 120-170 hpf (**E**) but not in 40-60 hpf (**D**).

Head-tactile input initiates fast escape before 70 hpf whereas acousticovestibular input effectively induces short-latency escape after 80 hpf.

The short-latency (3-6 ms) escape elicited by OV stimulation requires acousticovestibular input in larvae > 120 hpf (Chapter 3), suggesting that the developmental shortening of escape latency reflects functional maturation of escape network which is activated by acousticovestibular input. Thus, I next assessed the contribution of acousticovestibular input onto the fast escape by ablation of the OV. Unlike in the developed larvae (120-170 hpf) where the OV-lesioning abolished the short-latency escape (< 6 ms, Fig. 4-2B, E), newly-hatched larvae (40-70 hpf) still showed fast escapes with the same latencies as intact fish (p>0.3, Mann-Whitney U test) in response to water stimulation applied to the lesioned OV (Fig. 4-2A, D and 4-3). Initial angular velocity of the tail flexion also did not affected apparently by the lesion. As shown in Fig.

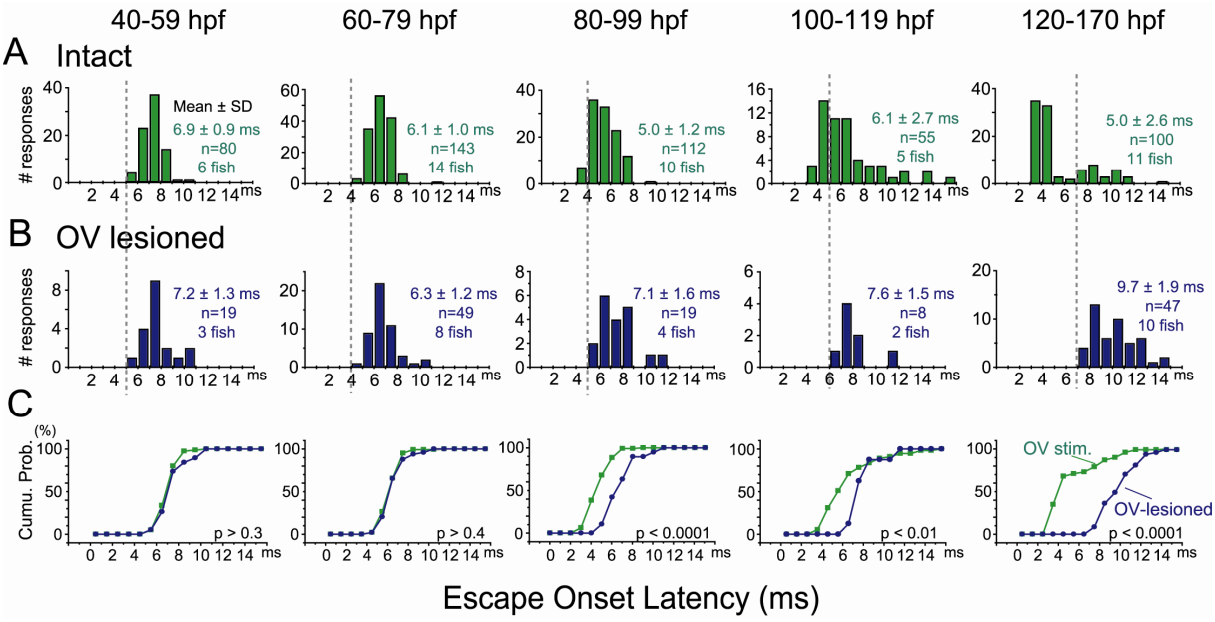

Figure 4-3. Acousticovestibular input is necessary for short-latency escape after 80 hpf. **A, B,** Frequency distributions of the onset latency of fast escape elicited by water pulse applied to intact (**A**) or lesioned OV (**B**) of semi-fixed larvae at various developmental stages. Average onset latency (Mean ± SD) and the number of trials and fish for each stage are denoted. **A,** In intact larvae, the minimal onset latency decreased gradually from 5 ms at 40-59 hpf to 3 ms after 80 hpf. Furthermore, the distribution profile was changed from uninomodal into bimodal after 100 hpf. **B,** After OV lesion, the escape onset was delayed after 80 hpf. Typically, escape with shorter onset latencies than 5 or 6 ms (left to dotted lines) was not observed. By contrast, the onset was not affected in the younger larvae before 80 hpf. **C,** Cumulative probability plots of **A** and **B**. Statistical difference (p) between **A** and **B** for each stage was assessed by the Mann-Whitney U-test .

4-3, when I quantified the latency distribution with the time window of 20 hours, the OV-lesioning resulted in a significant delay in the escape latency after 80 hpf ($p < 0.01$, Mann-Whitney U test). In particular, escape with shorter latency than 5 (80-100 hpf) or 6 ms (> 100 hpf) was never observed after the lesion. Thus, it is strongly suggested that the acousticovestibular input is necessary to initiate short-latency escape acquired after 80 hpf.

Small or no effects of OV lesioning onto escape initiation also suggest that fast escape in newly-hatched zebrafish is initiated by stimulation of the head skin. The head-cutaneous input seems to be mediated predominantly by the trigeminal nerve since the pharmacological poisoning of lateral line hair cells with neomycin did not affect the escape onset (50-65 hpf, 5.7±0.8 ms, $p > 0.05$, Kolmogorov-Smirnov test, n = 18, 3 fish) as in the developed larvae (> 120 hpf, see Chapter 3). To confirm this notion, I performed selective laser-ablation of trigeminal ganglion (gV) in newly-hatched larvae (50-65 hpf) as in Chapter 3. When a water pulse was applied to the gV-lesioned side, evoked tail response was never elicited opposite to (0 %,

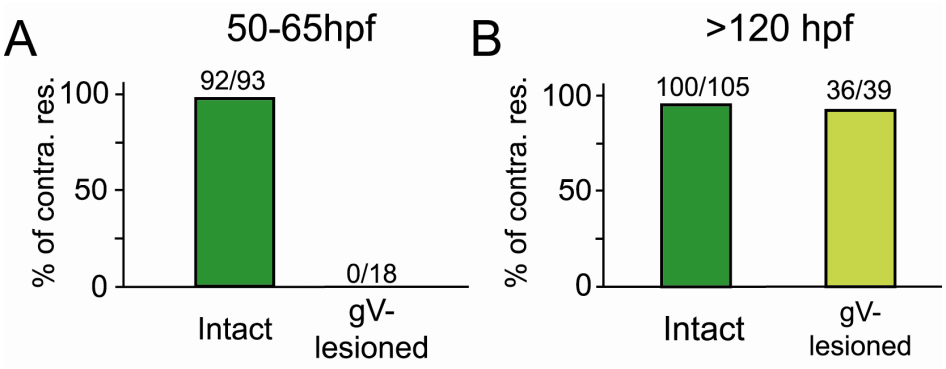

Figure 4-4. Trigeminal nerve input is necessary for fast escape elicited by head-touch stimulus before 70 hpf. Directionality of fast (latency: < 15 ms) tail flip evoked by the water stimulus applied to the OV of intact animal (left bars) or the OV on gV-lesioned side (right bars) is represented by the fraction of the tail flip toward the contralateral side to the water pulse. Number of contralateral tail flips per that of total trials accompanied with tail flip is denoted above each bar. **A,** At 50-65 hpf, almost all the tail flips were directed toward the contralateral, however, no contralateral tail flip but only ipsilateral ones were observed after ablation of the gV. **B,** At 120-170 hpf, contralateral tail flip was still observed as in intact animal after lesioning the gV. See also Fig. 3-4 for distribution of onset latency.

n = 18, 4 fish), but all toward the stimulus (Fig. 4-4A). Such behavioral deficit does not seem to come from non-specific damages associated with the ablation because the gV-lesioned larvae still showed contralateral tail flip when the water stimulation was applied the gV-intact side (100 %, n = 21, 3 fish), as in intact larvae (99 %, n = 93, 8 fish) (Fig. 4-4A). In contrast, gV-lesioning did not affected the directionality of the escape in the developed larvae at > 120 hpf (Intact: 95 %, n = 105, 10 fish, gV-lesioned: 92%, n = 39, 4 fish, $p > 0.05$, comparison of two proportions)(Fig. 4-4B)(see also Chapter 3). Thus, I conclude that the trigeminal nerve plays an essential role in the initiation of fast escape in newly-hatched zebrafish. After the acousti-covestibular input develops, however, fast escape is elicited toward correct direction by auditory, vestibular and/or lateral line inputs.

The M-cell is not essential for short-latency fast escape in young larvae

It is suggested from the previous chapters that, in the developed larva at > 120 hpf, acousticovestibular input activates the M-cell to initiate short-latency (< 6 ms) escape whereas head-tactile input initiates delayed-latency (> 6 ms) escape without activating the M-cell. Field potential recordings, however, suggested that the M-cell in newly-hatched larvae fires an action potential during escape (Eaton and Farley, 1975; Eaton et al., 1977). Thus, there may be a functional development of hindbrain escape network during acquisition of vibratory-induced fast escape, particularly in the functional relationships between the M-cell and non-M-cells.

To investigate this possibility, I evaluated the effects of selective ablation of the M-cell onto fast escape in larvae at 50-65 hpf (Fig. 4-5A). Here, the ablation was performed with pulsed-laser application to the M-cell visualized by the EGFP fluorescence in the Tol026 transgenic line, where the M-cell and many dorsal reticulospinal neurons express EGFP by the time of hatching (Tanimoto et al., 2009). After the M-cell ablation, water pulse applied to the OV still elicited fast escape opposite to the stimulus (4 fish, n = 25). Surprisingly, the evoked fast escape was virtually indistinguishable from that of M-cell intact fish (latency, 6.7±1.0 ms, tail flexion angle, 36.4 ± 6.7 degrees, n = 78, 6 fish) not only in the latency distribution (onset latency, 7.2 ± 1.0 ms, $p > 0.05$, Kolmogorov-Smirnov test) but also in the initial tail flexion angle

(37.2 ± 6.9 degrees, $p > 0.6$)(Fig. 4-5B), although fast escape with short latency from 5 to 6 ms was not observed after the lesion. These results indicate that the fast escape by head-tactile input before 70 hpf does not require the M-cell and can be initiated via non-M-pathway. Lack of further shortening in the minimum onset latency (6 ms) suggest that the non-M-escape pathway activated by head-tactile stimulation is well established by the time of hatching.

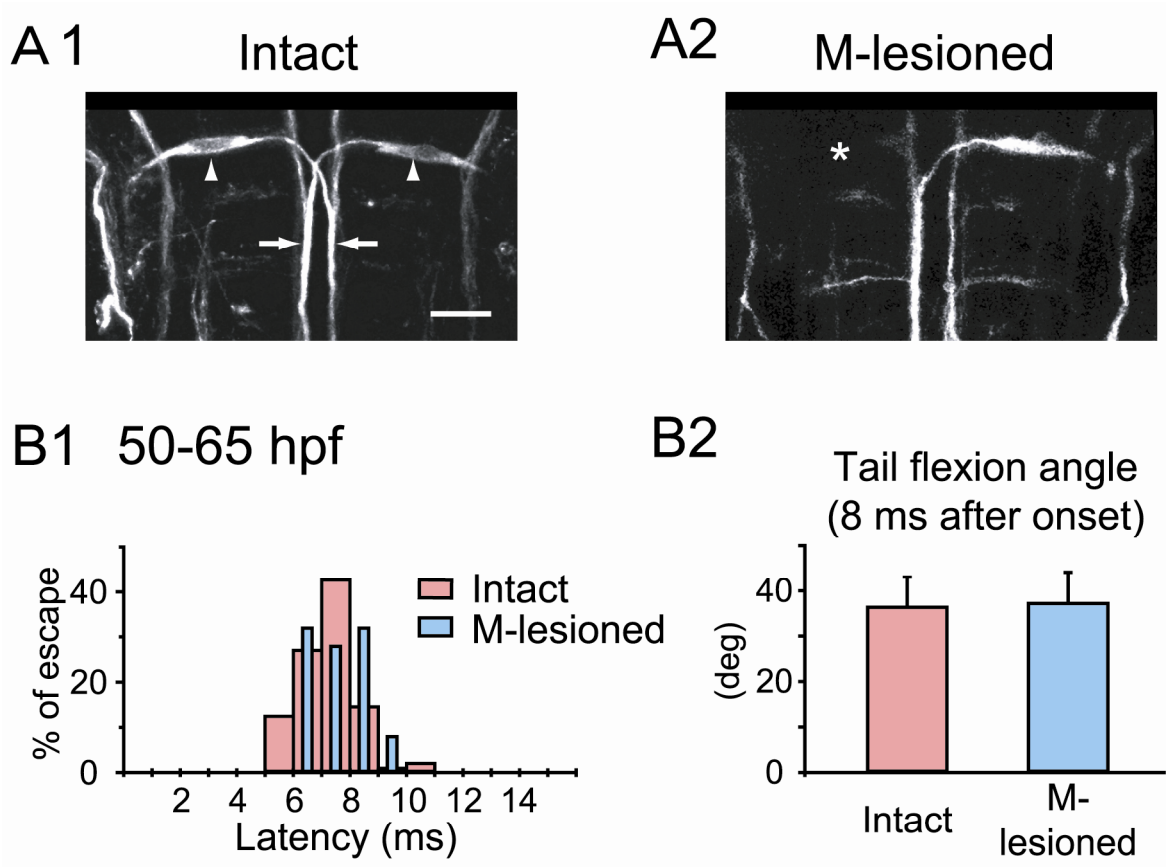

Figure 4-5. The M-cell is not essential for fast escape before 70 hpf. **A,** Cell bodies (arrowheads), lateral dendrites and crossing axons (arrows) of both M-cells are labeled with the 3A10 antibody in an intact 60-hpf larva (**A1**). Staining of each of them from the left M-cell was lost (asterisk) after the laser irradiation in another 60-hpf larva (**A2**). Scale bar: 30 μm. **B,** M-lesioned larva (blue) at 50-65 hpf still showed similar fast escape to intact fish (pink) in terms of probability distribution of the onset latency (**B1**) and the initial tail flexion angle (**B2**).

Discussion

Before 70 hpf, larval zebrafish shows escape behavior in response to head-tactile stimulus, which is mediated by trigeminal nerve afferent. After 80 hpf, zebrafish acquires sound/vibration-induced fast escape which is elicited with short latency by activation of statoacoustic nerve (VIIIn) afferent and the M-cell (M-escape). Head tactile stimulus also elicits fast escape at the later stage, which has longer onset latency than M-escape, but does not seem to require M-cell firing (non-M-escape).

Development of acousticovestibular input underlying acquisition of sound/vibration-induced escape

The present study shows that sound/vibration-induced escape is acquired later than touch-induced escape, which may depend on later acquisition of auditory responsiveness of the M-cell. Morphological as well as physiological evidences, however, have shown that the auditory afferent pathway from inner ear hair cells to the M-cell through statoacoustic nerve starts to form well before 40 hpf in zebrafish (Tanimoto et al., 2009). The hair cells in the OV and the VIIIn ganglion neurons appear before 24 hpf (Haddon and Lewis, 1996). Earliest contact of the VIIIn afferent on lateral dendrite of the M-cell occurred at 23 hpf (Kimmel et al., 1990). Furthemore, peripheral projections from the VIIIn connect with the hair cells before 27 hpf (Tanimoto et al., 2009). Thus, not the formation of the auditory pathway but subsequent functional development of it onto the M-cell is suggested to be critical for the acquisition of sound/vibration-induced escape. Tanimoto and his colleagues (2009) showed that natural sound stimulation elicits postsynaptic current (PSC) in the M-cell first at 46 hpf and that its onset latency decreases and its amplitude increases during subsequent development. They also demonstrated that the appearance and development of acoustic response in the M-cell coincids with those of microphonic potentials in the OV and suggested that acquisition of the acoustic response depends on functional maturation of the inner ear, possibly determined by expression of the nompC transient receptor potential channel critical for the mechanotransduction in the hair cell (Sidi et al., 2003). Therefore, the functional maturation of the inner ear by 80 hpf may determines the ac-

quisition of the sound/vibration-induced fast escape. This view may be generally applicable to developmental acquisition of behaviors related to inner-ear function because vestibulo-ocular reflex also acquired between 70-80 hpf (Easter and Nicola, 1997).

Contributions of the M-cell to fast escape in early developmental stages

The most simple explanation for the lack of significant effect of M-cell ablation (Fig. 4-5) is that the M-cell in newly-hatched larvae does not fire in response to head-tactile stimulation or M-cell firing does not deliver effective motor output enough to activate spinal neurons for fast bending of the body. Several lines of evidences, however, have been against the first possibility. Eaton and his colleagues (1975; 1977) reported that the head-tactile stimulation of the head of newly-hatched zebrafish (3-4 dpf, raised at 25-26 ºC) elicited extracellular field potential of action potential at the vicinity of the M-cell soma. Recently, firing of the M-cell in response to head-tactile stimulation was directly shown by whole-cell recording of the M-cell at 36 hpf (Tanimoto and Oda, unpublished observations). Yet, whether the M-cell fires during escape in newly-hatched larvae still remains to be elucidated. As for the second possibility, the M-cell has extended its axon to the end of the spinal cord (Eaton and Farley, 1973) with establishing morphologically mature synaptic contacts to primary motoneurons in the spinal cord (Jontes et al., 2000) by the time of hatching. However, the efficiency of the connections also remains to be elucidated physiologically. The third possibility for the luck of significant effect of M-cell ablation is that M-cell firing is effective enough to initiate escape, as in the developed larvae, but the onset of the escape is comparable to the non-M-cell pathway. The latency of M-cell firing in newly-hatched larva may be considerably longer than that in the developed larva because of the long latency and small amplitude of sound-evoked PSC in the M-cell as discussed above.

Altogether, teleost fishes, so-called hearing specialists (Popper and Fay, 1999) such as zebrafish and goldfish, acquire the acoustically evoked M-escape system in addition to the tactile-evoked escape system later in development to escape as quickly as possible from a hostile sound source before it reaches and injures the fish.

References for chapter 4

Bate M (1999) Development of motor behaviour. Curr Opin Neurobiol 9:670-675.

Burgess HA, Granato M (2007) Sensorimotor gating in larval zebrafish. J Neurosci 27:4984-4994.

Domenici P, Blake R (1997) The kinematics and performance of fish fast-start swimming. J Exp Biol 200:1165-1178.

Drapeau P, Saint-Amant L, Buss RR, Chong M, McDearmid JR, Brustein E (2002) Development of the locomotor network in zebrafish. Prog Neurobiol 68:85-111.

Easter SS, Jr., Nicola GN (1997) The development of eye movements in the zebrafish (Danio rerio). Dev Psychobiol 31:267-276.

Eaton RC, Farley RD (1973) Development of the Mauthner Neurons in embryos and larvae of the zebrafish, *Brachydanio rerio*. Copeia:674-682.

Eaton RC, Farley RD (1975) Mauthner neuron field potential in newly hatched larvae of the zebra fish. J Neurophysiol 38:502-512.

Eaton RC, Farley RD, Kimmel CB, Schabtach E (1977) Functional development in the Mauthner cell system of embryos and larvae of the zebra fish. J Neurobiol 8:151-172.

Fetcho JR (2006) The utility of zebrafish for studies of the comparative biology of motor systems. J Exp Zoolog B Mol Dev Evol.

Fetcho JR, Higashijima S, McLean DL (2008) Zebrafish and motor control over the last decade. Brain Res Rev 57:86-93.

Ghysen A, Dambly-Chaudiere C (2004) Development of the zebrafish lateral line. Curr Opin Neurobiol 14:67-73.

Haddon C, Lewis J (1996) Early ear development in the embryo of the zebrafish, Danio rerio. J Comp Neurol 365:113-128.

Hatta K (1992) Role of the floor plate in axonal patterning in the zebrafish CNS. Neuron 9:629-642.

Jontes JD, Buchanan J, Smith SJ (2000) Growth cone and dendrite dynamics in zebrafish embryos: early events in synaptogenesis imaged in vivo. Nat Neurosci 3:231-237.

Kimmel CB, Patterson J, Kimmel RO (1974) The development and behavioral characteristics of the startle response in the zebra fish. Dev Psychobiol 7:47-60.

Kimmel CB, Hatta K, Metcalfe WK (1990) Early axonal contacts during development of an identified dendrite in the brain of the zebrafish. Neuron 4:535-545.

Lewis KE, Eisen JS (2003) From cells to circuits: development of the zebrafish spinal cord. Prog Neurobiol 69:419-449.

Mendelson B (1986a) Development of reticulospinal neurons of the zebrafish. I. Time of origin. J Comp Neurol 251:160-171.

Mendelson B (1986b) Development of reticulospinal neurons of the zebrafish. II. Early axonal outgrowth and cell body position. J Comp Neurol 251:172-184.

Moorman SJ (2001) Development of sensory systems in zebrafish (Danio rerio). Ilar J 42:292-298.

Nagayoshi S, Hayashi E, Abe G, Osato N, Asakawa K, Urasaki A, Horikawa K, Ikeo K, Takeda H, Kawakami K (2008) Insertional mutagenesis by the Tol2 transposon-mediated enhancer trap approach generated mutations in two developmental genes: tcf7 and synembryn-like. Development 135:159-169.

Popper AN, Fay RR (1999) The auditory periphery in fishes. In: Comparative Hearing: Fish and Amphibians (Fay RR, Popper AN, eds), pp 43-100. New York: Springer-Verlag.

Saint-Amant L, Drapeau P (1998) Time course of the development of motor behaviors in the zebrafish embryo. J Neurobiol 37:622-632.

Sidi S, Friedrich RW, Nicolson T (2003) NompC TRP channel required for vertebrate sensory hair cell mechanotransduction. Science 301:96-99.

Stickney HL, Barresi MJ, Devoto SH (2000) Somite development in zebrafish. Dev Dyn 219:287-303.

Tanimoto M, Ota Y, Horikawa K, Oda Y (2009) Auditory input to CNS is acquired coincidentally with development of inner ear after formation of functional afferent pathway in zebrafish. J Neurosci 29:2762-2767.

Whitfield TT, Riley BB, Chiang MY, Phillips B (2002) Development of the zebrafish inner ear. Dev Dyn 223:427-458.

General discussion

In this thesis, I have demonstrated the direct correlation between activities of reticulospinal (RS) neurons and escape behavior in larval zebrafish. My results show that there are two types of fast escape in the intact brain: one is initiated by the single action potential of the M-cell and has a short onset latency (M-escape); the other is initiated without firing of the M-cell and has a longer onset latency than M-escape (non-M-escape), as observed in previous studies after ablation of the M-cell (Kimmel et al., 1980; Eaton et al., 1982; DiDomenico et al., 1988; Zottoli et al., 1999) (Chapter 1). In the initiation of M- or non-M-escape, the M-cell and its segmental homologs are suggested to act complementarily rather than cooperatively (Chapter 2). The escape pathways in the hindbrain are activated differently via different sensory inputs: auditory/vestibular input elicits M-escape, whereas head-tactile input preferentially induces non-M-escape (Chapter 3). As previously demonstrated (Kimmel et al., 1974), fast escape elicited by auditory/vestibular stimulus appears at a late stage of development (> 80 hpf), whereas tactile-induced escape appears earlier. In addition, lesioning of the M-cell does not affect the initiation of escape at the early stages of development (Chapter 4). Taken together, these data show that tactile-induced non-M-escape appears earlier in development and auditory/vibratory induced M-escape is established later.

Optical recording of neuronal activity in behaving larval zebrafish

The findings of the present study were possible primarily because of the recent development of techniques for *in vivo* Ca^{2+} imaging of neurons in an intact larval zebrafish whose tail is free to move, which have allowed us to examine the direct correlation between activities of RS neurons and escape behavior of teleost fish. The advantage of this approach is that we can determine how a particular neuron is activated during a measurable motor behavior. This is considerably different from the conventional electrophysiological techniques for *in vivo* intra- or extracellular recordings. Intracellular recordings made

by conventional methods allowed us to identify the activated neuron, but the animal had to be paralyzed during recordings, so that we had to deduce the associated behavior through electromyography of the muscle of interest (Hackett and Faber, 1983; Hackett and Greenfield, 1986) or through ventral root volleys (Svoboda and Fetcho, 1996). Extracellular recordings made by conventional methods allowed the animal to be active rather than paralyzed, but it was generally difficult to identify the neurons being fired or to measure the activities of many neurons other than the M-cell (Zottoli, 1977; Eaton et al., 1981; Weiss et al., 2006). In contrast, the optical approach employed here allowed us to obtain fluorescence responses from particular neurons, which had been retrogradely labeled with a fluorescent Ca^{2+} indicator, noninvasively, with simultaneous monitoring of animal behavior. The retrograde-labeling technique used in the present study enabled me to obtain high-contrast images of individual RS neurons with low background staining, because the indicator was taken up only by neurons that projected their axons to the site of the dye injection (Gahtan and O'Malley, 2001). The injection site was far from the recording area, ensuring that the local circuit in the brain was kept intact. Taking advantage of the new possibilities unlocked by this technique, I demonstrated the activities of paired M-cells during escape as the first challenge (Fig. 1-3 and 4). One problem I faced was that, using a conventional confocal microscope, I was able to image only a few neurons within a single focal plane. To overcome this limitation, I developed a novel confocal microscope that can image multiple neurons in optical planes that are distant (dozens of micrometers) from each other by introducing a high-speed confocal scanner and a high-speed focusing device. Measuring the M-cell together with its homolog, MiD3cm, at different depths enabled me to find a complementary relationship between the activities of these RS neurons (Fig. 2-3).

One limitation of the optical recording technique is that it offers only indirect measurement of neuronal activity through the associated Ca^{2+} increase. The Ca^{2+} response is much slower (on the order of seconds) than the membrane potential (on the order of milliseconds). Therefore, whole-cell recording allows us to measure the timing and the number of action potentials more accurately. Fortunately, in the present study, I was able to estimate the number of action potentials associated with the sensory-evoked Ca^{2+} response, by comparing the observed Ca^{2+} response with that of an antidromic action potential (Fig. 1-3 and 2-1).

Although retrograde labeling is a promising method that allows us to obtain excellent images of particular neurons of interest, it can not be applied to RS neurons with short axons or those in newly-hatched larva. A powerful way to overcome this problem is through the utilization of genetically encoded Ca^{2+} indicators (Higashijima et al., 2003). In particular, the single-wavelength indicator GCaMP2 (Diez-Garcia et al., 2005) is applicable to the optical setup in the present study. Expressing GCaMP2 in the RS neurons under the control of Mauthner-specific promotors such as that of the low-voltage gated potassium channel (Nakayama and Oda, 2004) may resolve one of the most important outstanding issues: that of the correlation between M-cell activity and fast escape in newly hatched larva (see discussion in Chapter 4).

Unique features of teleost RS neurons allow us to examine functional architecture of hindbrain in detail

Across vertebrates, the overall organization of the brainstem reticular formation is one of columns of cells arranged longitudinally along the length of the medulla and pons (Butler and Hodos, 2005). Within these columns, there are dorsoventral and rostrocaudal subdivisions called reticular nuclei. Each reticular nucleus can be distinguished from the others by the size of the cells within it as well as by its connections with other parts of the nervous system. Accordingly, the functional roles of the RS neurons within the reticular nuclei are usually studied at the level of the nucleus, especially in mammals (Dampney, 1994; Orlovsky et al., 1999; Yeomans et al., 2002) and in lampreys (Ullen et al., 1997; Fagerstedt et al., 2001; Dubuc et al., 2008). By contrast, all RS neurons in zebrafish and goldfish can be distinguished from others by their morphology; this situation provides us with a unique opportunity to examine their functions at the level of the individual cell (Kimmel et al., 1982b; Kimmel et al., 1985; Metcalfe et al., 1986; Lee and Eaton, 1991; Lee et al., 1993). The discrete appearance of teleost RS neurons has allowed us to investigate the relationships among them reproducibly, especially with regard to their segmental arrangement (Metcalfe et al., 1986), at the level of physiology (O'Malley et al., 1996; Liu and Fetcho, 1999; Oda and Nakayama, 2003; Nakayama and Oda, 2004; Neki et al., 2007) as well as development (Mendelson, 1986a, b; Hanneman et al., 1988) and axonal arborization (Gahtan and O'Malley, 2003).

The segmentally homologous RS neurons are hypothesized to be generated by the duplication and subsequent evolutionary divergence of hindbrain segments from an ancestral segment (Metcalfe et al., 1986). As a result of this process, the RS neurons within each set of the segmental homologs are expected to be related to each other developmentally (Metcalfe et al., 1986) or functionally (Kimmel et al., 1982b; Lee and Eaton, 1991; Lee et al., 1993). Of all the sets, the M-series neurons have been studied most intensively in order to test this hypothesis. Each M-series neuron is the first RS neuron to be born in its segment (Mendelson, 1986a), and the first to start extending its axon (Mendelson, 1986b). All M-series neurons express the same antigen in their early developmental stages (Hanneman et al., 1988). Functionally, the M-series neurons are coactivated by an escape-eliciting head tap (O'Malley et al., 1996), and the ablation of all of them was reported to abolish fast escape (Liu and Fetcho, 1999), suggesting that they are involved in the control of fast escape. Yet the M-series neurons are not exact copies of one another. Even in their morphology, they show fairly different axonal branching patterns in the spinal cord (Gahtan and O'Malley, 2003). In addition, they exhibit considerably different excitability: the M-cell fires only once at the onset of depolarization, whereas its homologs exhibit bursts of action potentials depending on the depolarizing current (Nakayama and Oda, 2004). These diversifications probably contribute to the production of escape behaviors in an adaptive manner (cf. Eaton and Emberley, 1991; Foreman and Eaton, 1993): specifically, the M-cell determines the onset and initial direction of the fast escape (Zottoli, 1977; Eaton et al., 1981; DiDomenico et al., 1988; Nissanov et al., 1990; Weiss et al., 2006), especially in response to the acousticovestibular input, whereas MiD2cm and MiD3cm are assumed to send varying motor outputs to the spinal cord by transmitting the duration of the sensory inputs into the trains of action potentials (Nakayama and Oda, 2004). Furthermore, the present study demonstrated that the M-cell and MiD3cm are involved in different ways in fast escapes elicited by different modes of sensory input (Chapter 3). Taken together, the duplication of hindbrain segments may have produced a group of morphologically homologous neurons mediating a particular behavior and the subsequent diversification of the segmental homologs may have led an expansion of the behavioral repertoire of the animal evoked by various types of stimulation.

The segmental homology among RS neurons in the teleost hindbrain is also consistent with the columnar organization of reticular nuclei, because segmental homologs, by definition (Metcalfe et al., 1986), share the morphological characteristics of neurons in a reticular nucleus as described above: 1) cell bodies at the same position in each corresponding segment, as if they were aligned in a column along the rostrocaudal axis, and 2) similar dendritic patterns, which suggest synaptic input from the common brain region (cf. Nakayama and Oda, 2004; Sato et al., 2007). Thus, a set of segmental homologs apparently corresponds to a set of neurons in a reticular nucleus. Segregation of sensory inputs onto morphologically similar neurons, as demonstrated in the present study, may be also observed in the reticular nuclei of other vertebrates.

Functional development of sensorimotor integration in reticulospinal system

It is noteworthy that the acquisition of sound/vibration-induced escape (Kimmel et al., 1974), which probably reflects the functional development of statoacoustic input to the M-cell (see discussion in Chapter 4), coincides with the morphological development of the M-cell (Kimmel, 1972). It has been reported previously that ablation of the ipsilateral OV before hatching impairs the growth of lateral dendrite of the M-cell in zebrafish (Kimmel et al., 1982a). In axolotls, elimination of the primordium of the statoacoustic ganglion reduced dendritic branching of the ipsilateral M-cell, while implantation of an additional primordium next to the original enhanced it (Goodman and Model, 1988). These findings suggest that the statoacoustic nerve afferents regulate the morphological development of the M-cell. This may be a mechanism by which developing sensory systems actively promote morphological, and probably also functional, diversification of RS neurons.

References for general discussion

Butler AB, Hodos W (2005) Comparative Vertebrate Neuroanatomy: Evolution and Adaptation, Second Edition. Hoboken, NJ: John Wiley and Sons, Inc.

Dampney RA (1994) Functional organization of central pathways regulating the cardiovascular system. Physiol Rev 74:323-364.

DiDomenico R, Nissanov J, Eaton RC (1988) Lateralization and adaptation of a continuously variable behavior following lesions of a reticulospinal command neuron. Brain Res 473:15-28.

Diez-Garcia J, Matsushita S, Mutoh H, Nakai J, Ohkura M, Yokoyama J, Dimitrov D, Knopfel T (2005) Activation of cerebellar parallel fibers monitored in transgenic mice expressing a fluorescent Ca2+ indicator protein. Eur J Neurosci 22:627-635.

Dubuc R, Brocard F, Antri M, Fenelon K, Gariepy JF, Smetana R, Menard A, Le Ray D, Viana Di Prisco G, Pearlstein E, Sirota MG, Derjean D, St-Pierre M, Zielinski B, Auclair F, Veilleux D (2008) Initiation of locomotion in lampreys. Brain Res Rev 57:172-182.

Eaton RC, Emberley DS (1991) How stimulus direction determines the trajectory of the Mauthner-initiated escape response in a teleost fish. J Exp Biol 161:469-487.

Eaton RC, Lavender WA, Wieland CM (1981) Identification of Mauthner-initiated response patterns in goldfish: Evidence from simultaneous cinematography and electrophysiology. J Comp Physiol [A] 144:521-531.

Eaton RC, Lavender WA, Wieland CM (1982) Alternative neural pathways initiate fast-start responses following lesions of the Mauthner neuron in goldfish. J Comp Physiol [A] 145:485-496.

Fagerstedt P, Orlovsky GN, Deliagina TG, Grillner S, Ullen F (2001) Lateral turns in the Lamprey. II. Activity of reticulospinal neurons during the generation of fictive turns. J Neurophysiol 86:2257-2265.

Foreman MB, Eaton RC (1993) The direction change concept for reticulospinal control of goldfish escape. J Neurosci 13:4101-4113.

Gahtan E, O'Malley DM (2001) Rapid lesioning of large numbers of identified vertebrate neurons: applications in zebrafish. J Neurosci Methods 108:97-110.

Gahtan E, O'Malley DM (2003) Visually guided injection of identified reticulospinal neurons in zebrafish: a survey of spinal arborization patterns. J Comp Neurol 459:186-200.

Goodman LA, Model PG (1988) Superinnervation enhances the dendritic branching pattern of the Mauthner cell in the developing axolotl. J Neurosci 8:776-791.

Hackett JT, Faber DS (1983) Mauthner axon networks mediating supraspinal components of the startle response in the goldfish. Neuroscience 8:317-331.

Hackett JT, Greenfield LJ (1986) The behavioral role of the Mauthner neuron impulse. Behav Brain Sci 9:729-730.

Hanneman E, Trevarrow B, Metcalfe WK, Kimmel CB, Westerfield M (1988) Segmental pattern of development of the hindbrain and spinal cord of the zebrafish embryo. Development 103:49-58.

Higashijima S, Masino MA, Mandel G, Fetcho JR (2003) Imaging neuronal activity during zebrafish behavior with a genetically encoded calcium indicator. J Neurophysiol 90:3986-3997.

Kimmel CB (1972) Mauthner axons in living fish larvae. Dev Biol 27:272-275.

Kimmel CB, Patterson J, Kimmel RO (1974) The development and behavioral characteristics of the startle response in the zebra fish. Dev Psychobiol 7:47-60.

Kimmel CB, Eaton RC, Powell SL (1980) Decreased fast-start performance of zebrafish larvae lacking Mauthner neurons. J Comp Physiol [A] 140:343-350.

Kimmel CB, Powell SL, Kimmel RJ (1982a) Specific reduction of development of the Mauthner neuron lateral dendrite after otic capsule ablation in Brachydanio rerio. Dev Biol 91:468-473.

Kimmel CB, Powell SL, Metcalfe WK (1982b) Brain neurons which project to the spinal cord in young larvae of the zebrafish. J Comp Neurol 205:112-127.

Kimmel CB, Metcalfe WK, Schabtach E (1985) T reticular interneurons: a class of serially repeating cells in the zebrafish hindbrain. J Comp Neurol 233:365-376.

Lee RK, Eaton RC (1991) Identifiable reticulospinal neurons of the adult zebrafish, Brachydanio rerio. J Comp Neurol 304:34-52.

Lee RK, Eaton RC, Zottoli SJ (1993) Segmental arrangement of reticulospinal neurons in the goldfish hindbrain. J Comp Neurol 329:539-556.

Liu KS, Fetcho JR (1999) Laser ablations reveal functional relationships of segmental hindbrain neurons in zebrafish. Neuron 23:325-335.

Mendelson B (1986a) Development of reticulospinal neurons of the zebrafish. I. Time of origin. J Comp Neurol 251:160-171.

Mendelson B (1986b) Development of reticulospinal neurons of the zebrafish. II. Early axonal outgrowth and cell body position. J Comp Neurol 251:172-184.

Metcalfe WK, Mendelson B, Kimmel CB (1986) Segmental homologies among reticulospinal neurons in the hindbrain of the zebrafish larva. J Comp Neurol 251:147-159.

Nakayama H, Oda Y (2004) Common sensory inputs and differential excitability of segmentally homologous reticulospinal neurons in the hindbrain. J Neurosci 24:3199-3209.

Neki D, Nakayama H, Fujii T, Oda Y (2007) Functional connection from Mauthner cell to homologous reticulospinal neurons in the goldfish hindbrain. Neurocsci Res 58:S92.

Nissanov J, Eaton RC, DiDomenico R (1990) The motor output of the Mauthner cell, a reticulospinal command neuron. Brain Res 517:88-98.

Oda Y, Nakayama H (2003) Common synaptic drive from Mauthner cell to segmentally homologous reticulospinal neurons in teleost hindbrain. In: 2003 Abstract Viewer/Itinerary Planner, p Program No. 78.79. Washington, DC: Society for Neuroscience Online.

O'Malley DM, Kao YH, Fetcho JR (1996) Imaging the functional organization of zebrafish hindbrain segments during escape behaviors. Neuron 17:1145-1155.

Orlovsky GN, Deliagina TG, Grillner S (1999) Initiation of locomotion. In: Neuronal control of locomotion: from mollusc to man, pp 205-214. New York: Oxford University Press.

Sato T, Hamaoka T, Aizawa H, Hosoya T, Okamoto H (2007) Genetic single-cell mosaic analysis implicates ephrinB2 reverse signaling in projections from the posterior tectum to the hindbrain in zebrafish. J Neurosci 27:5271-5279.

Svoboda KR, Fetcho JR (1996) Interactions between the neural networks for escape and swimming in goldfish. J Neurosci 16:843-852.

Ullen F, Deliagina TG, Orlovsky GN, Grillner S (1997) Visual pathways for postural control and negative phototaxis in lamprey. J Neurophysiol 78:960-976.

Weiss SA, Zottoli SJ, Do SC, Faber DS, Preuss T (2006) Correlation of C-start behaviors with neural activity recorded from the hindbrain in free-swimming goldfish (Carassius auratus). J Exp Biol 209:4788-4801.

Yeomans JS, Li L, Scott BW, Frankland PW (2002) Tactile, acoustic and vestibular systems sum to elicit the startle reflex. Neuroscience and Biobehavioral Reviews 26:1-11.

Zottoli SJ (1977) Correlation of the startle reflex and Mauthner cell auditory responses in unrestrained goldfish. J Exp Biol 66:243-254.

Zottoli SJ, Newman BC, Rieff HI, Winters DC (1999) Decrease in occurrence of fast startle responses after selective Mauthner cell ablation in goldfish (Carassius auratus). J Comp Physiol [A] 184:207-218.

Acknowledgements

I am so grateful to Prof. Yoichi Oda for giving me a chance to research on the fascinating escape networks in teleost fish. I greatly appreciate for his patient instruction, consistent encouragement, critical discussions throughout this research. He is the very father of my science. I am grateful to Dr. Edward Ruthazer for his comments and grammatical corrections on the original article. I am also grateful to Drs. Shin Takagi, Hiromi Hirata, and Akira Nukazuka for their continuous encouragement and discussions during my days in Nagoya. I thank Prof. Hiroyuki Takeda, Dr. Kazuki Horikawa and Ms. Yasuko Sato for providing the *Tol026* transgenic zebrafish and Prof. Hitoshi Okamoto and the National Bio Resource Project for providing the *zCREST2/isl1-GFP* transgenic zebrafish. I also thank Mses. Keiko Fukuda, Mikiko Nakashoji, Yukako Kinbara and Natsuyo Nakata for their collaboration, and Mses. Mayu Goto, Mahoko Hirose, Keiko Tanaka and Chikako Chujo for their assistance. I am also grateful to Profs. Fujio Murakami, Hisato Kondoh and Ichiro Fujita for their critical readings and helpful comments on the thesis. At last, I would like to thank Prof. Nobuhiko Yamamoto for his helpful advice and encouragement during the graduate course and critical comments and suggestions for preparing the thesis.

Bibliography

【Original article】

Tsunehiko Kohashi and Yoichi Oda (2008) Initiation of Mauthner- or non-Mauthner-mediated fast escape evoked by different modes of sensory input. J Neurosci 28:10641-10653.

【Review】

平田　普三, 小橋　常彦, 小田　洋一 (2008) 硬骨魚類の逃避運動制御メカニズム 実験医学 26 (12): 1916-1923

【Symposiums】

小橋　常彦, 谷本　昌志, 小田　洋一: ゼブラフィッシュの逃避運動と後脳ニューロンの同時光学計測 日本顕微鏡学会第63回学術講演会 新潟コンベンションセンター(新潟) 2007.5.20-22

小田洋一, 中山寿子, 小橋常彦:Functional organization of segmentally homologous reticulospinal neurons in teleost hindbrain 第28回日本神経科学大会, 2005.7.26-28, SY1-01-6, パシフィコ横浜(横浜)

【Oral presentations】

小橋　常彦, 小田　洋一: Functional Segregation of Segmentally Homologous Reticulospinal Neurons in Hindbrain for Control of Fast Escape in Zebrafish. 第14回小型魚類研究会, 岡崎コンファレンスセンター(岡崎) 2008.9.20-21

Tsunehiko Kohashi and Yoichi Oda: Functional segregation of segmentally homologous reticulospinal neurons in hindbrain for control of fast escape in zebrafish: International seminar Evolutionary Studies

in Behavioral Neuroscience; Shonan Village Center (Hayama), 2008.6.25-27

小橋　常彦, 小田　洋一: Development of fast escape initiated by the Mauthner cell in zebrafish; 第29回日本神経科学大会, OS2P7-13, 国立京都国際会館(京都)2006.7.19-21

小橋常彦, 小田洋一:ゼブラフィッシュの逃避運動発現を担う後脳分節間相同ニューロンの階層的活動様式. 第52回中部日本生理学会、名古屋大学 IB 情報館(名古屋), 2005.9.29-30、

小橋常彦, 小田洋一:Combined activity in segmentally homologous hindbrain neurons during escape behavior of zebrafish 第28回日本神経科学大会、O3F-04, パシフィコ横浜(横浜), 2005.7.26-28

【Poster presentations】

Tsunehiko Kohashi and Yoichi Oda: Initiation of Mauthner- or non-Mauthner- mediated fast escape evoked by different modes of sensory input in zebrafish 576.9/PP13, the 38th annual meeting of the Society for Neuroscience, Washington Convention Center (Washington DC) , 2008.11.15-19

小橋　常彦, 中田　奈津代, 小田　洋一: Development of hindbrain circuits for fast escape in zebrafish 第31回日本神経科学大会 P1-k03 東京国際フォーラム(東京) 2008.7.9-11

小橋　常彦, 小田　洋一: Different pathways for Mauthner and Non-Mauthner escapes in zebrafish 第30回日本神経科学大会 P2-e19 パシフィコ横浜(横浜)2007.9.10-12

谷本　昌志, 小橋　常彦, 小田　洋一: ゼブラフィッシュの逃避運動の発達にともなうマウスナー細胞への感覚入力の再編成 日本分子生物学会2006フォーラム 3P-374 名古屋国際会議場(名古屋)2006.12.6-8

小橋 常彦, 小田 洋一 Functional relationships of segmentally homologous hindbrain neurons in controlling escape behaviors of zebrafish 第27回日本神経科学大会 P1-242 大阪国際会議場(大阪)2004.9.21-23

小橋 常彦, 白木 千津子, 小田 洋一 In vivo imaging of segmentally homologous reticulospinal neurons in zebrafish hindbrain activated during escape behaviors 第26回日本神経科学大会 P3-A-094 名古屋国際会議場(名古屋)2003.7.23-25